Année 2006 - 2007

THÈSE

présentée à

l'Université Paul Verlaine-Metz

par Chien-Cheng HUANG

pour l'obtention du grade de Docteur

Spécialité : Physique

Statics, Dynamics, and Rheological Properties of Micellar Solutions by Computer Simulation

Thèse en cotutelle avec l'Université Libre de Bruxelles, Belgique

Soutenue le 25 septembre 2007 devant la commission d'examen

M. Wim Briels	Professeur, Twente University, Pays-Bas	**Rapporteur**
M. Roland G. Winkler	Professeur, Forschungszentrum Jülich, Allemagne	**Rapporteur**
M. Michel Mareschal	Professeur, Université Libre de Bruxelles	**Examinateur**
M. Joachim Wittmer	DR CNRS, Institut Charles Sadron, Strasbourg	**Examinateur**
Mme Hong Xu	Professeur, Université Paul Verlaine-Metz	**Directeur de Thèse**
M. Jean-Paul Ryckaert	Professeur, Université Libre de Bruxelles	**Directeur de Thèse**

Remerciements

Dans le cadre d'une thèse en cotutelle entre le Laboratoire de Physique des Milieux Denses de l'Université Paul Verlaine-Metz et le Laboratoire de Physique des Polymères de l'Université de Libre de Bruxelles, j'ai été amené à travailler au sein de deux laboratoires, expérience très enrichissante d'un point de vue scientifique et humain.

J'exprime, tout d'abord, mes reconnaissances envers le Prof. Hong Xu pour sa pédagogie, sa grande disponibilité et son soutien ainsi que pour la formation qu'elle m'a dispensée. Je tiens à remercier ensuite le Prof. Jean-Paul Ryckaert pour toutes les discussions productives que nous avons eu ensemble et le partage de son savoir dans le domaine de la physique. Je leur remercie pour leur soutien au jour le jour et pour leur qualité humaine. Merci à vous deux de m'avoir donné un si bel exemple de rigueur et d'honnêteté scientifique.

Je remercier également Dr. Joachim Wittmer et le Prof. Marc Baus pour les nombreuses idées sur les voies à explorer ainsi que pour les discussions très enrichissantes.

Je remercie grandement Monsieur Georges Destrée pour les aides sur les techniques de simulations.

Je souhaite aussi remercier Monsieur François Crevel pour les nombreuses discussions.

Je voudrais également remercier l'ensemble des membres du jury de thèse, et en particulier le Prof. Roland G. Winkler et le Prof. Wim Briels pour avoir accepté la charge de rapporteurs de cette thèse. Merci au Prof. Michel Mareschal d'avoir bien voulu présider le jury et Dr. Joachim Wittmer pour l'intérêt qu'il a porté à ce travail.

Enfin, je tiens également à remercier ma famille et mes proches pour leur confiance et leur soutien constant.

Abstract

Statics, dynamics, rheology and scission recombination kinetics of self assembling linear micelles are investigated at equlibrium state and under shear flow by computer simulations using a newly proposed mesoscopic model. We model the micelles as linear sequences of Brownian beads whose space-time evolution is governed by Langevin dynamics. A Monte Carlo algorithm controls the opening of a bond or the chain-end fusion. A kinetic parameter ω modelling the effect of a potential barrier along a kinetic path, is introduced in our model. For equilibrium state we focus on the analysis of short and long time behaviors of the scission and recombination mechanisms. Our results show that at time scales larger than the life time of the average chain length, the kinetics is in agreement with the mean-field kinetics model of Cates. By studying macroscopic relaxation phenomena such as the average micelle length evolution after a T-jump, the monomer diffusion, and the zero shear relaxation function, we confirm that the effective kinetic constants found are indeed the relevant parameters when macroscopic relaxation is coupled to the kinetics of micelles. For the non-equilibrium situation, we study the coupled effects of the shear flow and the scission-recombination kinetics, on the structural and rheological properties of this micellar system. Our study is performed in semi-dilute and dynamically unentangled regime conditions. The explored parameter ω range is chosen in order for the life time of the average size chain to remain shorter than its intrinsic (Rouse) longest relaxation time. Central to our analysis is the concept of dynamical unit of size Λ, the chain fragment for which the life time τ_Λ and the Rouse time are equal. Shear thinning, chain gyration tensor anisotropy, chain orientation and bond stretching are found to depend upon the reduced shear rate $\beta_\Lambda = \dot{\gamma}\tau_\Lambda$ while the average micelle size is found to decrease with increasing shear rate, independently of the height of the barrier of the scission-recombination process.

Contents

Introduction

In the field of self-assembling structures, supramolecular polymers are attracting nowadays much attention [1, 56]. The terminology of supramolecular polymer applies to any polymer-like flexible and cylindrical superstructure obtained by the reversible linear aggregation of one or more type of molecules in solution or in melt. These supramolecular polymers are typical soft matter systems and the chain length distribution which determines their properties, is very sensitive to external conditions (temperature, concentration, external fields, salt contents, etc...). Wormlike micelles are one of the most common type of supramolecular polymer [2]. Self-assembled stacks of discotic molecules [20] and chains of bifunctional molecules [21] are other examples. All these examples differ by the nature of the intermolecular forces involved in the self-assembling of the basic units, but they lead to a similar physical situation bearing much analogy with a traditional system of polydisperse flexible polymers when their length becomes sufficiently large with respect to their persistence length. The specificity and originality of these supramolecular polymers comes from the fact that these chains are continuously subject to scissions at random places along their contour and subject to end to end recombinations, leading to a dynamical equilibrium between different chain lengths species.

It is well known and schematically illustrated in figure 1 that some surfactant molecules in solution can self-assemble and form wormlike micelles [2]. As their mass distribution is in thermal equilibrium, they are therefore sometimes termed "equilibrium polymers" (EP) [1]. Similar system of equilibrium polymer are formed by liquid sulfur [33, 34, 35], selenium [36] and some protein filaments [37]

The micellar solutions exhibit fascinating rheological behavior which has been recently reviewed and discussed theoretically [56]. Quite commonly, under shear flow in a Couette cell, an originally isotropic micellar solution undergoes a shear-banding

transition [3], producing a two phases system spatially organized in a concentric manner with both phases lying either close to the inner or to the outer cylinder of the rheometer. As the viscosity of both phases is different, a velocity profile with two slopes is observed through the gap. This non-equilibrium phase separation is the object of numerous studies [56]. The shear thinning and orientational ordering of wormlike micelles [55] resembles the usual phenomenon observed in polymer solutions but, in many micellar solutions close to the overlap concentration[4], one can also observe a shear-thickening behavior whose microscopic origin is still a matter of debate nowadays. Much better understood is the trend of entangled micellar solutions to display a Maxwell fluid rheological behavior [2]. The simple exponential relaxation behavior has been theoretically explained by the reptation-reaction model[56], taking into account the scission-recombination mechanism by which local entanglements can be released by chain scission. The theoretical treatment of the scission-recombination process within the rheological theoretical approaches, is usually based on a simple mean-field (MF) approach in which correlations between successive kinetic events are fully neglected. The way to take into consideration such correlated transitions has been detailed by O'Shaughnessy and Yu [12] in order to explain some high frequency features of the rheological behavior of micellar systems. As the latter kinetics model interprets the stress relaxation as the result of local effects between successive correlated transitions where chain ends produced by a scission recombine with each other after a small diffusive excursion of the chain ends, such a rheological behavior was called "diffusion-controlled" (DC) by opposition to the standard MF model.

Computer simulations at the mesoscopic scale offers an interesting route towards the understanding of the generic properties of wormlike micelles solutions on the basis of a well controlled microscopic (or mesoscopic) model. The first accent within the simulation approach was put on testing the chain length distribution for various algorithms producing, on a lattice or in continuum space, temporary linear self assembling structures. Earlier Monte Carlo simulations using an asymmetric Potts model were performed to study static properties of equilibrium polymers [38, 39, 40]. Rouault and Milchev proposed a dynamical Monte Carlo algorithm [41], based on the highly efficient bond fluctuation model (BFM) [42, 43]. In great detail, Wittmer and co-workers [13, 22] investigate the static properties of EP in dilute and semi-dilute solutions using the same BFM. They confirmed scaling predictions of the mean chain length in dilute and

semi-dilute limits. Rouault [15] verified the dependence of mean chain length with concentration using an off-lattice Brownian dynamics simulation. Dynamics at equilibrium and direct simulation of systems in shear flow were also much investigated over the last ten years. Kroger and co-workers study EP at equilibrium [58] and under shear flow [17] by Molecular Dynamics using the particular pair potential FENE-C model. This model is a variant of the traditional pair potential of the LJ+FENE type used to model (permanent) polymers, a pair potential which diverges both as r goes to zero (repulsive forces) and at a distance $r = R_c$ where the corresponding attractive force between neighboring monomers also diverges. The FENE-C potential is a truncated form of the usual form which is set to a constant beyond a certain distance $r = r_m < R_c$ value, creating a finite potential well for a bounded pair with respect to the unbounded pair ($r > r_m$). In this way, the covalent bond can break or recombine as the pair distance crosses the r_m value. Using the same model, Padding and Boek [16] investigated the recombination kinetics and the stress relaxation of wormlike micellar systems. They found that at high concentrations, the kinetics is close to a diffusion-controlled mechanism. Milchev and co-works [26] study micelle conformations and their size distribution by an off-lattice microscopic model, to study solutions of EP in a lamellar shear flow while Padding and Boek investigate the influence of shear flow on the formation of rings in a EP system using FENE-C model [44]. All these studies predict a decrease of the average micelle size as a result of the shear flow. Other simulation studies envisage that ultimately, various simulations at different length and time scale will have to be combined to fill the huge gap between the atomistic length and time scales where the precise chemistry is relevant and the mesoscopic scale where rheological properties can really be probed by simulation. Studies of this type mixing both the atomistic and mesoscopic approaches to study wormlike micelles rheology are under progress[57].

The aim of our thesis on isotropic wormlike micelles solutions is to analyze, on the basis of a dynamical simulation at the mesoscopic level, the influence on the macroscopic relaxation phenomena of the dynamical coupling between the usual "flexible polymer" relaxation processes and the "scission-recombination" kinetics. We will restrict ourselves to unentangled solutions (working slightly below or above the isotropic semi-dilute threshold with a very flexible mesoscopic equilibrium polymer model) to avoid the prohibitive computer time needed to follow relaxation phenomena governed by entangled dynamics. The relevance of the MF kinetics model and the microscopic

origin of the scission-recombination rate constants is one important target of our study. Unentangled supramolecular polymers dynamics was indeed found to be relevant in selenium rheology. At the occasion of this experimental rheological study, Faivre and Gardissat [36] proposed an extension of the traditional Rouse theory to include the scission kinetic effects on the Rouse modes relaxation. They predicted the way the zero shear rate viscosity decreases as the scission and recombination kinetic constants increase, introducing the concept of dynamical subunit whose size fixes the relaxation time which governs the shear modulus relaxation.

The thesis is organized as follows: The theoretical aspects of wormlike micelles statics (distribution of micelle sizes) and the dynamics (Cates MF kinetic model, Faivre and Gardissat theory[36])are gathered in chapter I.

In chapter II, we detail the particular mesoscopic Langevin Dynamics model which is adopted throughout our thesis. Given our aims, this model has the particularly useful feature that the static properties (in particular the distribution of chain lengths) and the dynamics of the scission-recombination can be tuned separately so that we will often investigate how the relaxation at a unique state point (from a static point of view) is modified by tuning the kinetic rate constants.

Chapter III reports the results of a series of simulations at equilibrium, performed by Langevin Dynamics. Both a dilute and a semi-dilute state points are treated. We check our results regarding the distribution of chain sizes with respect to theoretical prediction and analyze in detail the microscopic origin of the relevant rate constants.

Chapter IV reports a systematic study of a single semi-dilute state point of micellar solution under shear flow. Here two kinds of parameters, the shear rate and the scission-recombination rate constants, are systematically varied. We discuss the evolution of the average micelle size with shear rate and relate it to a different evolution of the two types of rate constants (scission and recombination). We also discuss the nature of the relevant reduced shear rate and extrapolate our viscosity data to zero shear rate, allowing us to test the Faivre-Gardissat theory's predictions [36].

Our general conclusions are gathered in the last chapter V.

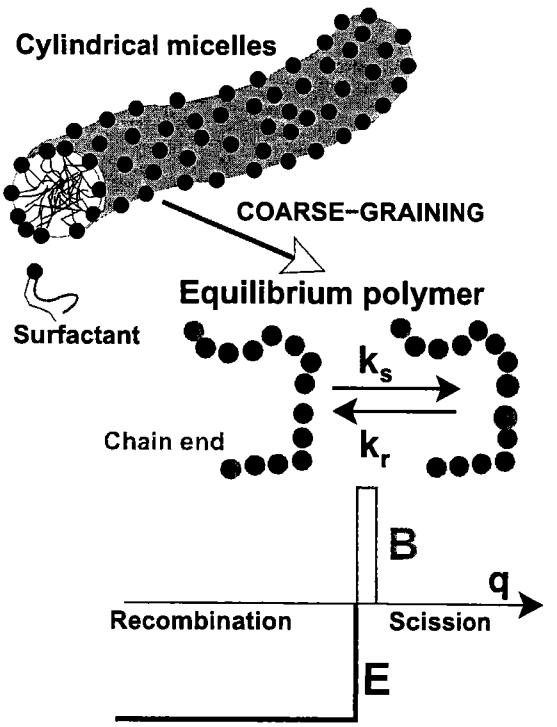

Figure 1: Some surfactant molecules in solution self-assemble and form long wormlike micelles which continuously break and recombine. Their mass distribution is, hence, in thermal equilibrium and they present an important example of the vast class of systems termed "equilibrium polymers"[1].The free energy E of the (hemispherical) end cap of these micelles has been estimated [2] to be of order of $10k_BT$. This energy penalty (together with the monomer density) determines essentially the static properties and fixes the ratio of the scission and recombination rates, k_s and k_r. Additionally, these rates are influenced by the barrier height B which has been estimated to be similar to the end cap energy. Both important energy scales have been sketched schematically as a function of a generic reaction coordinate q (see chapter 8 of reference [23]).Following closely the analytical description [2, 22, 13] these micellar systems are represented in this study by coarse-grained effective potentials in terms of a standard bead-spring model. The end cap free energy becomes now an energy penalty for scission events, i.e., the creation of two unsaturated chain ends. The dynamical barrier is taken into account by means of an attempt frequency $\omega = \exp(-B/k_BT)$. If ω is large, successive breakage and recombination events for a given chain can be assumed to be uncorrelated and the recombination of a newly created chain ends will be of standard mean-field type. On the other hand, the (return) probability that two newly created chain ends recombine immediately must be particularly important at large ω. These highly correlated "diffusion controlled" [12] recombination events do not contribute to the effective macroscopic reaction rates which determine the dynamics of the system.

Chapter 1

Theoretical Framework

In this chapter we will briefly present the theoretical framework of cylindrical micelles and some standard polymer theoretical aspects which are pertinent to the flexible micelles system. In Section 1, we introduce the statistical mechanics derivation of the distribution of chain lengths and of the corresponding average chain length. Then in section 2, for the scission-recombination kinetics at equilibrium, we study the theoretical formalism of equilibrium polymers (EP) developed by Cates and co-workers [9, 2], based on a mean-field approximation. And the third section of this chapter will focus on the linear viscoelasticity of EP. In this section, a framework for linear viscoelacity of dilute polymer solutions, and intrinsic shear modulus by the Rouse model are presented. Finally, we briefly review the theory of Faivre and Gardissat [36] where a modification of the standard Rouse theory of linear viscosity of a polydisperse polymer system is proposed.

1.1 Statistical mechanics derivation of the distribution of chain lengths

To treat a system of wormlike micelles theoretically, it is convenient to work at the mesoscopic scale using a model of linear flexible polymers made of L monomers of size b linked together by a non permanent bonding scheme. Within the system, individual chain lengths fluctuate by bond scission and by fusion of chain ends of two different chains. Statistical mechanics can be employed to predict the equilibrium distribution of chain lengths[2]. In terms of the equilibrium chain number density $c_0(L)$, the average chain length L_0 and the total monomer density ϕ are given by

$$L_0 = \frac{\sum_{L=0}^{\infty} L c_0(L)}{\sum_{L=0}^{\infty} c_0(L)} \tag{1.1}$$

$$\phi = \sum_{L=0}^{\infty} L c_0(L) = \frac{M}{V} \tag{1.2}$$

where M denotes the total number of monomers in the system and V is the volume.

Conceptually, we consider the Helmholtz free energy $F(V,T;\{N(L)\},N_s)$ of a mixture of chain molecules of different length L in solvent where, in addition to the temperature T, the volume V and the number of solvent molecules N_s, the number of chains of each specific length $N(L)$ is fixed. Let $F(V,T;M,N_s)$ be the Helmholtz free energy of a similar system where only the total number of solute monomers M is fixed. The equilibrium chain length distribution $c_0(L) = N(L)/V$ will result from the set $\{N(L)\}$ which satisfies the condition

$$F(V,T;M,N_s) = min_{\{N(L)\}} \left[F(V,T;\{N(L)\},N_s) + \mu \sum_{L=0}^{\infty} L N(L) \right] \tag{1.3}$$

The parameter μ is the Lagrange multiplier associated with the constraint that the individual number of chains $N(L)$ must keep fixed the total number of monomers $M = \sum_0^{\infty} L N(L)$. Minimization requires that the first derivative with respect to any $N(L')$ variable (L'=1,2, ...) is zero, giving

$$\frac{\delta F(V,T;\{N(L)\},N_s)}{\delta N(L')} + \mu L' = 0; L' = 1,2,... \tag{1.4}$$

We expect the entropic part of the total free energy $F(V,T;\{N(L)\},N_s)$ to be the sum of translational and chain internal configurational contributions which both depend upon the way the M monomers are arranged into a particular chain size distribution. For the translation part, the polydisperse system entropy is estimated as the ideal mixture entropy S_{id}

$$S_{id}(V,T;\{N(L)\},N_s) = -k_B \sum_L N(L) \ln \left(C N(L) \right) + S^{solv} \tag{1.5}$$

where $C = b^3/V$ is a dimensionless constant independent of L and where S^{solv} is the solvent contribution, independent of the $N(L)$ distribution. The configurational entropy of an individual chain with L monomers is written as $S_1(L) = k_B \ln \Omega_L$, in

terms of Ω_L, the total number of configurations of the chain. Adding the configurational contributions to S_{id} as given by eq.(1.5), the total entropy becomes

$$S(V,T;\{N(L)\},N_s) = -k_B \sum_L N(L)\left[\ln\left(CN(L)\right) - \ln\Omega_L\right] + S^{solv} \tag{1.6}$$

We now turn to the energy $E(V,T;\{N(L)\},N_s)$ of the same system. If $E_1(V,T;L)$ represents the internal energy of a chain of L monomers and E_s the energy of a solvent molecule, the energy can be written as

$$E(V,T;\{N(L)\},N_s) = \sum_L N(L)E_1(V,T;L) + N_s E_s(V,T) \tag{1.7}$$

The key contribution in E_1 is the chain end-cap energy E which corresponds to the chain end energy penalty required to break a chain in two pieces. We will suppose that $E_1(L) = E + L\tilde{\epsilon}$ where $\tilde{\epsilon}$ is an irrelevant energy per monomer as $M\tilde{\epsilon}$, its total contribution to the system energy, is independent of the chain length distribution.

The present approximation of the total free energy of the system is thus given by incorporating in the general expression (1.3) the expressions (1.6) and (1.7), giving

$$\beta F(V,T;\{N(L)\},N_s) = \sum_L N(L)\left[\ln N(L) + \ln C - \ln\Omega_L + \beta E + \beta\tilde{\epsilon}L\right] \tag{1.8}$$

where irrelevant constant solvent terms have been omitted as we only need the first derivative of the free energy with respect to $N(L)$, which now takes the form

$$\frac{\delta\beta F}{\delta N(L)} = \ln N(L) + \ln C - \ln\Omega_L + \beta E + \beta\tilde{\epsilon}L + 1. \tag{1.9}$$

With this expression, the minimization condition on $N(L)$ becomes

$$\ln N(L) + \ln C - \ln\Omega_L + \beta E + 1 + \mu' L = 0 \tag{1.10}$$

where $\mu' = (\beta\mu + \beta\tilde{\epsilon})$. We note at this stage that the second derivative of $\beta F(V,T;\{N(L)\}) + \mu' \sum_L LN(L)$ with respect to $N(L)$ and $N(L')$ variables gives the non negative result $\frac{\delta_{LL'}}{N(L)}$, indicating that the extremum is indeed a minimum.

Solving for $N(L)$ in eq.(1.10), we get

$$N(L) = C'^{-1}\exp -(\mu' L + \beta E - \ln\Omega_L) \tag{1.11}$$

where $C' = eC$ while, according to eq. (1.2)), μ' must be such that

$$\sum_L L\exp -(\mu' L + \beta E - \ln\Omega_L) = MC' \tag{1.12}$$

The equilibrium $N(L)$ variables are also related to the equilibrium chain length average L_0 (see eq. (1.1)), so that

$$\sum_L \exp -(\mu' L + \beta E - \ln \Omega_L) = \frac{MC'}{L_0} \tag{1.13}$$

To progress, we now need to specify the explicit L dependence of Ω_L. The traditional single chain theories of polymer physics provide universal expression of Ω_L in terms of the polymer size, the environment being simply taken into account through the solvent quality and the swollen blob size in the semi-dilute (good solvent) case.

1.1.0.1 The case of mean field or ideal chains

The basic mean-field or ideal chain model for a L segments chain gives

$$\Omega_L^{id} = \left[C_1 z^L\right] \tag{1.14}$$

where z is the single monomer partition function and C_1 a dimensionless constant. Adapting eq.(1.11), one has

$$N(L) = \frac{C_1}{C'} \exp -(\beta E) \exp\left(-\mu" L\right) \tag{1.15}$$

where $\mu" = \mu' - \ln z$ must, according to eq. (1.12), be such that

$$\sum_L L \exp -(\mu" L) = \frac{1}{\mu"^2} = \frac{MC'}{C_1 \exp -(\beta E)} \tag{1.16}$$

while eq.(1.13) takes the form

$$\sum_L \exp -(\mu" L) = \frac{1}{\mu"} = \frac{MC'}{L_0 C_1 \exp -(\beta E)} \tag{1.17}$$

In eqs.(1.16) and (1.17), sums over L from 1 to ∞ have been approximated by the result of their continuous integral counterparts.

Combining eqs.(1.15), (1.16) and (1.17), one gets the final expression for the chain number densities

$$c_0(L) = \frac{\phi}{L_0^2} \exp\left(-\frac{L}{L_0}\right) \tag{1.18}$$

with the average polymer length given by

$$L_0 = B_1^{1/2} \phi^{\frac{1}{2}} \exp\left(\frac{\beta E}{2}\right). \tag{1.19}$$

where $B_1 = eb^3/C_1$ is a constant depending upon the monomer size b and the prefactor in the number of ideal chain configurations in eq.(1.14).

1.1.0.2 The case of dilute chains in good solvent

Polymer solutions are in a dilute regime when chains do not overlap and in semi-dilute regime when chains do strongly overlap while the total monomer volume fraction is still well below its melt value. In the semi-dilute regime in good solvent condition, chains remain swollen locally over some correlation length, known as the swollen blob size χ, but they are ideal over larger distances as a result of the screening of excluded volume interactions between blobs.

Specifically, for a given monomer number density ϕ, the blob size is given by the condition that the blob volume $\chi^3 = b^3 L^{*3\nu}$ is equal to the total volume V divided by the total number of blobs M/L^* in the swollen blob. This gives estimates in terms of the reduced number density $\phi' = b^3\phi$,

$$L^* = \phi'^{(\frac{1}{1-3\nu})} \tag{1.20}$$

$$\chi = b\phi'^{(\frac{\nu}{1-3\nu})} \tag{1.21}$$

where $\nu = 0.588$ in present good solvent conditions[8].

In living polymers characterized by a monomer number density ϕ and some averaged chain length L_0, the semi-dilute conditions correspond to the case $L_0 >> L^*$. We discuss in this subsection the theory for the dilute case where $L_0 << L^*$. We will come back to the semi-dilute case in the next subsection.

Self-avoiding walks statistics apply to dilute chains in good solvent, and we thus adopt the number of configurations[6, 7](See especially page 128 of the book of Grosberg and Khokhlov [7])

$$\Omega_L^{EV} = C_1 L^{(\gamma-1)} z^L \tag{1.22}$$

for a chain of size L, where γ is the (entropy related) universal exponent equal to 1.165, z is the single monomer partition function and C_1 a dimensionless constant.

Incorporating expression (1.22) in eq. (1.11), one gets

$$N(L) = \frac{V}{B_1} \exp -(\beta E) L^{(\gamma-1)} \exp -(\mu" L) \tag{1.23}$$

where B was introduced in eq.(1.19) and where $\mu" = \mu' - \ln z$ must be fixed by eq.(1.2)

$$\sum_L L^\gamma \exp -(\mu" L) = B_1 \phi \exp (\beta E) \tag{1.24}$$

while eq.(1.13) takes here the form

$$\sum_L L^{(\gamma-1)} \exp -(\mu" L) = \frac{B_1\phi}{L_0} \exp(\beta E) \tag{1.25}$$

If L is treated as a continuous variable, eqs (1.24) and (1.25) can be rewritten in terms of the Euler Gamma function satisfying $\Gamma(x) = x\Gamma(x-1)$ as

$$\int_0^\infty L^\gamma \exp -(\mu" L) dL = \frac{\Gamma(\gamma+1)}{\mu"^{(\gamma+1)}} = B_1\phi \exp(\beta E) \tag{1.26}$$

$$\int_0^\infty L^{(\gamma-1)} \exp -(\mu" L) dL = \frac{\Gamma(\gamma)}{\mu"^{\gamma}} = \frac{B_1\phi}{L_0} \exp(\beta E) \tag{1.27}$$

From eqs (1.26) and (1.27), one gets

$$\mu" = \frac{\gamma}{L_0} \tag{1.28}$$

$$B_1\phi \exp(\beta E) = \frac{\Gamma(\gamma+1)}{\gamma^{(\gamma+1)}} L_0^{(\gamma+1)} \tag{1.29}$$

These results lead then finally to the Schulz-Zimm distribution of chain lengths, namely

$$c_0(L) = \frac{\exp(-\beta E)}{B_1} L^{(\gamma-1)} \exp(-\gamma \frac{L}{L_0}) \tag{1.30}$$

and an average polymer length given by

$$L_0 = \left(\frac{\gamma^\gamma}{\Gamma(\gamma)}\right)^{\frac{1}{1+\gamma}} B_1^{\frac{1}{1+\gamma}} \phi^{\frac{1}{1+\gamma}} \exp\left(\frac{\beta E}{(1+\gamma)}\right). \tag{1.31}$$

1.1.0.3 The semi-dilute case

We consider here the semi-dilute case in good solvent where the average length of living polymers L_0 is much larger than the blob length L^*. The usual picture of a semi-dilute polymer solution is an assembly of ideal chains made of blobs of size χ. Using this approach, Cates and Candau [2] and later J.P. Wittmer et al [13] derived the relevant equilibrium polymer size distribution. In this subsection, we adapt their derivation to the theoretical framework presented above.

Let Ω_b be the number of internal configurations per blob and z' some coordination number for successive blobs. As there are $n_b = L/L^*$ blobs for a chain of L monomers, we write the total number of internal configurations of a chain of size L as

$$\Omega_L^{SD} = C_1 L^{*(\gamma-1)} \Omega_b^{L/L^*} z'^{L/L^*} \tag{1.32}$$

where γ is the universal exponent in the excluded volume chain statistics met earlier for chains in dilute solutions. The important factor $L^{*(\gamma-1)}$ can be seen as an entropy correction for chain ends just like E was an energy correction to $L\tilde{\epsilon}$. This entropic term which involves the number of monomers per blob, is needed to take into account that when a chain breaks, its two ends are subject to a reduced excluded volume repulsion. The other factors in eq. (1.32) will lead to terms linear in L after taking the logarithm and thus will be absorbed in the Lagrange multiplier definition, as seen earlier in similar cases for ideal and dilute chains. The resulting expression of $N(L)$ in terms of the Lagrange multiplier (cf. eq.(1.15)) can then be written by analogy as

$$N(L) = \frac{C_1}{C'} \exp - [\beta E - (\gamma - 1) \ln L^*] \exp(-\mu L) \tag{1.33}$$

Proceeding as in the ideal case (simply replacing at every step the constant βE by $\beta E - (\gamma - 1) \ln L^*$, one recovers in the semi-dilute case the simple exponential distribution

$$c_0(L) = \frac{\phi}{L_0^2} \exp(-\frac{L}{L_0}) \tag{1.34}$$

with a slightly different formula for the average polymer length

$$L_0 \propto \phi^\alpha \exp\left(\frac{\beta E}{2}\right) \tag{1.35}$$

where $\alpha = \frac{1}{2}(1 + \frac{\gamma-1}{3\nu-1})$ is about 0.6.

1.2 A kinetic model for scissions and recombinations

The interest for wormlike micelles dynamics came from the experimental observation that entangled flexible micelles often display, after an initial strain, a simple exponential stress relaxation. The mechanism of such relaxation is different from that of usual dead polymer entangled melts. In the latter system, stress relaxation requires that individual chains leave the strained topological tube created by the entangled temporary network by a reptation mechanism. A theoretical model, taking into account the extra relaxation mechanism caused by scissions and recombinations of micelles, leads [9] to an exponential decay of the shearing forces with a decay Maxwell time equal to $\tau \approx \sqrt{\tau_b \tau_{rep}}$ where τ_{rep} is the chain reptation time and τ_b is the mean life time of a chain of average size in the system.

We will assume in the following that the Cates's scission-recombination model governing the population dynamics, originally devised to explain entangled equilibrium polymer melt rheology, should also apply to the kinetically unentangled regime which is explored in the present work.

This Cates kinetic model [9] assumes that

- the scission of a chain is a unimolecular process, which occurs with equal probability per unit time and per unit length on all chains. The rate of this reaction is a constant k_s for each chemical bond, giving

$$\tau_b = \frac{1}{k_s L_0} \tag{1.36}$$

  for the lifetime of a chain of mean length L_0 before it breaks into two pieces.

- recombination is a bimolecular process, with a rate k_r which is identical for all chain ends, independently of the molecular weight of the two reacting species they belong to. It is assumed that recombination takes place with a new partner with respect to its previous dissociation as chain end spatial correlations are neglected within the present mean field theory approach. It results from detailed balance that the mean life time of a chain end is also equal to τ_b.

Let $c(t, L)$ be the number of chains per unit volume having a size L at time t. On the basis of the model, the following kinetic equations can be written [9]

$$\begin{aligned} \frac{dc(t,L)}{dt} &= -k_s L c(t,L) + 2k_s \int_L^\infty c(t,L')dL' \\ &+ \frac{k_r}{2}\int_0^L c(t,L')c(t,L-L')dL' - k_r c(t,L)\int_0^\infty c(t,L')dL' \end{aligned} \tag{1.37}$$

where the two first terms deal with chain scission (respectively disappearance or appearance of chains with length L) while the two latter terms deal with chain recombination (respectively provoking the appearance or disappearance of chains of length L).

It is remarkable that the static solution of this empirical kinetic model leads to an exponential distribution of chain lengths. Indeed, direct substitution of solution $c_0(L)$ in the above equation leads to the detailed balance condition:

$$\phi\frac{k_r}{2k_s} = L_0^2 \tag{1.38}$$

the ratio of the two kinetic constant being thus restricted by the thermodynamic state. Detailed balance means that for the equilibrium distribution $c_0(L)$, the number of scissions is equal to the number of recombinations per unit time and volume. The total number of scissions and recombinations per unit volume and per unit time, denoted respectively as n_s and n_r, can be expressed as

$$n_s = k_s \frac{\phi}{L_0^2} \int_0^\infty L \exp(-L/L_0) dL = k_s \phi \tag{1.39}$$

$$n_r = \frac{k_r}{2} \frac{\phi^2}{L_0^4} \int_0^\infty dL' \int_0^\infty dL" \exp(-\frac{L'}{L_0}) \exp(-\frac{L"}{L_0}) = \frac{\phi^2 k_r}{2L_0^2} \tag{1.40}$$

and it can be easily verified that detailed balance condition equation 1.38 implies $n_s = n_r$.

Mean field theory assumes that a polymer of length L will break on average after a time equal to $\tau_b = (k_s L)^{-1}$ according to a Poisson process. This implies that the distribution of first breaking times (equal to the survival times distribution) must be of the form

$$\Psi(t) \propto \exp(-\frac{t}{\tau_b}) \tag{1.41}$$

for a chain of average size. Detailed balance then requires that the same distribution represents the distribution of first recombination times for a chain end[2]. Accordingly, throughout the rest of this chapter, the symbol τ_b will represent as well the average time to break a polymer of average size or the average time between end chain recombinations. In the same spirit, we stress that among the different estimates of τ_b proposed in this work, some are based on analyzing the scission statistics while others are based on the recombination statistics.

Two additional points may be stressed at this stage:

- The mean field model in the present context has been questioned [12] because in many applications, there are indications that a newly created chain end often recombines after a short diffusive walk with its original partner. In that case, a possibly large number of breaking events are just not effective and the kinetics proceeds thus differently.

- Given the statistical mechanics analysis in the previous subsection, we see that the equilibrium distribution of chain lengths resulting from the simple empirical kinetic model is perfectly compatible with the equilibrium distribution in polymer

solutions at the θ point (ideal chains) or for semi-solutions (ideal chains of swollen blobs). The kinetic model is still pertinent, given its simplicity, in the case of dilute solutions in good solvent as the chain length distribution although non exponential, is not very far from it.

1.2.1 Macroscopic thermodynamic relaxation

In equation (1.35) the average length L_0 depends on the thermodynamic variables of the system such as the temperature, the pressure, and the volume fraction of monomers ϕ. Under a sudden change in one of the thermodynamic variables (for example, the temperature), the distribution of the length of the chains in equation (1.37) relaxes to a new equilibrium exponential distribution characterized by a new average length L_∞. The corresponding theory of macroscopic thermodynamic relaxation has been given by Marques and Cates [27] and tested using a Monte Carlo study by Michev and Rouault [46]. This is in general a complicated, nonlinear decay which can be monitored experimentally by light scattering which probes the evolution of the average length. The theory is based on the equations of distribution of length of chain (1.34) and the kinetic model of Cates [9] i.e. equation (1.37). The characteristic time provides information about the kinetics of the system.

Marques and Cates [27] show that for any amplitude of the perturbation which conserves the total volume fraction of monomers (for instance, a temperature modification having an arbitrary time-dependence), the distribution function $c(t, L)$ of equation (1.37) remains exponential versus L. Indeed, they show that

$$c(t, L) = \phi f^2(t) \exp\{-Lf(t)\} \tag{1.42}$$

is a non-linear eigenfunction of equation (1.37) with a eigenvalue $f(t)$ that obeys

$$\frac{df}{dt} = k_s \left[1 - \frac{\phi k_r}{2k_s} f^2(t)\right], \tag{1.43}$$

where k_r and k_s the kinetic constants of the new equilibrium state, after, e.g. a T-jump. The time evolution of $f(t)$ for a thermodynamic jump is then the solution of (1.43) with the initial condition $f(t = 0) = 1/L_0$. One obtains [27]:

$$f(t) = L_\infty^{-1} \tanh\left(\frac{t + t_0}{2\tau}\right) \texttt{ if } L_0 > L_\infty \tag{1.44}$$

$$f(t) = L_\infty^{-1} \coth\left(\frac{t + t_0}{2\tau}\right) \texttt{ if } L_0 < L_\infty \tag{1.45}$$

where the constant t_0 is given by

$$t_0 = 2\tau \tanh\left(\frac{L_\infty}{L_0}\right) \text{ if } L_0 > L_\infty \tag{1.46}$$

$$t_0 = 2\tau \coth\left(\frac{L_\infty}{L_0}\right) \text{ if } L_0 < L_\infty, \tag{1.47}$$

and the time

$$\tau = \frac{1}{2k_s L_\infty} \tag{1.48}$$

These equations describe the recovery of $c(t, L)$ and $\langle L(t)\rangle$ the average chain length, following a sudden change in temperature which is given by

$$\langle L(t)\rangle = \frac{1}{f(t)} \tag{1.49}$$

We see that by measuring the non-equilibrium τ the relaxation time of the mean chain length, one can get an estimate of the microscopic scission rate constant k_s.

1.3 Linear viscoelasticity of unentangled micelles

To describe the dynamics of cylindrical micelles in solution, each micelle can be modelled as a linear collection of L identical fragments (L being proportional to the length of the micelle), subject to Brownian motion to represent the dynamical effect of the bath (the coupling to the rest of the degrees of freedom), subject to connecting forces between adjacent fragments to enforce the linear structure of the micelle and possibly subject to pair interactions between non connected fragment pairs. If, as the relative distance between adjacent fragments increases, the connecting tension force is not bounded to a finite value to allow an intrinsic possibility of scission (e.g. the FENE-C model of Kroger[17]), the scission and recombination processes must be incorporated independently in the model. The latter must specify the way through which individual bonds can break (chain scission) or reform (chain end recombinations) by a pair potential swap for the involved pair of fragments. The micelle dynamics thus needs to combine all these various ingredients, implying that individual chain entities will survive for a finite life time during which ordinary polymer relaxation takes place.

Within a theoretical approach of the dynamical properties of micellar solutions where the emphasis lies in the search for analytical predictions, it is useful to explore the validity of the traditional Rouse model to represent the "dead polymer" dynamics

part (valid as long as an entity survives), when it can be assumed that excluded volume and entanglement effects are absent or weak. In the present purely theoretical discussion, we thus restrict ourselves to the unentangled dynamics of θ solvent chains. We briefly review the basic ingredients and essential results of the Rouse model for "dead chains", including linear viscoelasticity and we report the extension of this theory to polymer chains when they are the object of scissions and recombinations, along the lines proposed by Faivre and Gardissat [36].

1.3.1 The Rouse model

The Rouse model treats all chains as being independent. Consider a "dead chain" of N elements at temperature T, where each fragment is subject to a friction force proportional to its instantaneous velocity with friction coefficient ξ and to a random force modelled as a 3D white noise stochastic process whose statistical properties are given by the fluctuation-dissipation theorem in terms of T and ξ. The only interactions considered in the Rouse model are harmonic spring forces with spring constant k between neighboring beads to ensure the linear connectivity. Under this dynamics, the average squared distance between adjacent monomers defines a typical mean distance b given by $b^2 = 3k_BT/k$, where k_B is the Boltzmann constant. The mean squared end-to-end distance is simply $(N-1)b^2$.

Chain dynamics considered via the end-to-end vector time relaxation function leads at long times to an exponential decay with the main (Rouse) relaxation time

$$\tau_R = \tau_0 N^2 \tag{1.50}$$

where $\tau_0 = \frac{\xi b^2}{3k_BT\pi^2}$, indicating that the global relaxation time of a chain of size N is proportional to N^2.

The way to derive this important result requires the introduction of modes (Rouse modes), defined as

$$\bar{X}_q(t) = \frac{1}{N}\sum_{j=1}^{N} A_{qj}\bar{R}_j(t); q = 0, 1, 2, \cdots (N-1) \tag{1.51}$$

where $\bar{R}_j$ is the coordinate of the j^{th} monomer in a chain and $\bar{\bar{A}}$ a square matrix with elements

$$A_{qj} = \cos\left[\frac{q\pi}{N}(j-\frac{1}{2})\right]; q = 0, 1, 2, \cdots (N-1); j = 1, 2, \cdots N \tag{1.52}$$

According to this definition, the mode $q = 0$ represents the center of mass diffusive motion, while the other (N-1) modes $q > 0$ are associated to the collective motion of sub-chains of size N/q. The time autocorrelation of these internal chain modes are

$$< \bar{X}_q(t)\bar{X}_q(0) >=< X_q^2 > \exp\left(-\frac{t}{\tau_q}\right) \tag{1.53}$$

where

$$\tau_q = \frac{\xi b^2}{3k_B T\pi^2}\left(\frac{N}{q}\right)^2 \tag{1.54}$$

which shows that the Rouse time is the relaxation time associated to the mode $q = 1$, while the relaxation time of higher index modes decreases as $1/q^2$. For completeness, the mode amplitudes are given by

$$< X_q^2 >= \frac{Nb^2}{2\pi^2}\frac{1}{q^2} \tag{1.55}$$

Rouse theory leads to an expression of the time autocorrelation of the chain end-to-end vector $\bar{S} = \bar{R}_N - \bar{R}_1$

$$< \bar{S}(t).\bar{S}(0) >= (N-1)b^2\frac{\sum_q' \tau_q \exp\left(-t/\tau_q\right)}{\sum_q' \tau_q} \tag{1.56}$$

where the prime in the sums means that the latter only involves the odd q mode indices. This result shows a typical Rouse theory relaxation function: it is a sum of terms implying the different mode relaxation, which explains that at long times, only the slowest mode survives and the behavior of the time autocorrelation becomes exponential with characteristic time τ_R.

1.3.2 The Rouse model implications on the viscous response of a monodisperse polymer solution

We now discuss the intrinsic shear modulus $G(t)$ of a monodisperse polymer solution which reflects the viscoelastic response of the system in the linear regime (limit of very small shear rates). The Newtonian shear viscosity is related to the shear modulus through

$$\eta_0 = \int_0^\infty G(t)dt \tag{1.57}$$

Rouse theory for a monodisperse solution of "dead" polymers of size N at monomer number density ϕ gives [48]

$$G(t) = \frac{\phi}{N}k_B T\sum_{q=1}^{N-1}\exp(-2t/\tau_q) = \frac{\phi}{N}k_B T\sum_{q=1}^{N-1}\exp(-2tq^2/\tau_R) \tag{1.58}$$

This important result indicates that, because of the independence of the dynamics of the various chains in the system, Rouse theory gives for a collective and intensive quantity like $G(t)$ an expression which is proportional to the solute concentration while its viscoelastic behavior is strictly identical to the single chain viscoelastic relaxation process. Therefore, the shear modulus again appears as a sum of terms expressing the specific contributions of the various single chain modes in the relaxation process, with at long times, a simple exponential time decay with characteristic time τ_R. By time integration, according to eq.(1.57), the shear viscosity is then given (for $N >> 1$) by

$$\eta_0 = \frac{\pi^2}{12}\frac{\phi k_B T}{N}\tau_R \tag{1.59}$$

where τ_R is given in eq. (1.50).

1.3.3 The theory of Faivre and Gardissat and the viscoelasticity of micelles

The above subsection is dealing with a monodisperse dilute solution of "dead" chains. The stress relaxation function of a micellar system is in reality the object of a coupling between the stress relaxation and the scission-recombination process if the time scale of the second process is shorter than the viscoelastic times scales. In our work, we adapt the theory proposed by Faivre and Gardissat [36], originally developed to interpret rheological data of liquid selenium. Faivre and Gardissat [36] proposed a modification of the standard Rouse theory of linear viscosity of a polydisperse polymer system [8] to incorporate the influence of the scission events.

If we have a polydisperse system of polymers with normalized weight function W_p, the relaxation modulus given by the Rouse model should be given by

$$G(t) = \sum_{p=1}^{\infty} W_p G_p(t) \tag{1.60}$$

where $G_p(t)$ concerns the "polymer" part of chain of size p which, within the Rouse model, reads (see eq.(1.58))

$$G_p(t) = G_0 \frac{1}{p} \sum_{q=1}^{p} \exp\left[-2\frac{t}{\tau_0}\left(\frac{q}{p}\right)^2\right], \tag{1.61}$$

where p is the polymerization degree, $G_0 = \phi k_B T$ a material constant, and τ_0 the local dynamic relaxation time which depends on the solvent viscosity. Notice that for

physical reasons we have $q \leq p$ in the sum of Rouse modes for any upper limit p. As mentioned earlier, the stress relaxation is a superposition of exponentials, each term corresponds to the contribution to the relaxation of a particular Rouse mode. All terms have the same amplitude but decay with a characteristic time

$$\tau_q^p = \tau_0 \frac{p^2}{q^2} \tag{1.62}$$

which depends on the p/q ratio which is the number of monomers per wave length for that particular mode. If bond scission occurs independently and uniformly along the chain with rate k_s (per unit time and per bond), the lifetime of a chain of p/q monomers should be

$$\tau_b = \frac{q}{k_s p} \quad . \tag{1.63}$$

The Rouse mode q in the original chain of length p should therefore have a survival probability which decays in time as $\exp(-k_s(p/q)t)$, hence the idea of multiplying the contribution of each mode to the relaxation of $G(t)$ by this survival probability to take into account the effect of bond scissions. This leads to the expression

$$G_p'(t) = G_0 \frac{1}{p} \sum_{q=1}^{p} \exp\left[-k_s \frac{p}{q} t - 2\frac{t}{\tau_0}\left(\frac{q}{p}\right)^2\right]. \tag{1.64}$$

When the life time τ_b of the chain of average size is shorter than the internal Rouse relaxation time of the same chain $\tau_0 L_0^2$, the viscoelastic response is independent of the mean chain length L_0 but depends upon a new intrinsic time τ_Λ which corresponds to the relaxation of a dynamical unit of size Λ defined by the equality of the Rouse relaxation time $\tau_0 \Lambda^2$ and the life time, $(k_s \Lambda)^{-1}$:

$$\tau_0 \Lambda^2 = (k_s \Lambda)^{-1} \quad . \tag{1.65}$$

It leads to

$$\Lambda = (\tau_0 k_s)^{-1/3} \tag{1.66}$$

and

$$\tau_\Lambda = \tau_0^{1/3} k_s^{-2/3} \tag{1.67}$$

so that equation (1.64) can be rewritten as

$$G_p'(t) = G_0 \frac{1}{p} \sum_{q=1}^{p} \exp\left(-\frac{t}{\tau_\Lambda}\left[\frac{p}{q\Lambda} + 2\left(\frac{q\Lambda}{p}\right)^2\right]\right). \tag{1.68}$$

Identifying the number of Rouse beads with the number of beads in present work, using a known distribution of lengths of the chains of our system (1.18), the weight function for our equilibrium polymers is

$$W_p = \frac{1}{L_0} \exp\left(-\frac{p}{L_0}\right). \tag{1.69}$$

So that $G(t)$ for the equilibrium polymers is now given by

$$G(t) = \sum_{p=1}^{\infty} W_p G_p'(t). \tag{1.70}$$

Note that this expression differs slightly from the Faivre and Gardissat final expression as apparently, in equation (18) of reference [36], they assume a relaxation time for a segment of p monomers to be half of the usual Rouse time. (Note also that in their paper, the symbol τ_0 corresponds to half the time τ_0 used in our work).

Chapter 2

The mesoscopic model of worm-like micelles

The main goal our thesis is to exploit simulation techniques to improve our understanding of the link between the macroscopic behavior and microscopic aspects of the structure and the dynamics of self-assembling micellar systems at equilibrium and under shear flow. As it is pragmatically impossible to reach large enough scales of length and time to determine those macroscopic properties using an atomistic level molecular dynamics simulation approach, we adopt a mesoscopic model and a Langevin Dynamics approach as done regularly in the studies on micellar systems. As sketched in figure 1, micelles can be represented as linear sequences of Brownian beads which, in addition to their usual Langevin Dynamics space-time evolution, can either fuse together to form longer structures or break down into two pieces. The kinetics can be modelled by a microscopic kinetic Monte-Carlo algorithm which generates new bonds between chain ends adjacent in space or which breaks existing bonds between adjacent monomers. The free energy E to creat this new end caps for these micelles becomes an energy penalty for scission events, i.e., the creation of two unsaturated chain ends. This scission energy determines the static propeties and influences the scission and recombination rates, k_s and k_r. In this model, the scission energy E of micelles is controlled by a scission energy parameter W which is defined as an additive potential term which influences the switching probability between bonded and unbounded potentials. The barrier energy of recombination B also influences the kinetic rate constants. The advantage of our model is that the dynamical barrier height B can be taken into account by means of the attempt frequency ω associated to the Monte Carlo potential swap. If ω is small,

successive breakage and recombination events for a given chain can be assumed to be uncorrelated and the recombination of newly created chain ends will be of standard mean-field type. On the other hand, the (return) probability that two newly created chain ends recombine immediately must be particulary important at large ω. These highly correlated "diffusion controlled" [12] recombination events do not contribute do the effective macroscopic reaction rates which determine the dynamics of the system.

The mesoscopic model is based on a standard polymer model with repulsive Lennard-Jones interactions between all monomer pairs and an attractive FENE (finitely extensible nolinear elastic) potential [24] to enforce (linear) connectivity. For the scission and recombination events, a Monte Carlo procedure is set up to switch back and forth between the bounded potential and the unbounded potential. This new model is thus at the same time justified by its link with a standard polymer model and by the advantage that the scission/recombination attempt frequency is a control parameter governing dynamics, without affecting the thermodynamic and structural properties of the system.

2.1 The potential [19]

We consider a set of micelles consisting of (non-cyclic) linear assemblies of Brownian particles. Within such a linear assembly, the bond potential $U_1(r)$ acting between adjacent particles is expressed as the sum of a repulsive Lennard-Jones (shifted and truncated at its minimum) and an attractive part of the FENE type [24]. The pair potential $U_2(r)$ governing the interactions between any unbounded pair (both intramicellar and intermicellar) is a pure repulsive potential corresponding to a simple Lennard-Jones potential shifted and truncated at its minimum. This choice of effective interactions between monomers implies good solvent conditions.

Using the Heaviside function $\Theta(x) = 0$ or 1 for $x < 0$ or $x \geq 0$ respectively, explicit expressions (see figure 2.1) are

$$U_2(r) = 4\epsilon \left[(\frac{\sigma}{r})^{12} - (\frac{\sigma}{r})^6 + \frac{1}{4} \right] \Theta(2^{1/6}\sigma - r)) \tag{2.1}$$

$$U_1(r) = U_2(r) - 0.5kR^2 \ln\left(1 - [\frac{r}{R}]^2\right) - U_{min} - W \tag{2.2}$$

In the second expression valid for $r < R$, $k = 30\epsilon/\sigma^2$ is the spring constant and $R = 1.5\sigma$ is the value at which the FENE potential diverges. U_{min} is the minimum value of the sum of the two first terms of the second expression (occurring at $r_{min} =$

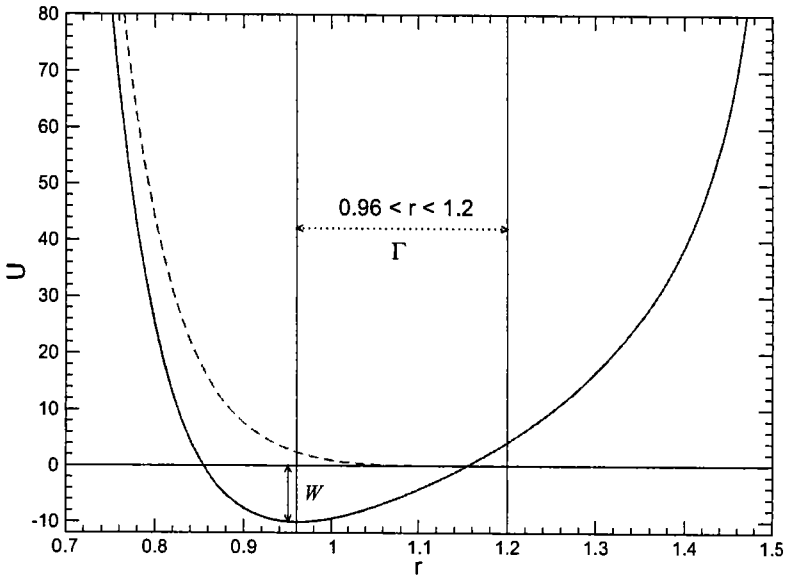

Figure 2.1: Bounded potential $U_1(r)$ (continuous curve) and unbounded potential $U_2(r)$ (dashed line) between a pair of monomers. W is a parameter tuning the energy required to open the bond. The figure also shows the Γ region where potential swaps (corresponding to bond scissions or bond recombinations) are allowed during the Brownian dynamics simulation. The unit of length is σ, and for the energy is ϵ.

0.96094σ for the adopted parameters) while W is a key parameter which corresponds to the typical energy gain (loss) when an unbounded (bounded) pair is the object of a recombination (scission).

2.2 The Langevin Dynamics

The Langevin equation describes the Brownian motion of a set of interacting particles. The action of the fluid is split into a slowly evolving viscous force and a rapidly fluctuating random force. For a free particle in one dimension the equation is expressed as

$$m_i \dot{\bar{v}}_i(t) = -\xi \bar{v}(t)_i + \bar{F}_i(t) + \bar{R}_i(t) \tag{2.3}$$

where $barv_i$ is the velocity of particle i with mass m_i at time t, $\bar{F}_i$ the systematic force, ξ the friction coefficient, and $\bar{R}_i$ represents the sum of the forces due to the incessant collision of the fluid molecules. It is regarded as a stochastic force and is satisfying the

condition (fluctuation-dissipation theorem) [47]:

$$< R_{i\alpha}(t)R_{j\beta}(t') >= 2\xi k_B T\delta_{ij}\delta_{\alpha\beta}\delta(t-t') \tag{2.4}$$

where the greek-letter subscripts $\alpha\beta$ refer to the x, y or z components.

2.2.0.1 Brownian Dynamics (BD)

If we assume that the time scales for momentum relaxation and position relaxation are well separated, then it is possible to consider only time intervals longer than the momentum relaxation times. In the diffusive regime the momentum of the particles has relaxed and equation (2.3) can be modified by setting to zero the momentum variation (left hand side of equation (2.4)). Then the "position Langevin equation" is given as

$$\frac{d\bar{r}_i}{dt} = \frac{\bar{F}_i(t)}{\xi} + \frac{\bar{R}_i(t)}{\xi} \tag{2.5}$$

Earlier simulations within the present work were executed using an algorithm based on (2.5) [25]. The single BD step of particle i subject to a total force $\overline{F}_i$ is simply

$$\bar{r}_i(t+\Delta t) = \bar{r}_i(t) + \frac{\bar{F}_i}{\xi}\Delta t + \bar{\Delta}_i(\Delta t) \tag{2.6}$$

where the last term given by

$$\bar{\Delta}_i(\Delta t) = \int_t^{t+\Delta t} \bar{R}_i(t')dt'/\xi \tag{2.7}$$

corresponds to a vectorial random Gaussian quantity with first and second moments given by

$$< \Delta_{i\alpha}(\Delta t) > = 0 \tag{2.8}$$

$$< \Delta_{i\alpha\beta}(\Delta t)\Delta_{j\beta}(\Delta t) > = 2(\frac{k_B T}{\xi})\Delta t\delta_{\alpha\beta}\delta_{ij} \tag{2.9}$$

for arbitrary particles i and j and where $\alpha\beta$ stand for the x, y, z Cartesian components.

At this stage, it is useful to fix units. In the following, we will adopt the size of the monomer σ as unit of length, the ϵ parameter as energy unit and we will adopt $\xi\sigma^2/(3\pi\epsilon)$ as time unit. We also introduce the reduced temperature $k_B T/\epsilon = T^*$, so that in reduced coordinates (written here with symbol*) the random displacement $\Delta^*_{i\alpha}$ is

$$< \Delta^*_{i\alpha} > = 0 \tag{2.10}$$

$$< \Delta^*_{i\alpha}\Delta^*_{j\beta} > = \frac{2}{3\pi}\Delta t^*\delta_{\alpha\beta}\delta_{ij}\, T^* \tag{2.11}$$

which means that each particle, if isolated in the solvent, would diffuse with a RMSD of $\sqrt{2T^*/\pi}$ per unit of time. In the following, all quantities will be expressed in reduced coordinates without the $*$ symbol.

2.2.0.2 Langevin Dynamics velocity Verlet scheme

Most of the simulation of the present work are performed using Langevin Dynamics (LD) velocity Verlet algorithmes based on the work of [50]. The explict expressions are

$$\bar{r}_i(t+\Delta t) = \bar{r}_i(t) + c_1\bar{v}_i(t)\Delta t + c_2\frac{\bar{F}_i(t)}{m}\Delta t^2 + \delta\bar{r}_i^G \tag{2.12}$$

$$\bar{v}_{i(1/2)} = c_0\bar{v}_i(t) + \left(\frac{c_0c_2}{c_1}\right)\frac{\bar{F}_i(t)}{m}\Delta t + \delta\bar{v}_i^G \tag{2.13}$$

$$\bar{v}_i(t+\Delta t) = \bar{v}_{i(1/2)} + \frac{1}{(\gamma\Delta t)}\left(1-\frac{c_0}{c_1}\right)\frac{\bar{F}_i(t+\Delta t)}{m}\Delta t \tag{2.14}$$

where the first equation updates the position, the second equation updates the "half" step velocities and the third equation completes the velocity move. $\gamma = \xi/m$, the coefficients for the above equations are:

$$c_0 = e^{-\gamma\Delta t} \tag{2.15}$$

$$c_1 = (\gamma\Delta t)^{-1}(1-c_0) \tag{2.16}$$

$$c_2 = (\gamma\Delta t)^{-1}(1-c_1) \tag{2.17}$$

$$c_3 = (\gamma\Delta t)^{-1}\left(\frac{1}{2}-c_1\right) \tag{2.18}$$

where $e^{\gamma\Delta t}$ is approximated by its power expansion for $\gamma\Delta t < 1$. Each pair of vectorial component of $\delta\mathbf{r}^G$, $\delta\mathbf{v}^G$, i.e. $\delta r_{i\alpha}^G$, $\delta v_{i\alpha}^G$ is sampled from a bivariate Gaussian distribution[49] defined as

$$\rho\left(\delta r_{i\alpha}^G, \delta v_{i\alpha}^G\right) = \frac{1}{2\pi\sigma_r\sigma_v\left(1-c_{rv}^2\right)^{1/2}} \times \exp\left\{-\frac{1}{2\left(1-c_{rv}^2\right)}\left(\left(\frac{\delta r_{i\alpha}^G}{\sigma_r}\right)^2 + \left(\frac{\delta v_{i\alpha}^G}{\sigma_v}\right)^2 - 2c_{rv}\left(\frac{\delta r_{i\alpha}^G}{\sigma_r}\right)\left(\frac{\delta v_{i\alpha}^G}{\sigma_v}\right)\right)\right\} \tag{2.19}$$

with zero mean values, variances given by

$$\sigma_r^2 = \left\langle\left(\delta r_{i\alpha}^G\right)^2\right\rangle = \Delta t^2\frac{k_BT}{m}(\gamma\Delta t)^{-1}\left(2-(\gamma\Delta t)^{-1}\left(3-4e^{-\gamma\Delta t}+e^{-2\gamma\Delta t}\right)\right) \tag{2.20}$$

$$\sigma_v^2 = \left\langle\left(\delta v_{i\alpha}^G\right)^2\right\rangle = \frac{k_BT}{m}\left(1-e^{-2\gamma\Delta t}\right) \tag{2.21}$$

and the correlation coefficient c_{rv} determined by

$$c_{rv} = \left\langle \delta r_{i\alpha}^G \delta v_{i\alpha}^G \right\rangle = \Delta t \frac{k_B T}{m} (\gamma \Delta t)^{-1} \left(1 - e^{-\xi \Delta t}\right)^2 \frac{1}{\sigma_r \sigma_v} \tag{2.22}$$

Each pair of cartesian components $\delta r_{i\alpha}^G$ and $\delta v_{i\alpha}^G$ are obtained by the appropriate Gaussian distribution according to:

$$\delta r_{i\alpha} = \sigma_r \eta_1 \tag{2.23}$$

$$\delta v_{i\alpha} = \sigma_v \left(c_{rv}\eta_1 + \eta_2 \left(\sqrt{1 - c_{rv}^2}\right)\right) \tag{2.24}$$

where η_1 and η_2 are two independent random numbers with Gaussian distribution of zero average and unit variance.

2.2.1 Nonequilibrium LD technique

In this sub-section we briefly present the technique adopted for imposing the shear flow onto the system. We limit the study to a stationary, isovolumic and homogeneous planar Couette flow characterized by a velocity field $\bar{u}(r) = \bar{\bar{k}}^T r$ as illustrated in figure 2.2, where the velocity gradient $\bar{\bar{k}}$ is constant in space and time.

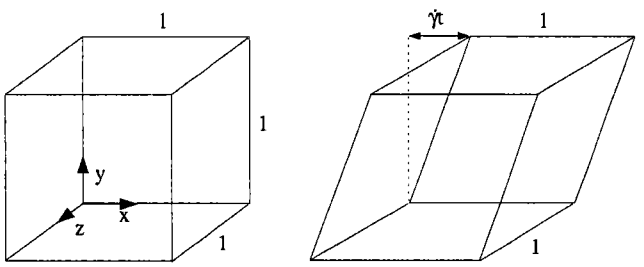

Figure 2.2: Sketch of planar Couette flow.

For a planar Couette flow in the x direction with a shear along the y axis, the velocity gradient k is defined as

$$\bar{\bar{k}} = \begin{vmatrix} 0 & 0 & 0 \\ \dot{\gamma} & 0 & 0 \\ 0 & 0 & 0 \end{vmatrix}$$

where $\dot{\gamma}$ is shear rate. With the imposition of the solvent velocity field, the equation of motion becomes

$$m_i \dot{\bar{v}}_i(t) = -m\xi_i \left(\bar{v}_i(t) - \bar{u}\left(r_i\right)\right) + \bar{F}_i(t) + \bar{R}_i(t) \tag{2.25}$$

A modification of the periodic boundary conditions proposed by [51] has been adopted

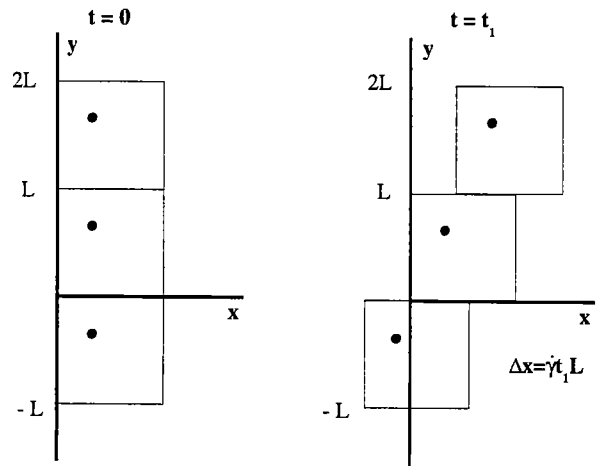

Figure 2.3: Sketch of shear boundary conditions for planar Couette flow.

for establishing the shear flow. The scheme used is shown in figure 2.3. In essence, the infinite periodic system is subjected to a uniform shear in xy plane. The box above is moving at a speed $\dot{\gamma}L$ in the positive x direction. The box below moves at a speed $\dot{\gamma}L$ in the negative x direction. When a particle in the primary box with coordinates (x, y) crosses a horizontal border one of its images enters from the opposite side at $x' = x - \dot{\gamma}tL_y$ with velocity $v' = v - \dot{\gamma}L_y$

2.3 Monte-Carlo procedure

The bonding network is itself the object of random instantaneous changes provided by a Monte-Carlo (MC) algorithm [19] which is built according to the standard Metropolis scheme [49].

The probability $P_{m,n}$ to go from a bounding network m to a different one n is written as

$$P_{m,n} = A^{trial}_{m,n} P^{acc}_{m,n} \tag{2.26}$$

where $A^{trial}_{m,n}$ is the trial probability to reach a new bounding network n starting from the old one m, within a single MC step. This trial probability is chosen here to be symmetric as usually adopted in Metropolis Monte Carlo schemes, and is chosen to be

different from zero only if both bounding networks n and m differ by the status of a single bond, say the pair of monomers (ij). To satisfy microreversibilty, the acceptance probability $P^{acc}_{m,n}$ for the trial $(m \longrightarrow n)$ must be given by

$$P^{acc}_{m,n} = Min[1, \exp(-\frac{(U(\{r\},n) - U(\{r\},m))}{k_B T})]. \tag{2.27}$$

In the present case, as a single pair (ij) changes its status, the acceptance probability takes the explicit form

$$P^{acc}_{m,n} = Min[1, \exp(-\frac{(U_2(r_{ij}) - U_1(r_{ij}))}{k_B T})] \tag{2.28}$$

$$P^{acc}_{m,n} = Min[1, \exp(-\frac{(U_1(r_{ij}) - U_2(r_{ij}))}{k_B T})] \tag{2.29}$$

for bond scission and bond recombination respectively.

The way to specify the trial matrix $A^{trial}_{m,n}$ starts by defining a range of distances, called Γ and defined by $0.96 < r < 1.20$ within the range $r < R$. For $r \in \Gamma$, a change of bounding is allowed as long as the two restricting rules stated above are respected. Consider the particular configuration illustrated by figure 2.4 where M=7 monomers located at the shown positions, are characterized by a connecting scheme made explicit by representing a bounding potential by a continuous line. The dashed line between monomers 5 and 6 represents the changing pair with distance $r \in \Gamma$ which is a bond $U_1(r)$ in configuration m but is just an ordinary intermolecular pair $U_2(r)$ in configuration n.

For further purposes, we have also indicated in figure 2.4 by a dotted line all pairs with $r \in \Gamma$ which are potentially able to undergo a change from a non bounded state to a bounded one in the case where the (56) pair, on which we focus, is non bounded (state n). Note that the bond (35) is not represented by a dotted line eventhough the distance is within the Γ range: a bond formation in that case is not allowed as it would lead to a cyclic conformation. Note also that in state n, monomer 5 could thus form bonds either with monomer 2 or with monomer 6 while monomer 6 can only form a bond with monomer 5.

We now state the algorithm and come back later on the special $(m \longrightarrow n)$ transition illustrated in figure 2.4.

During the LD dynamics, with an attempt frequency ω per arm and per unit of time, a change of the chosen arm status (bounded $U_1(r)$ to unbounded $U_2(r)$ or unbounded

to bounded) is tried. If it is accepted as a "trial move" of the bounding network, it obviously implies the modification of the status of a paired arm belonging to another monomer situated at a distance $r \in \Gamma$ from the monomer chosen in the first place.

The trial move goes as follows: a particular arm is chosen, say arm 1 of monomer i, and one first checks whether this arm is engaged in a bounding pair or not.

- If the selected arm is bounded to another arm (say arm 2 of monomer j) and the distance between the two monomers lies within the interval $r_{ij} \in \Gamma$, an opening is attempted with a probability $1/(N_i + 1)$, where the integer N_i represents the number of monomers available for bonding with monomer i, besides the monomer j (N_i is thus the number of monomers with at least one free arm whose distance to the monomer carrying the originally selected arm i lies within the interval Γ, excluding from counting the monomer j and any particular arm leading to a ring closure). If the trial change consisting in opening the (ij) pair is refused (either because the distance is not within the Γ range or because the opening attempt has failed in the case $N_i > 0$), the MC step is stopped without bonding network change (This implies that the LD restarts with the (ij) pair being bonded as before).

- If the selected arm (again arm 1 of monomer i) is free from bonding, a search is made to detect all monomers with at least one arm free which lie in the "reactive" distance range $r \in \Gamma$ from the selected monomer i (Note that if monomer i is a terminal monomer of a chain, one needs to eliminate from the list if needed, the other terminal monomer of the same chain in order to avoid cyclic micelles configurations). Among the monomers of this "reactive" neighbour list, one monomer is then selected at random with equal probability to provide an explicit trial bonding attempt between monomer i and the particular monomer chosen from the list. Note that if the list is empty, it means that the trial attempt to create a new bond involving arm 1 of monomer i has failed and no change in the bonding network will take place.

In both cases, if a trial change is proposed, it will be accepted with the probability $P^{acc}_{m,n}$ defined earlier. If the change is accepted, LD will be pursued with the new bonding scheme (state n) while if the trial move is finally rejected, LD restarts with the original bonding scheme corresponding to state m.

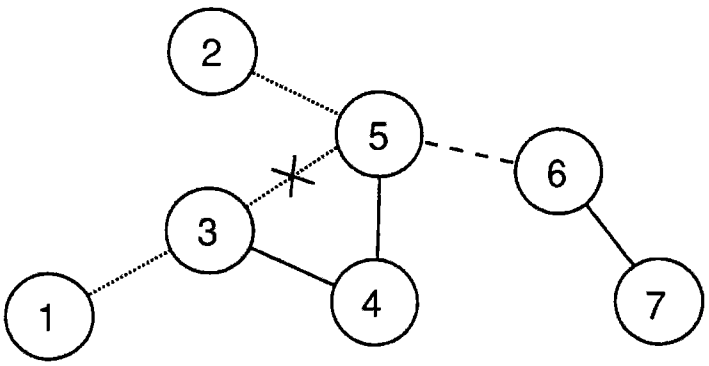

Figure 2.4: Exemplary configuration of a 7 monomers system in state n where monomers 3,4 and 5 form a trimer and monomers 6 and 7 a dimer. All pairs of monomers with mutual distances within the Γ region are indicated by a dotted or a dashed line. In the text, we consider the Monte Carlo scheme for transitions between states n and m which only differ by the fact that in state n and m the 5-6 pair is respectively open or bounded. The n $\rightarrow$ m transition corresponds to the creation of a pentamer by connecting a dimer and a trimer while the m $\rightarrow$ n transition leads to the opposite scission. The cross symbol on link 3-5 indicates that in state n, when looking to all monomers which could form a new link with monomer 5, monomer 3 is excluded because it would lead to a cyclic polymer which is not allowed within the present model.

Coming back to figure 2.4, we now show that the MC algorithm mentioned above garantees that the matrix A_{mn}^{trial} is symmetric, an important issue as it leads to the micro-reversibility property when combined with the acceptance probabilities described earlier. Let us define as $P_{arm} = 1/2N$ the probability to select a particular arm, a uniform quantity.

If configuration m with pair (56) being "bounded" is taken as the starting configuration, the number of available arms to form alternative bonds with monomer 5 and monomer 6 are respectively $N_5 = 1$ and $N_6 = 0$. Therefore, applying the MC rules described above, the probability to get configuration n where the pair (56) has to be unbounded is given by the sum of probabilities to arrive at this situation through selection of the arm of monomer 5 engaged in the bond with monomer 6 or through selection of the arm of monomer 6 engaged in a bond with monomer 5. This gives

$$A_{m,n}^{trial} = P_{arm} * \frac{1}{N_5 + 1} + P_{arm} \frac{1}{N_6 + 1} = \frac{3}{2} * P_{arm} \tag{2.30}$$

If configuration n with pair (56) being "unbounded" is taken as the starting configuration, the application of the MC rules lead to the probability to get configuration m

where the pair (56) has to be bounded is given by the sum of probabilities to arrive at this situation through selection of the free arm of monomer 5 (which has two bounding possibilities, namely with monomers 2 and 6) or through selection of the free arm of monomer 6 which can only form a bond with monomer 5. This gives

$$A_{n,m}^{trial} = P_{arm} * \frac{1}{2} + P_{arm} = \frac{3}{2} * P_{arm} \tag{2.31}$$

showing the required matrix symmetry.

Chapter 3

Equilibrium Properties

We have exploited the model introduced in chapter II in a series of Langevin Dynamics (LD) simulations at equilibrium with different bonding energy parameter W and different number density ϕ, and hence, in this chapter, we will present the resulting equilibrium static and dynamic properties of cylindrical micelles.

Within the static properties, the theoretical prediction of the chain size distribution has been given by Cates [2] and tested in great detail by Monte Carlo simulation by Wittmer *et al.* [13, 52] who also investigated conformational properties of chains at equilibrium. For static properties, our aim is thus mainly to check that our results on a different model are compatible with the analysis of the previous works [13, 52].

The two main parameters governing the static properties are the monomer density ϕ and the end cap energy E. Our choice of these two parameters is set up with the aim to simulate three thermodynamic states corresponding to a dilute solution and two semi-dilute solutions at the same ϕ but different E, leading to the system with two average chain lengths ~ 56 and ~ 150.

For static properties, the distribution of chain lengths, the gyration radius, and the end-to-end distance versus chain length will be analyzed and compared with previous studies. We have also investigated $g_{ee}(r)$ the pair correlation function of end monomers and $P(r)$ the distribution of bond lengths which are quantitative pertinent in the microscopic formulation of the kinetic rate constants.

The dynamic properties of the micelles which are given and interpreted in this chapter form the core of the work. The detailed trajectory of diffusing micelles which are continuously breaking and recombing allows us to analyze the microscopic origin of rate constants in terms of structural features (e.g. chain end pair correlation function)

and dynamic quantities to be related to the statistics of life times of a newly created chain end. For the latter, we show that the Poisson statistics dominates at long times while a fraction of correlated recombinations happen at short times. Exploiting these microscopic features, we characterize the macroscopic scission energy E and the barrier of recombination B and estimate their values for various state points investigated.

Some macroscopic dynamic properties are then studied with an accent on the modification of various dynamic relaxation processes due to the scission-recombination process. We investigate the monomer diffusion and the stress relaxation function. Finally, we perform a T-jump experiment in order to point out that the previously estimated macroscopic kinetic constants are indeed the key parameters governing the relaxation of the chain length distribution.

3.1 Static properties

The main aim of this section is to test the model of chapter II by comparing the structural properties, including the average chain length, the distribution of chain lengths and the conformations of the chains, with the theory [9, 27] and previous simulation works [13, 52].

3.1.1 List of simulation experiments and chain length distribution

The model is studied at three state points. The number of monomers, the number density ϕ, the energy parameter W, and the attempt frequency ω per arm are chosen for

1. A solution at the number density $\phi = 0.05$ and an energy parameter $W = 8$. The number of monomers is M=1000. The attempt frequencies of bond scission/recombination per arm ω are 0.1, 0.5, 1 and 5. This choice will be shown to lead to a dilute solution.

2. A solution at the number density $\phi = 0.15$ and an energy parameter $W = 10$. The number of monomers is M=1000. The attempt frequencies of bond scission/recombination per arm ω are 0.1, 0.5, 1 and 5. (will be shown to be a semi-dilute solution)

3. A solution at the number density $\phi = 0.15$ and an energy parameter $W = 12$. The number of monomers is M=5000. The attempt frequencies of bond scission/recombination per arm ω are 0.02, 0.06, 0.1, 0.5 and 1 (will be shown to be a semi-dilute solution).

Each system evolves according to the Langevin Dynamics algorithm with time step $\Delta t = 0.005$ and is subject to random trials of bond scission/recombination with the arm attempt frequency ω. All the experiments and the results of static properties which include the average chain length L_0, the mean square end-to-end vector, the radius of gyration and L_0/L^*, the number of blobs in a chain of length L_0, are listed in the table 3.1. Where $\langle R^2 \rangle$ and $\langle R_g^2 \rangle$ are defined as

$$\langle R^2 \rangle_{L_0} = \sum_{n=1}^{L_0-1} \sum_{m=1}^{L_0-1} \langle \bar{r}_n \cdot \bar{r}_m \rangle \tag{3.1}$$

$$\langle R_g^2 \rangle_{L_0} = \frac{1}{2L_0^2} \sum_{n=1}^{L_0} \sum_{m=1}^{L_0} \langle (\bar{R}_n - \bar{R}_m)^2 \rangle , \tag{3.2}$$

where $\bar{r}_n = \bar{R}_{n+1} - \bar{R}_n$. And L^* is defined by equation (1.21) (also see section 3.1.2).

As shown in the table, we observed that all the static properties are independent of ω and therefore, all data can be averaged over all ω values.

3.1.1.1 The dilute case

From Table 3.1, it can be observed that the first state point experiment ($W = 8, \phi = 0.05$) is a dilute solution since its average chain length $L_0 = 11.48(1)$ is much smaller than its crossover value at the monomer number density as calculated by equation (1.20), $L^* = 50.5$. Dilute solution conditions are confirmed by the chain length distribution shown in figure 3.1. For dilute conditions, a distribution given by (1.30) is expected [13, 52]. We fit our data with a single parameter B_1 of function (1.30), where L_0 is given its computed average value and where γ is given its expected value, $\gamma = 1.165$ [13]. The fit gives $B_1 = 1.08$. This curve is significantly better than the simple exponential distribution expected for ideal or semi-dilute chain. If γ is left as a second free parameter in the fit, it gives $\gamma = 1.161$ which is also very close to its expected value.

Table 3.1: List of simulation experiments and the values of static properties. W is the scission energy parameter, ϕ the number density, T_s the total simulation time, ω the attempt frequency, L_0 the average chain length, $\sqrt{\langle R^2 \rangle_{L_0}}$ the end-to-end distance of the average chain, and $\sqrt{\langle R_g^2 \rangle_{L_0}}$ its radius gyration. L_0/L^* is the ratio of the average chain length over the blob length L^*

W	ϕ	T_s	ω	L_0	$\sqrt{\langle R^2 \rangle_{L_0}}$	$\sqrt{\langle R_g^2 \rangle_{L_0}}$	L_0/L^*
8	0.05	$2.5 * 10^5$	0.1	11.48(6)	4.93(2)	1.9(2)	0.2
8	0.05	$2.5 * 10^5$	0.5	11.46(2)	4.92(1)	1.9(1)	0.2
8	0.05	$2.5 * 10^5$	1.	11.50(3)	4.94(1)	1.9(1)	0.2
8	0.05	$2.5 * 10^5$	5.	11.51(2)	4.95(1)	1.9(1)	0.2
10	0.15	$2.5 * 10^5$	0.1	56.2(6)	12.2(1)	4.8(2)	4.7
10	0.15	$2.5 * 10^5$	0.5	56.2(1)	12.4(1)	4.9(3)	4.7
10	0.15	$2.5 * 10^5$	1.	56.2(2)	12.3(1)	4.9(3)	4.7
10	0.15	$2.5 * 10^5$	5.	56.6(2)	12.4(1)	4.9(4)	4.7
12	0.15	$6.25 * 10^5$	0.02	151(4)	20.9(5)	8.3(4)	12.6
12	0.15	$4.5 * 10^5$	0.06	153(4)	21.5(7)	8.5(5)	12.6
12	0.15	$4.5 * 10^5$	0.1	150.7(5)	21.2(2)	8.4(3)	12.6
12	0.15	$3 * 10^5$	0.5	150.3(5)	20.9(1)	8.4(2)	12.5
12	0.15	$3 * 10^5$	1	150.4(6)	20.92(3)	8.5(4)	12.5

3.1.1.2 The semi-dilute case

Both the second state point ($W = 10, \phi = 0.15$) and the third state point ($W = 12, \phi = 0.15$) experiments are found to be in semi-dilute regime, since their average chain lengths are 56.4(1) and 151.4(4), respectively, which are several times larger than their crossover value $L^* \approx 12$ at $\phi = 0.15$ according to equation (1.20). Semi-dilute solution conditions are confirmed by the observation of a simple exponential distribution of chain lengths. In figure 3.2 and figure 3.3, we show, for the second and the third state point experiments respectively, the agreement of our data with the expected simple exponential distribution (1.34).

3.1.2 Chain length conformational analysis

In this subsection we are interested in the conformational properties of micelles in equilibrium and studied as a function of chain size within our polydisperse system. We have calculated the mean square end-to-end distance and the mean square radius of gyration $< R^2 > (L)$ and $< R_g^2 > (L)$ averaged over subsets of chains of length L.

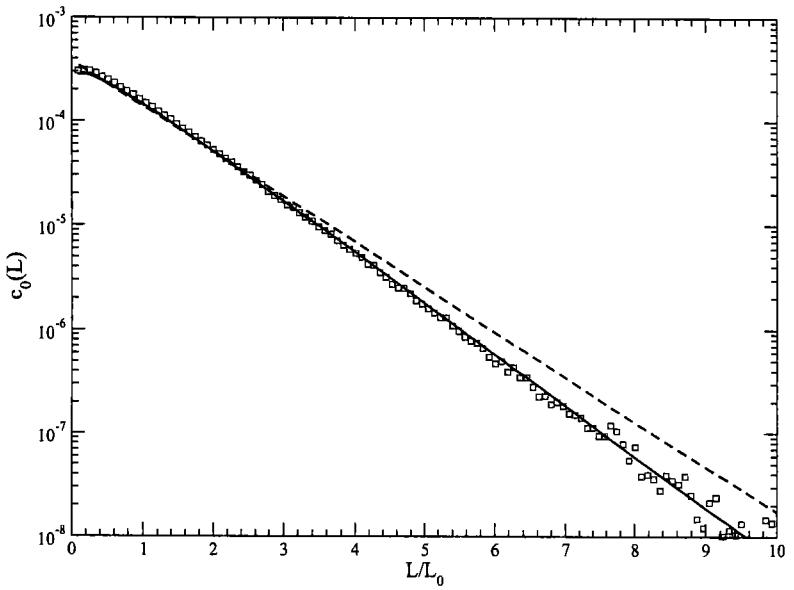

Figure 3.1: Distribution of chain lengths for the dilute case in good solvent. The data (*squares*) are fitted using equation (1.30) with the single parameter B_1 and imposed value $\gamma = 1.165$ (*continuous curve*). The fit gives $B = 1.08$. The dashed line shows the simple exponential distribution $c_0(L) \propto \exp(-L/L_0)$ which does not fit the data.

Figure 3.4 and figure 3.5 are the results for the dilute state point and the two semi-dilute state points experiments respectively. As shown in figure 3.4 relative to the dilute case, the *squares* and *circles* represent our data of $< R^2 >$ and $< R_g^2 >$ respectively. With the *solid line* and the *dashed line*, we indicate, for long chains ($L \gtrsim 25$), standard power law scaling $L^{2\nu}$ with $\nu = 0.588$. The data show a reasonable agreement of this asymptotic regime in the range of application.

The chains in the semi-dilute system are expected to behave as ideal chains for $L \gg L^* \approx 12$ where L^* is estimated from equation.(1.20) with $\phi = 0.15$. Figure 3.5 shows the $\langle R^2 \rangle$ and $\langle R_g^2 \rangle$ of the two semi-dilute cases. Results of $\langle R^2 \rangle$ and $\langle R_g^2 \rangle$ for the two cases, are superimposed. We indicate for the long chains the ideal chain conformation $\langle R^2 \rangle$ and $\langle R_g^2 \rangle \propto L$. The agreement of the fitting lines with simulation data appears to start at $L \gtrsim 60$.

The conformational properties of the chain in the two semi-dilute cases are found

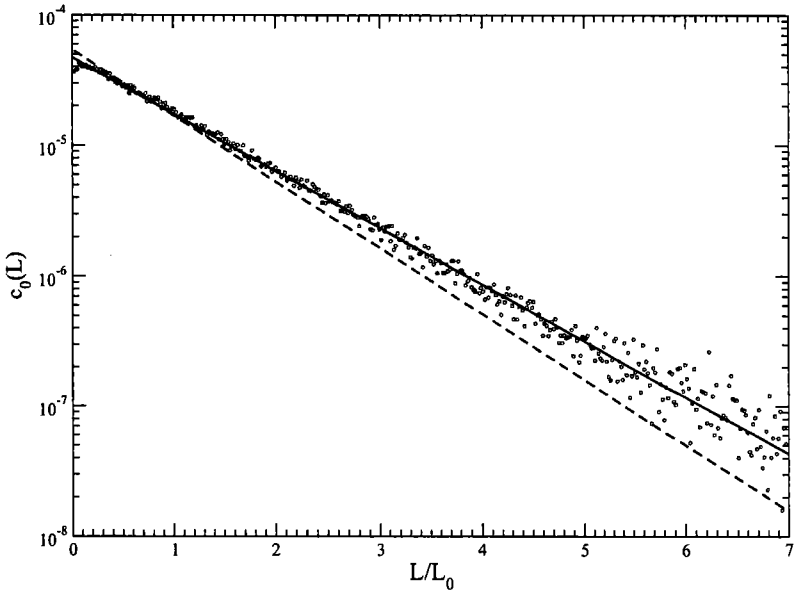

Figure 3.2: Distribution of chain lengths for the state point $W = 10, \phi = 0.15$ (accumulated over all ω values). The data (*circles*) are fitted very well by the simple exponential function, equation (1.34), with imposed average chain length $L_0 = 56.4$. The *Dashed line* shows the function $\exp(-1.165L/L_0)$ which does not fit the data.

to be identical as expected. The size R of a chain of length $L > L^*$ is

$$R = bL^{*\nu}\left(\frac{L}{L^*}\right)^{0.5} \tag{3.3}$$

where b is the monomer size and ν is the good solvent scaling exponent while L^* (function of ϕ only) is the same in both cases.

3.1.3 Pair correlation function of chain ends and the distribution of bond length

Equilibrium polymers are polydisperse polymers endowed with scission and recombination processes. Whereas a scission can happen between any bounded pair, a recombination may happen only with two chain ends for linear chains. Thus it is interesting to study the spatial distribution of the chain ends and the bond length distribution. For the dilute case the population of bonds ready to open within the Γ range ($-0.96 < r < 1.2$) is $< N_{1\Gamma} >= 552$ and represents 61% of the bonded pairs $< N_1 >$, while the population of free arm pairs ready to close, again within the same Γ range, is

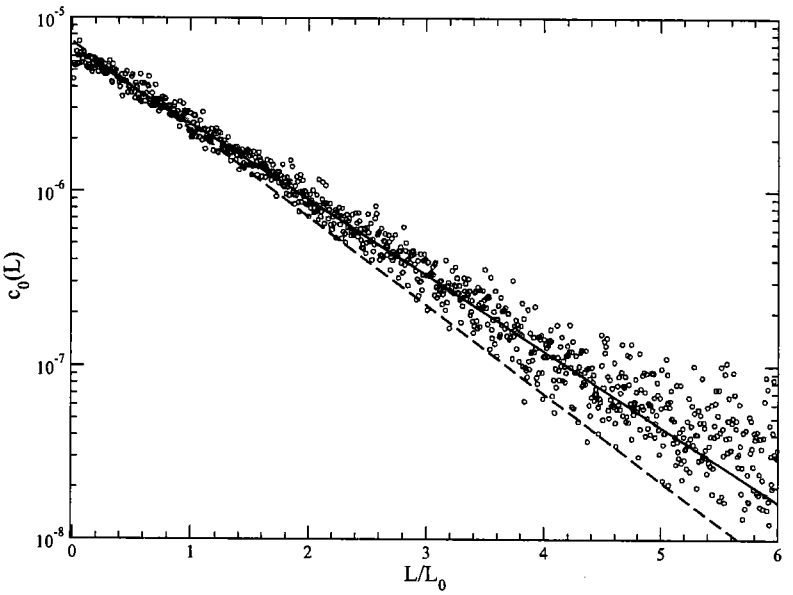

Figure 3.3: Distribution of chain lengths for the state point $W = 12, \phi = 0.15$ (accumulated over all ω values). The data (*circles*) are fitted very well by the simple exponential function, equation 1.34, with imposed average chain length $L_0 = 151.4$. The *Dashed line* shows the function $\exp(-1.165L/L_0)$ which does not fit the data.

only $< N_{2\Gamma} >= 1.16$. Figures 3.6 and 3.7 show respectively the pair correlation function $g_{ee}(r)$ (where the pairs between the two ends of the same chain are eliminated) for chain ends (unsaturated arms) and the distribution of the distances between bounded monomers, in particular within the Γ region where potential changes can occur by scission or recombination. The "free arm" fraction, namely $1 - N_1/M = 0.0957$, is close to $L_0^{-1} =< N_{ch}/M >= 0.0964$.

For the semi-dilute case (we show here only the case $W = 10$) the number of bonds ready to open in the Γ region is $< N_{1\Gamma} >= 597$, while the population of free arms pairs ready to close within Γ region is $< N_{2\Gamma} >= 0.183$. The pair distribution of chain ends and the distribution of distances of bounded pairs are respectively given in figures 3.6 and 3.7, where we have also plotted the dilute case data. We note that the $g_{ee}(r)$ function between free ends is not very different from the dilute case. The "free arm" fraction $1 - N_1/M = 0.021$ is 5 times smaller than in the dilute case, which is consistent with the chains average length being 5 times larger.

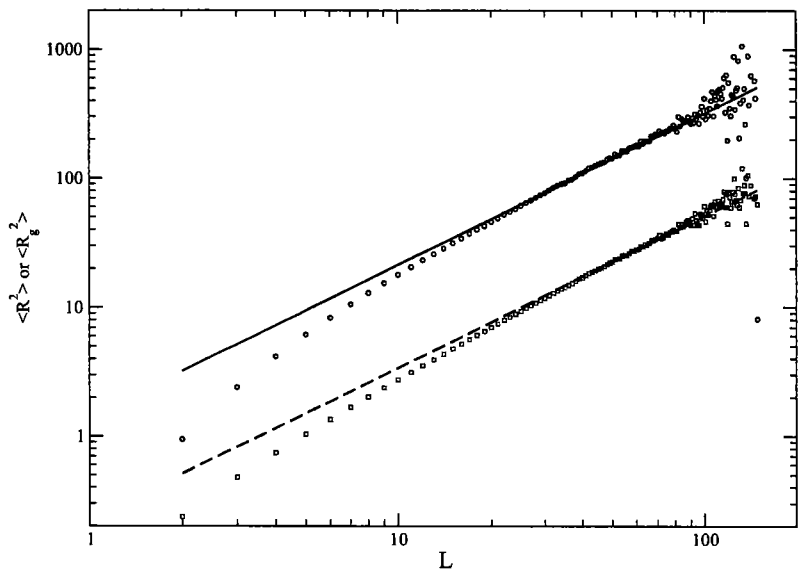

Figure 3.4: Conformational properties in the dilute case: $< R^2 >$ (squares, lower curve) and $< R_g^2 >$ (circles, upper curve) versus chain length L. The fitting functions which are power laws with fixed exponent $2\nu = 1.176$ (prefactors 0.226 for $< R_g^2 >$ and 1.461 for $< R^2 >$) fit the data for long chains only.

3.2 Dynamic properties

In this section we explore the results of the dynamic properties. Focusing on the two semi-dilute state points where chain dynamics is still essentially unentangled. We extract for various attempt frequencies ω of the phenomenological kinetic constants by a statistical analysis of all scission-recombination events recorded in our simulations. We check the micro-reversibility of the model at equilibrium state. We then perform a T-jump experiment, analyze the mean square displacement of the monomers, and estimate the stress autocorrelation function of our system, in order to point out that the previously estimated macroscopic kinetic constants are indeed the key parameters governing the dynamic properties of the EP system.

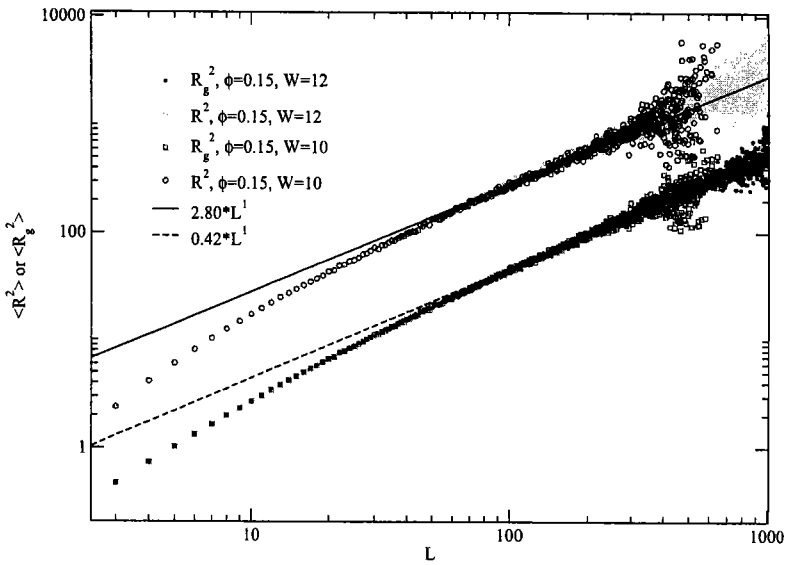

Figure 3.5: $< R^2 >$ and $< R_g^2 >$ versus chain length L in the two semi-dilute cases. The data for the two semi-dilute case ($W = 10$ and of $W = 12$) are superimposed. The fitting functions (linear in L) assume ideal chain statistics with prefactors 0.42 for $< R_g^2 >$ and 2.80 for $< R^2 >$. The lower curves show $< R^2 >$, whereas the upper $< R_g^2 >$

3.2.1 Kinetics Analysis

3.2.1.1 Scission and recombination events

The aim of this subsection is to understand the short and long time behavior of the distribution of the scission and recombination times and to determinate the macroscopic scission rate constant k_s and the recombination rate constant k_r. For different attempt frequencies ω investigated, the number of Monte-Carlo accepted scissions and accepted recombinations are obtained by simple counting during the simulation. In Table 3.2, we list the number n_s of "accepted" scissions and the number n_r of "accepted" recombinations per unit time and unit volume, for the two state points and for different ω. For each state point, we observe that the number of scissions per unit of time is, as expected, proportional to ω and we have also verified that the number of recombinations differs from the number of scissions only by marginal amounts (0.05%), which shows that the chain length distributions are well equilibrated during the simulation run for data analysis.

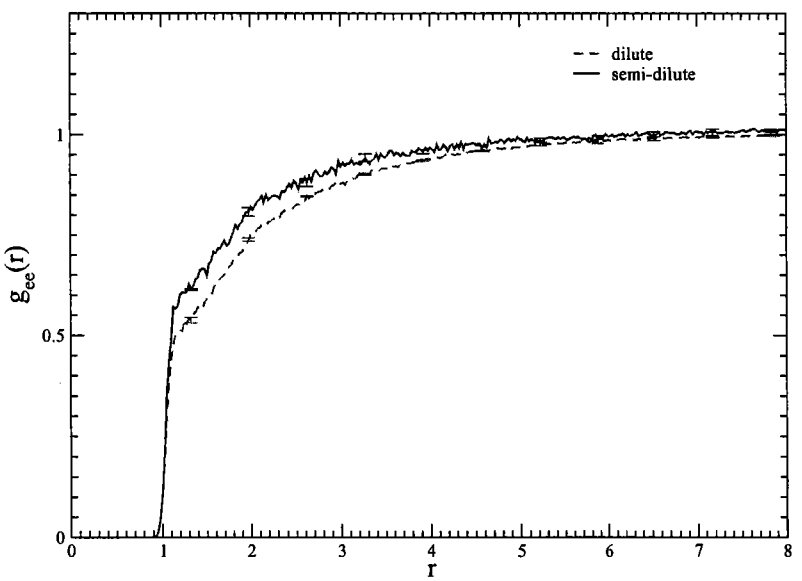

Figure 3.6: Chain end pair distribution function $g_{ee}(r)$ in the dilute ($\phi = 0.05$, $W = 8$) and semi-dilute ($\phi = 0.15$, $W = 10$) experiments. Note that the Γ region where the bounding changes take place correspond to the region of first (fast) increase of the distribution function around $r = 1$.

3.2.1.2 Distribution of First Recombination Times

The aim of this subsection is to present a method of estimating the rate constants. In our explored ω range, we find that a large fraction of elementary scissions are followed by recombinations of the same original chain monomers. This kind of recombinations which happens almost immediately after the scission event do not lead to any effective effect on the long time relaxation. To extract estimates of the rate constants defined by the kinetic model of Cates, it is thus important to eliminate the spurious transitions from the effective ones. The best way for this is certainly to approach the problem via a time scale separation between scission-recombination processes taking place on a fast time scale and effective transitions taking place on the reaction time scale τ_b.

The first approach is to analyze the distribution of first recombination times $\Psi(t)$ satisfying the renormalization

$$\int_0^\infty \Psi(t)dt = 1. \tag{3.4}$$

Hence, we have to compute the histogram of all first recombination times $t = t_2 - t_1$ (limited for pragmatic reasons to a time $T_{max} = 1000$) for an arm which became free

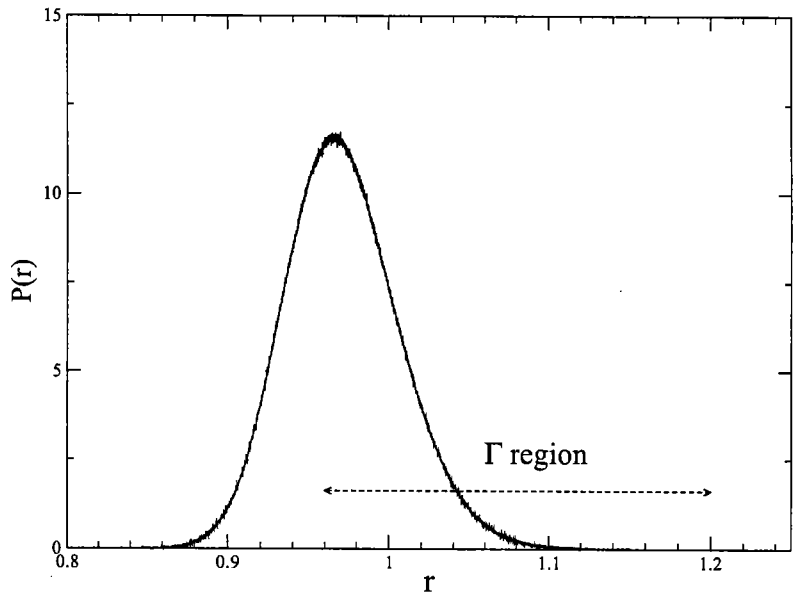

Figure 3.7: Normalized distribution function $P(r)$ of the distance between bounded monomers in the semi-dilute experiment. The corresponding function in the dilute solution experiment is marginally different from the semi-dilute case and is therefore not shown in the figure.

by scission at time t_1 and which recombines for the first time at time t_2. The short time behavior of the distribution can be analyzed by plotting the function versus time on a logarithmic scale. In figure 3.8, the resulting histogram $\Psi(t)$ for $\omega = 0.5$ is shown together with a partition of the recombination events between those which reform the same original pair and those where the arm we consider binds with a new partner with respect to the one it detached from in the first place. This function is properly normalized by imposing that its integral over the time interval of observation is the ratio of the total number of observed first recombinations over the total number of scissions used in the sampling. At short time ($t < 10$), there is a much higher probability for a recombination with the same partner. The theory of diffusion controlled recombination kinetics [12] predicts an algebraic decay $At^{-5/4}$ for $\Psi(t)$ and we observe that the self-recombination part of our data beyond $t = 1$ follows very well this power law decay. Similar power laws are observed for the simulation with other attempt frequencies, except at the hightest one ($\omega = 5$) where the slope is steeper by 20%. When ω becomes so large that the time ω^{-1} is smaller than the time required for a free arm to diffuse over

Table 3.2: Scission and recombination frequencies for the two semi-dilute cases for various scission-recombination attempt frequencies ω. n_s and n_r denote the number of scissions and of recombinations per unit time and per unit volume respectively.

W	ω	n_s	n_r
10	0.1	$3.29(4)10^{-6}$	$3.29(3)10^{-6}$
10	0.5	$1.64(1)10^{-5}$	$1.63(2)10^{-5}$
10	1	$3.31(3)10^{-5}$	$3.31(3)10^{-5}$
10	5	$1.652(4)10^{-4}$	$1.652(4)10^{-4}$
12	0.02	$1.05(4)10^{-7}$	$1.05(4)10^{-7}$
12	0.1	$5.28(4)10^{-7}$	$5.27(5)10^{-7}$
12	1	$5.348(9)10^{-6}$	$5.348(9)10^{-6}$

a distance Γ, the mechanism for quasi immediate recombination is different and largly decoupled from diffusion. In figure 3.8, the two curves corresponding to the two types of contributions cross each other around $t = 25$ and at later times, the recombination with another partner quickly dominates.

The self-recombinations dominating at short times are considered to make no change in chain topology, since the recombinations happen almost immediately following a scission. We consider these transitions as not effective. Actually, noneffective transitions may also come from more complex particular transition sequences. Consider a chain end monomer (say monomer i) lying close in space to another chain at the level of two adjacent monomers j and k. At high ω, a scission of the bond jk may be immediately followed by a recombination between j or k with monomer i. In turn, the ik or ij bond may reopen and recombine to restore the very first situation, ending with no effective transition without being detected through the criterion of a successive recombination with the same partner. The occurrence of such events is proven indirectly in the following by noting almost immediate chain end recombination with another partner (see figure 3.8).

The first recombination times data have further been analyzed by considering that $\Psi(t)$ is exponential decaying at long times. Figures 3.9 and 3.10 show the result on semi-logarithmic scale for the two state points and all ω studied. At long times the curves of $\Psi(t)$ are exponential with time. Imposing a fraction of effective transitions, κ, one can define

$$\Psi_{asymp}(t) = \frac{\kappa}{\tau_b} e^{-t/\tau_b}. \tag{3.5}$$

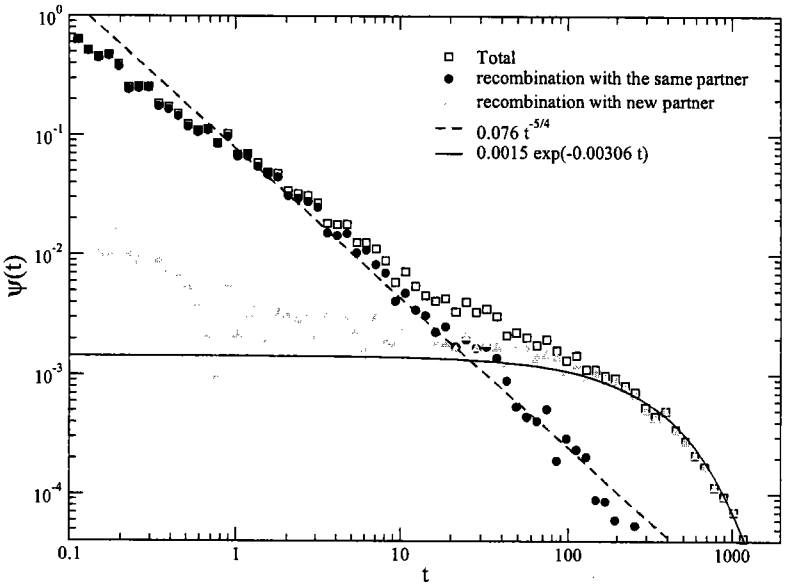

Figure 3.8: Distribution of first recombination times $\Psi(t)$ for the semi-dilute case ($W = 10$) for attempt frequencies $\omega = 0.5$ (open square). The partition between contributions from recombinations with the same partner (filled circles) or with a new partner (filled triangles) are distinguished. The dashed line (with slope -5/4) represents the power law $t^{-5/4}$ expected for short times. The solid line indicates the long time mean-field prediction (for $t > 30$).

Thus, the slope is interpreted as the inverse of the average life time of a chain end which is denoted as $\tau_b^{(1)}$. The ordinate intercept of the function fitted to $\Psi(t)$ at long time corresponds to $\frac{\kappa}{\tau_b}$, and can be use to determine κ. The value κ obtained using the function $\Psi(t)$ is denoted as $\kappa^{(1)}$. Specific values for the different $\omega's$ and $W's$ are indicated in Table 3.3.

Figure 3.11 shows the first recombination times at long times and at short times for the three ω for the cases $W = 10$ and $W = 12$. To indicate the universality at long time, we rescale t by τ_b and $\Psi(t)$ by $\Psi_{asymp}(\tau_b)$, forcing all curves to match at $\frac{t}{\tau_b} = 1$. The *dashed line* indicates the universal exponential which is indeed followed by all curves as $\frac{t}{\tau_b} > 1$. The short time part of the curves tends closer and closer to 1, as κ approaching to unity.

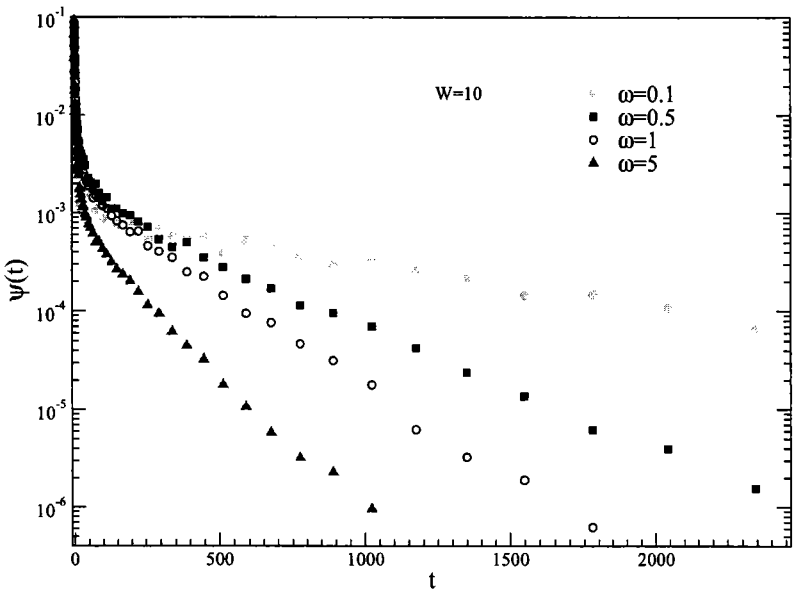

Figure 3.9: Distribution of first recombination times $\Psi(t)$ for the semi-dilute case ($W = 10$) for the four attempt frequencies $\omega = 0.1$ (*filled circles*), $\omega = 0.5$ (*filled square*), $\omega = 1$ (*opened circles*), and $\omega = 5$ (*filled triangles*). The average chain length L_0 for this state point is $L_0 = 56.4(1)$ and is independent of ω.

3.2.1.3 Cumulative Hazard Analysis

Another way to analyze the recombination kinetics is the hazard rate plotting technique advocated by Helfand [30] to analyze the rates of conformational transitions in butane and other short alkane molecules. We first summarize the theoretical foundations of the method, using the particular case of equilibrium polymer kinetics to directly illustrate the concepts. The cumulative hazard plot has the advantage of avoiding the necessity of binning recombination time data which become scars at long times. It also exploits statistically some additional information (useful for low rates) from portions of the $2M$ trajectories between a scission and the next recombination in a way which is truncated either at the beginning or at the end of the LD run.

Let $h(t)dt$ be the probability that a free arm, created at time $t = 0$ and which is still free at time t, undergoes a first recombination in the interval $[t, t + dt]$. Let $P(t)$ be the probability that a free arm, created at time $t = 0$, has undergone a (first) recombination between 0 and t.

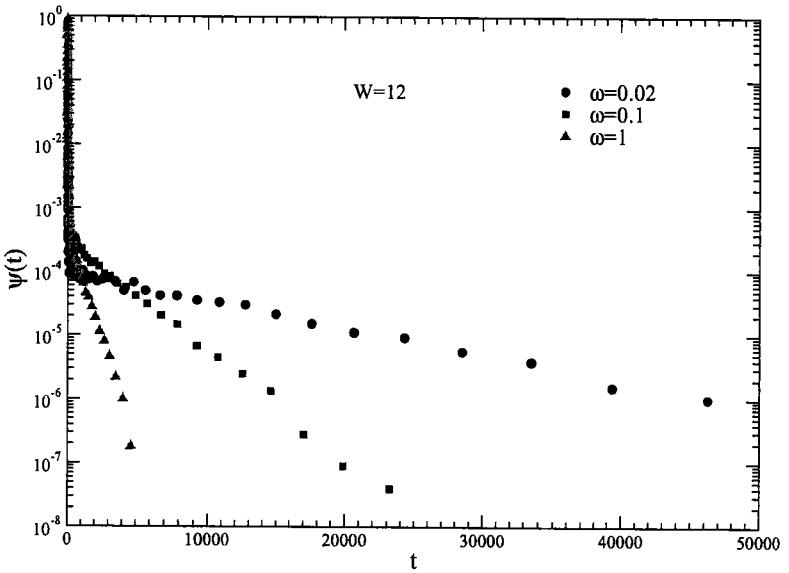

Figure 3.10: Distribution of first recombination times $\Psi(t)$ for the semi-dilute case ($W = 12$) for the three attempt frequencies $\omega = 0.02$ (dots), $\omega = 0.1$ (squares), and $\omega = 1$ (triangles). The average chain length L_0 for this state point is $L_0 = 151.4(4)$.

Using these definitions, the following steps can be written

$$[1 - P(t + dt)] = [1 - P(t)]\,(1 - h(t)dt) \tag{3.6}$$

$$\frac{d}{dt}[1 - P(t)] = -h(t)\,[1 - P(t)] \tag{3.7}$$

$$[1 - P(t)] = \exp\,(-\int_0^t h(t')dt') = \exp\,[-H(t)] \tag{3.8}$$

where $H(t) = \int_0^t h(t')dt'$ is the cumulative hazard. In the present case, we anticipate a complex process involving correlated events at short times $h(t) = h^{sh}(t)$ and a Poisson process emerging at long times with uniform frequency $lim_{t\to\infty} h(t) = \lambda$ where λ is the recombination rate constant. On the relevant time scale of the kinetics, one thus should find for the cumulative hazard function and the P(t) probability

$$H(t) = H_I + \lambda t \tag{3.9}$$

$$P(t) = 1 - \exp\,(-H_I)\exp\,(-\lambda t) \tag{3.10}$$

where H_I, the ordinate intercept of the function $H(t)$ versus t, can be seen as the time integral of $(h^{sh}(t) - \lambda)$ from 0 to ∞. If a good time scale separation exists,

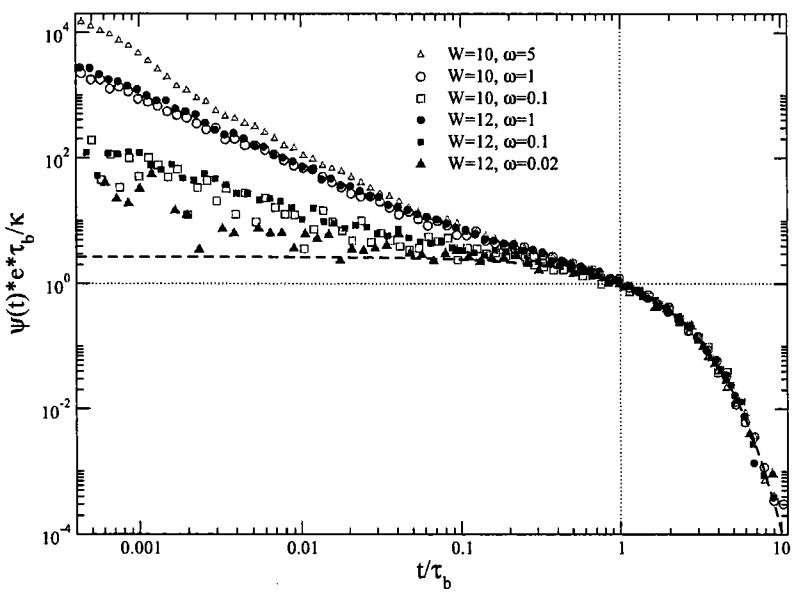

Figure 3.11: Rescaled first recombination times function $\psi(t)$ shows an universal exponential behavior after $\frac{t}{\tau_b}$. The dashed line indicates the universal exponential. The case $(W = 12, \omega = 0.02)$ is the most "mean field" case.

equation.(3.10) implies that $c \equiv P(0^+) = 1 - \exp(-H_I)$ is the fraction of correlated transitions, $\kappa^{(2)} = 1 - c$ being the estimate according to the present analysis of the average probability for a newly created free arm to recombine by the Poisson "mean field" kinetic process postulated by Cates in his theory [9].

We now explain how the estimate of the cumulative hazard function is effectively computed. We start by extracting from the LD trajectory a collection of times $\{\hat{t}\}$ where each member corresponds to the elapsed time between a scission of a particular arm at time t_1 and its next recombination at time t_2, so $\hat{t} = t_2 - t_1$. All the $2M$ arms of the system contribute to the $\hat{t}$ data sample which, for each arm, can contain several times of this kind between the start (at $t = 0$) and the end (at $t = T_{max}$) of the LD trajectory.

Moreover, if the first change of status of a particular arm since the beginning of the LD simulation is a recombination taking place at time t, we can say that this time is a lower bound $\hat{T}$ of an additional unknown elapsed time $\hat{t}$ between a scission (out of our reach) and the next recombination (we observed). Also, if the last change of arm

status before the end of the LD trajectory is a scission taking place at time t, then, the time $\hat{T} = T_{max} - t$ is a similar lower bound of yet another time of interest. The analysis thus furnishes a set of K times $\{\hat{t}\}$ and M lower bounds times $\{\hat{T}\}$) which are then separately ordered from the shortest time up to the longer one and indexed accordingly as $(\hat{t}_1, \hat{t}_2, \hat{t}_3, ..\hat{t}_K)$ and $(\hat{T}_1, \hat{T}_2, \hat{T}_3, ...\hat{T}_M)$. Let us consider successively all individual arm life times $\{\hat{t}\}$. For any time $\hat{t}_i$ of that collection, the probability that a free arm which had survived up to the previous time $\hat{t}_{i-1}$ changes its status and becomes engaged in the formation of new bond between times $\hat{t}_{i-1}$ and $\hat{t}_i$ is given with our available statistics by $1/N(\hat{t}_{i-1})$ where the denominator is the number of cases (including both types of times $\hat{t}$ and $\hat{T}$) where recombination takes place at a time longer than $\hat{t}_{i-1}$, i.e.

$$N(\hat{t}_{i-1}) = [K - (i-1)] + [M - m_{(i-1)}] \tag{3.11}$$

where $m_{(i-1)}$ is the index of largest $\hat{T}$ value which is still inferior to $\hat{t}_{i-1}$. In terms of these definitions, the cumulative hazard function $H(t)$ can be evaluated at each time $\hat{t}$

$$H(\hat{t}_i) = \sum_{j=1}^{i-1} \frac{1}{N(t_j)} \tag{3.12}$$

If the function is linear in time, it implies a Poisson process with a rate of transitions given by the slope of that linear portion.

Figure 3.12 and 3.13 shows the resulting cumulative hazard functions for the four ω values in the case $W = 10$ and the three ω values in the case $W = 12$. Fort the case $W = 10$, a linear behavior starts around $100 - 150$ for all ω and it lasts up to times of the order of 1000 where statistical noise sets in. As shown in figure 3.13, for the case $W = 12$, the linear behavior lasts up to very long times (up to $t \approx 50000$ for $\omega = 0.02$). The inset of the figure is a close view of the ordinate at origin of this case, showing that in the smallest attempt frequency case $\omega = 0.02$, having it's ordinate at origin $H_I \approx 0$, represents the most "mean field" case with $\kappa = 0.93$. For each case, the inverse slopes of the linear portions provide estimates $\tau_b^{(2)}$ of the mean life time of a chain end. Specific values for both thermodynamic states ($W = 10$ and 12) are gathered in Table 3.3. They are compatible with the values extracted from the histogram of first recombination times. Using the procedure described at the beginning of this subsection, one gets from the ordinate intercepts of $H(t)$ the κ estimate indicated in Table 3.3 for the two states points and various ω.

Table 3.3: Kinetic data for the two semi-dilute cases for various investigated ω values. The superscript (i) refers to the methodology used to get various estimates of a given quantity, namely $i = 1$ for the method based on the direct analysis of the distribution of first recombination times, and $i = 2$ for the cumulative hazard method. τ_b is the average first recombination time and also the typical life time of a chain of average length L_0. The estimate $\tau_b^{(i)}$ is obtained by the long time behavior of the relevant dynamical function used in methodology (i). $\kappa^{(i)}$ is the fraction of transitions which are effective as mentioned in method (i). Such transitions can be seen as those which do not belong to sequences of correlated transitions (chain scission followed by almost immediate recombination ending into no change in chains topology). $n_s^{(2)}$ is obtained on the basis of $k_s^{(2)}$ through equations (3.13 and 3.14). Q_s^{eq} and Q_r^{eq} are obtained through equations (3.20) and (3.21) respectively (see text). $\hat{Q}_s^{eq}$ and $\hat{Q}_r^{eq}$ are obtained from the structural functions (equations (3.22) and (3.26) respectively (see text)).

W	ω	$\kappa^{(1)}$	$\kappa^{(2)}$	$\tau_b^{(1)}$	$\tau_b^{(2)}$	$k_s^{(1)}10^5$	$k_s^{(2)}10^5$	$n_s^{(2)}10^6$	$Q_s^{eq} * 10^4$	Q_r^{eq}	$\hat{Q}_s^{eq} * 10^4$	$\hat{Q}_r^{eq}$
10	0.1	0.80	0.82(2)	1049	1026(22)	1.69	1.72	3.2	1.077	4.535	1.093	4.497
10	0.5	0.51	0.49(1)	347	321(5)	5.11	5.51	17.0	1.102	4.705	1.113	4.420
10	1	0.38	0.32(1)	226	231(3)	7.84	7.63	36.1	1.077	4.534	1.121	4.444
10	5	0.13	0.11(1)	145	140.5(8)	1.22	1.26	171.5	1.092	4.666	1.096	4.477
12	0.02	0.91	0.93(1)	10170	10422	6.49	6.39	10.3	-	-	-	-
12	0.1	0.73	0.72(1)	2501	2596	2.64	2.57	53.3	-	-	-	-
12	1	0.28	0.25(1)	705	699	9.37	9.54	5.7	-	-	-	-

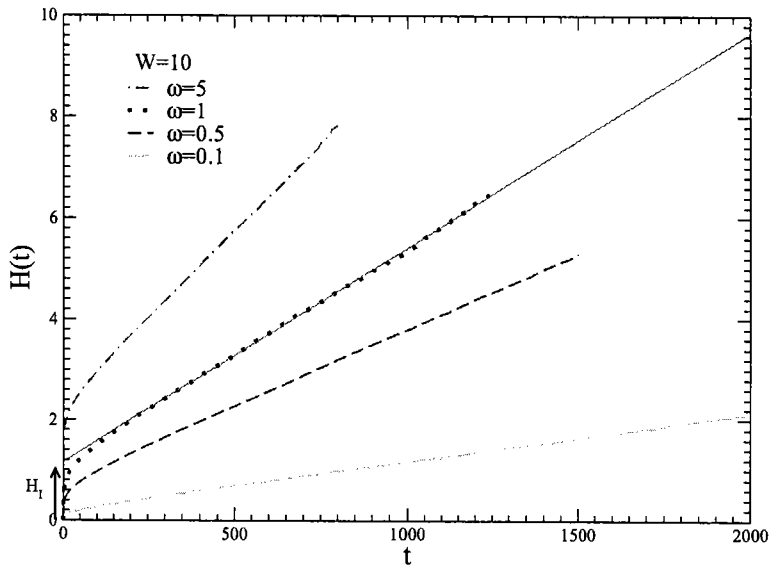

Figure 3.12: Cumulative Hazard curves of recombination times for the case $W = 10$. The average chain length L_0 for this state point is $L_0 = 56.4(1)$ and is independent of ω. Data are shown for various attempt frequencies, from bottom to top, namely $\omega = 0.1$ (continuous line), $\omega = 0.5$ (dashed line), $\omega = 1.0$ (dot line) and $\omega = 5$ (dot-dashed line). The straight line associated to the $\omega = 1$ case gives an example of the linear asymptote of $H(t)$ of slope $\lambda = 1/\tau_b$ and ordinate at origin H_I = -ln κ

3.2.1.4 Estimation of rate constants: comparison of the various methods

Explicitly, the scission rate constants k_s and k_r of the "mean-field" kinetic model can be estimated from our data in two distinct ways.

- On the basis of the total number of transitions n_s per unit time and per unit volume, and on the basis of an estimate of κ by one of the methods discussed above, the rates can be estimated from a trivial modification of equations (1.39,1.40), namely

$$\kappa n_s = k_s \phi = \frac{k_r \phi^2}{2L_0^2} \tag{3.13}$$

  where κn_s corresponds to the number of scissions per unit of time and per unit volume which lead to an effective recombination with a new partner.

- On the basis of the long time behavior of a dynamical function relevant to the particular methodology adopted, the "chain end" life time can be directly esti-

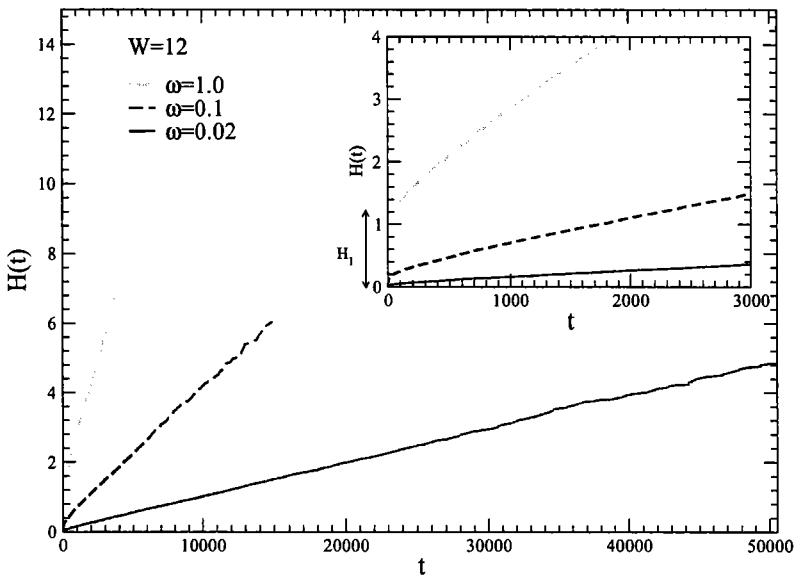

Figure 3.13: Cumulative Hazard curves of recombination times for the case $W = 12$. The average chain length L_0 for this state point is $L_0 = 151.4(4)$. Data are shown for various attempt frequencies, namely $\omega = 0.02$ (continuous line), $\omega = 0.1$ (dashed line), and $\omega = 1$ (dot-dashed line). Notice that the smallest attempt frequency case $\omega = 0.02$, having it's ordinate at origin $H_I \approx 0$, represents the most 'mean field' case with $\kappa = 0.93$

mated. As the latter is equivalent to the typical life time of a chain of average length denoted as τ_b, one gets rate constants through the equivalence

$$\tau_b = \frac{1}{k_s L_0} = \frac{2L_0}{k_r \phi} \tag{3.14}$$

where the last equality follows from detailed balance requirements. Two methodologies for the estimation the value of τ_b are discussed in the previous subsection and their corresponding k_s obtained via this relation are listed in the Table 3.3 as $k_s^{(1)}$ and $k_s^{(2)}$, respectively for the method of distribution of first recombination times and for the cumulative hazard analysis. We can easily check the values of k_s by comparing the values of n_s computed through equations (3.13, 3.14) and giving $k_s^{(1)}$ or $k_s^{(2)}$ with the values of n_s accounted directly during the simulations. Denoted as $n_s^{(2)}$ and listed in Table 3.3, the numbers of scissions (per per unit volume per unit time) obtained by using $k_s^{(2)}$ are compatible with n_s accounted directly during the simulations (listed in Table 3.3).

Looking at all values in the tables, we get an overall consistency between all methodologies. It indicates that all our strategies to extract the "macroscopic" rate constants do work. Among them, the cumulative hazard analysis appears the most straightforward to analyze once $H(t)$ is known and is particularly robust as noise influence seems minimal.

3.2.1.5 The microscopic analysis of the rate constants

The previous subsection has demonstrated that we need to be careful with the concept of scission/recombination kinetic events, as we have to distinguish the effective transition from the whole set of transitions which are potential swaps Monte-Carlo accepted moves. Hence, in the following we will add the subscript "st" to n_s to show that we consider all kinetic events. We have also added the subscript "eff" to n_s when we deal only with the effective numbers of transition. Let us first consider n_s^{st} (n_r^{st}) the total numbers of scissions or recombinations per unit of time per unit of volume. This allows us to define short time rate constants at equilibrium k_s^{st} and k_r^{st}, according to

$$n_s^{st} = k_s^{st}\left(1 - \frac{1}{L_0}\right)\phi \tag{3.15}$$

$$n_r^{st} = \frac{1}{2}k_r^{st}\left(\frac{\phi}{L_0}\right)^2 \tag{3.16}$$

where L_0 is the average micelle length at equilibrium. The term $(1 - \frac{1}{L_0}) \approx 1$ for $L_0 \gg 1$. Further, we introduce the bond scission probability Q_s^{eq} and the recombination probability Q_r^{eq}. The former quantity is the probability that a randomly selected bond is ultimately changed into two chain ends while the second quantity is defined such that $\frac{1}{2}\frac{\phi}{L_0}Q_r^{eq}$ is the probability for a randomly selected free arm to form a new bond with any other free arm available in the system. In terms of these, we have

$$k_s^{st} = 2\omega Q_s^{eq} = \frac{n_s^{st}}{\phi} \tag{3.17}$$

$$k_r^{st} = 2\omega Q_r^{eq}. \tag{3.18}$$

When following dynamical relaxation over mesoscopic times, much longer than the local dynamics time scale, $t \gg \tau_{micro} \approx 1$, only uncorrelated transitions (expected to be Poisson distributed) will be involved in the effective rate calculation. To determine these rate constants, we will use the concept of an effective transmission coefficient

$0 \leq \kappa(\omega) \leq 1$ introduced in the previous subsection. By assembling equations (3.15) to (3.18), the total number of effective transitions (per unit of time and per unit volume) can then be expressed as

$$\begin{aligned} & n_s^{eff}(\omega) = n_s^{st}\kappa(\omega) = 2\omega\kappa(\omega)Q_s^{eq}\phi \equiv k_s\phi \\ = \quad & n_r^{eff}(\omega) = n_r^{st}\kappa(\omega) = \frac{1}{2}\left(\frac{\phi}{L_0}\right)^2 2\omega\kappa(\omega)Q_r^{eq} \equiv \frac{1}{2}\left(\frac{\phi}{L_0}\right)^2 k_r \end{aligned} \tag{3.19}$$

where the last equalities for the two expressions define the scission and recombination rate constants. At equilibrium for the state $\phi = 0.15$, $W = 10$, we get an average micelle length $L_0 = 56.4 \pm 0.1$, independent of the arm change attempt frequency ω. The values of Q_s^{eq}, Q_r^{eq} and $\kappa(\omega)$ were listed in Table (3.3). The Q_s^{eq} were computed by

$$Q_s^{eq} = n_s^{st}\phi^{-1}(2\omega)^{-1}, \tag{3.20}$$

and Q_r^{eq} by

$$Q_r^{eq} = 2n_r^{st}\left(\frac{L_0}{\phi}\right)^2 (2\omega)^{-1} \tag{3.21}$$

It should be noted that the probabilities Q_s^{eq} and Q_r^{eq} are, for our microscopic model, only function of the thermodynamic state (ϕ, T), and not the attempt frequency ω.

Q_s^{eq} and Q_r^{eq} can be analyzed microscopically in terms of static structural functions, i.e. $P(r)$ the distribution of bond length and $g_{ee}(r)$ the pair correlation function of end-monomers.

1. For bond scissions between pairs of adjacent monomers distributed according to $P(r)$ (distribution normalized over r from 0 to R_c, where $R_c = 1.5$ is the value at which the FENE potential diverges), one has

$$Q_s^{eq} \equiv \int_\Gamma dr q_s(r) = \int_\Gamma dr P(r) P_s^{acc}(r) \tag{3.22}$$

$$P_s^{acc} \simeq p_n(r) Min(1, \exp(-\beta\Delta U(r))) \tag{3.23}$$

$$p_n(r) = \left\langle \frac{1}{N_i + 1} \right\rangle_r \tag{3.24}$$

where $p_n(r)$ is an extra probability factor appearing in our algorithm where N_i+1 is the total number of free ends which would be potentially available in the appropriate Γ region to reform a new bond with the originally selected monomer (see Section 2.3). As N_i is almost always 0 in the case of a semi-dilute solution and the approximation of equations (3.23) and (3.24) has no real quantitative influence. The term $Min(1, \exp(-\beta\Delta U(r)))$ is the probability with which a scission event is accepted by the Monte-Carlo process, where $\Delta U(r) = U_2(r) - U_1(r)$ is the difference of the two potentials considered in this model for a given r. The $q_s(r) = P(r)P_s^{acc}(r)$ function will be discussed in the next subsection.

2. For recombinations between end-monomers along the pair correlation function $g_{ee}(r)$ of end-monomers, the probability of recombination comes from the end-monomers in the Γ zone and from the probability to accept this closing. The probability of closing P_f is

$$P_f = \int_\Gamma dr g_{ee}(r) \frac{2\phi}{L_0} 4\pi r^2 P_r^{acc}(r) \equiv \frac{1}{2}\frac{\phi}{L_0} Q_r^{eq} \tag{3.25}$$

This gives Q_r^{eq} and q_r as

$$Q_r^{eq} \equiv \int_\Gamma dr q_r(r) = 4 \int_\Gamma dr g_{ee}(r) 4\pi r^2 P_r^{acc}(r) \tag{3.26}$$

$$P_r^{acc}(r) = Min(1, \exp(+\beta\Delta U(r))) \tag{3.27}$$

where $q_r(r)$ function will be discussed in the next subsection.

Using the distribution functions $P(r)$ and $g_{ee}(r)$ computed by the simulation, Q_s^{eq} and Q_r^{eq} for each state points are obtained from equation (3.22) to (3.27). The values are denoted as $\hat{Q}_s^{eq}$ and $\hat{Q}_r^{eq}$ and listed in the Table 3.3 for comparison with the value, denoted as Q_s^{eq} and Q_r^{eq}, obtained from n_s^{st} and n_r^{st}. The comparison shows a good agreement.

3.2.1.6 Micro-reversibility at equilibrium

With our algorithm, micro-reversibility is expected at equilibrium. This implies that we should obtain an equality between the number of scissions and recombinations per

unit time and volume, for any given interval $[r, r+dr]$ in the Γ region. Combining equations (3.15) to (3.27), the micro-reversibility then requires

$$q_s(r)(1 - L_0^{-1}) = \frac{1}{2}\frac{\phi}{L_0^2} q_r(r) \tag{3.28}$$

Using our results for $P(r)$ and $g_{ee}(r)$, this property is verified in figure 3.14. The small observed difference may be caused by the approximation of the term $\left\langle \frac{1}{N_i+1} \right\rangle_r$, by $\left\langle \frac{1}{N_i+1} \right\rangle_\Gamma$ averaged over the Γ interval. We observe also from figure 3.14 that $q_r(r)$ is independent of ω, as expected. The same observation has been noticed for $q_s(r)$ as well.

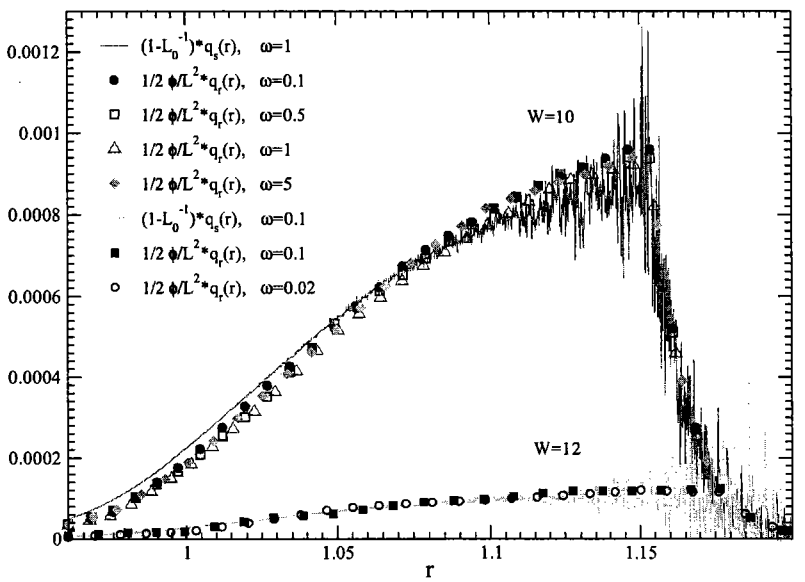

Figure 3.14: Test of micro-reversibility at equilibrium for the two state points (W=10, ω=0.1, 0.5, 1, 5 and W=12, ω=0.02, 0.1). For $W = 10$ case, $\frac{1}{2}\frac{\phi}{L_0^2} q_r(r)$ is shown for $\omega = 0.1$ (dots), 0.5 (empty squares), 1 (triangles), 5 (diamonds), and $(1 - \frac{1}{L_0} q_s(r))$ is shown for $\omega = 1$ (upper continuous line). For $W = 12$ case, $\frac{1}{2}\frac{\phi}{L_0^2} q_r(r)$ is shown for $\omega = 0.02$ (open circles), and 0.1 (filled squares), and $(1 - \frac{1}{L_0} q_s(r))$ is shown for $\omega = 0.1$ (lower continuous line) (see text)

3.2.1.7 Estimate of the macroscopic energy of scission E and the barrier energy of recombination B

As a variant, the kinetics can be reformulated in terms of a competition between pairs of free end-monomers which attempt to fuse and bonds which attempt to open, according to two processes of first order in terms of the number of pairs, used as kinetic variables. Let us define

$$\hat{N}_s(r) = P(r)\phi(1 - L_0^{-1}) \tag{3.29}$$

as the number of bonds per unit volume and per unit of length r having a length $r \in [0, R_c]$, which are available to a scission, and

$$\hat{N}_r(r) = 2\pi \frac{(2\phi)^2}{L_0^2} r^2 g_{ee}(r) \tag{3.30}$$

as the number of pairs of free end-monomer per unit of volume and per unit of length at a distance r. Integrating in both cases over the interval $r \in [0, R_c]$, one finds on the one hand the number of bounded pairs per unit of volume

$$N_s = \int_0^{R_c} dr \hat{N}_s(r) = \phi(1 - L_0^{-1}) \tag{3.31}$$

and on the other hand the quantity

$$N_r = \int_0^{R_c} dr \hat{N}_r(r) = 2\pi \frac{(2\phi)^2}{L_0^2} \int_0^{R_c} dr r^2 g_{ee}(r) \tag{3.32}$$

which is extracted from all pairs of free ends those which lie in the close neighborhood. This defines on the basis of criterion of proximity $r < R_c$, a chemical species of pair of "close" free ends. Let us stress here that this definition is independent of the choice of the interval $\Gamma \in [0, R_c]$, where kinetic effects are possible.

We can thus define a new kinetic constant k_f (closing of pair) which, applied to N_r, gives again the number of recombinations per unit of time and volume, quantity expressed according to the member of right-hand side of equation 3.19, that is

$$k_f N_r = \frac{1}{2} k_r \left(\frac{\phi}{L_0} \right)^2 . \tag{3.33}$$

By combining equations (3.19), (3.26), (3.32), and (3.33), the new kinetic constant is expressed in terms of the chain end pair correlation function $g_{ee}(r)$ as

$$k_f = 2\omega\kappa(\omega)\frac{4\pi\int_0^{R_c} drr^2 g_{ee}(r)P_r^{acc}(r)}{4\pi\int_0^{R_c} drr^2 g_{ee}(r)} = 2\omega\kappa(\omega)\left\langle P_r^{acc}\right\rangle_{R_c} \tag{3.34}$$

By combining equation (3.19), (3.22), (3.29), and (3.31), the kinetic constant k_s can be expressed in a symmetric way,

$$k_s = 2\omega\kappa(\omega)\frac{int_0^{R_c} drP(r)P_s^{acc}(r)}{\int_0^{R_c} drP(r)} = 2\omega\kappa(\omega)\left\langle P_s^{acc}\right\rangle_{R_c} \tag{3.35}$$

On the basis of the equality $k_f N_r = k_s N_s$, and expression (3.34),(3.35), we obtain the relation

$$N_s\left\langle P_s^{acc}\right\rangle_{R_c} = N_r\left\langle P_r^{acc}\right\rangle_{R_c} \tag{3.36}$$

The natural definition of the bonding energy (energy absorbed or released for the transitions) is

$$\exp(\beta E) \equiv \frac{N_s}{N_r} = \frac{\left\langle P_r^{acc}\right\rangle_{R_c}}{\left\langle P_s^{acc}\right\rangle_{R_c}} \tag{3.37}$$

The barrier to scission $\Delta_s = E + B$ and the barrier to recombination $\Delta_r = B$ can be expressed immediately via expressions (3.34) and (3.35) as

$$k_f \equiv \exp(-\beta B) \tag{3.38}$$

$$k_s \equiv \exp\left(-(\beta B + E)\right) \tag{3.39}$$

$$\beta B \equiv -\ln\left(2\omega\kappa(\omega)\left\langle P_r^{acc}\right\rangle_{R_c}\right) \tag{3.40}$$

where 2ω is the frequency of attempts of scissions or recombinations of "bonds" per unit of time. The expression (3.40) gives the barrier of energy to get a successful fusion per unit of time for an "interactive" pair of ends ($r < R_c$). In addition, the expression of the average length of the chains in the theory of (ideal) living polymers arises naturally from our definition of E in equation (3.37). Substituting the numbers of pairs in the member of right-hand side of equation (3.37) by their expression (3.31) and (3.32) and making the approximation of ideal chains $g_{ee}(r) = 1$, we find, as in chapter I (equation (1.19)),

$$L_0 = C^{1/2}\phi^{1/2}\exp\left(\frac{\beta E}{2}\right) \tag{3.41}$$

To test the quantitative aspects of the above discussion, we compute the value of N_r and N_s for each state point by using equations (3.31) and (3.32) based on the simulated $g_{ee}(r)$ and the mean micelle length L_0. Thus, the bonding energy E is obtained via equation (3.37) and the barrier of the recombination B is expressed via expression (3.39). The values of E and B for each equilibrium state point are listed in Table 3.4. The three first rows of Table 3.4 contain the cases of $W = 12$ for which the value of L_0 is found to be 151.4. One should be reminded that in expression (3.41), C is a constant depending upon the monomer size (chapter I).

We also notice from Table 3.4 that $E = W + constant$, implying $L_0 \propto \exp\left(\frac{\beta W}{2}\right)$. So our pair potential bonding energy parameter W plays the same role as E. Table 3.4 also gives our estimate of the barrier B. We observe that B is independent of E (or W) and that B increases when ω decreases, as expected.

Table 3.4: The values of macroscopic energy of scission E, the barrier energy of recombination B, and the indicator X (see text) for various investigated W and ω values. Because of the definition of E in terms of static quantities (equation (3.37)) the values of E are independent of ω.

W	ω	κ	N_s	$N_r * 10^4$	E	B	X
12	0.02	0.93	0.149	0.11	9.5	4.7	0.4
12	0.1	0.72	0.149	0.11	9.5	3.3	1.6
12	1	0.25	0.149	0.11	9.5	2.0	5.8
11	0.1	0.66	0.148	0.31	8.5	3.4	0.6
11	1	0.29	0.148	0.31	8.5	2.0	17.6
10	0.1	0.82	0.147	0.81	7.5	3.4	1.3
10	0.5	0.49	0.147	0.80	7.5	2.3	6.6
10	1	0.32	0.147	0.81	7.5	1.9	13
10	5	0.11	0.147	0.80	7.5	1.4	66

3.2.1.8 Mean chain length vs. scission energy E

We examine now the scaling law of the average chain length versus the energy parameter E. In order to have enough results, an additional thermodynamic state point at the same $T = 1$, $\phi = 0.15$, with $W = 11$ have been investigated using attempt frequency $\omega = 0.1$ and 1. For this state point ($W = 11$), we get $L_0 = 91.2$. We consider for these three semi-dilute solutions at the same ϕ the average chain length following the

function (1.19), written here as

$$L_0(W) = C^{1/2}\phi^{\frac{1}{2}} \exp\left(\beta\frac{E(W)}{2}\right) \tag{3.42}$$

where $E(W)$ is scission free energy [2] for a given value of parameter W. In figure 3.15, we plot in semi-log the average chain length (average over all the ω) of the case of $W = 10$, $W = 11$, and $W = 12$ as a function of E using the value of βE of Table 3.4. The slope of the fitting line is found to be 0.5, and a value of $C = 11.5(2)$. This confirms well the scaling law of Cates, i.e. equation (1.19) and also validates our estimate of E from statistical information at equilibrium.

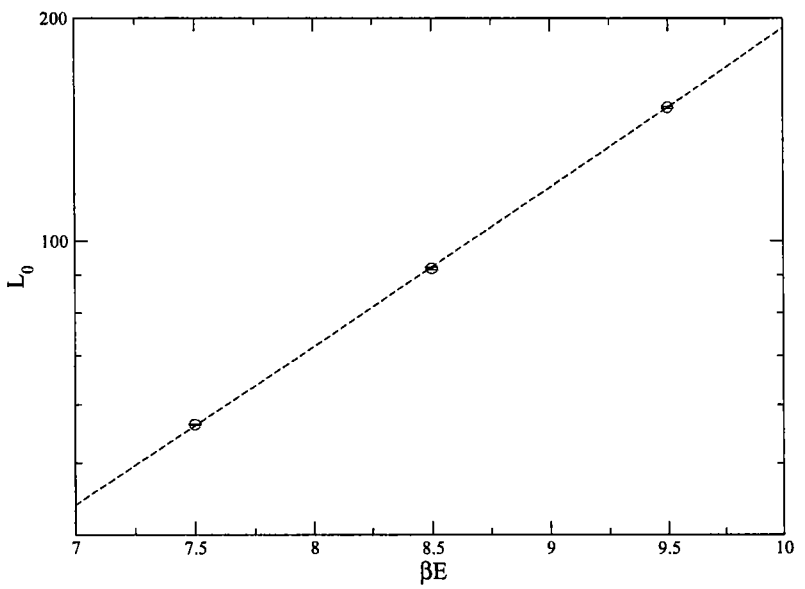

Figure 3.15: Average chain length L_0 versus energy of scission βE. The slope is found to be $\simeq 0.5$, which confirms the theoretical prediction (equation 1.19).

3.2.1.9 Relevance of different time scales for the kinetics

In this subsection, a discussion presented by O'Shaughnessy and Yu [12], closely related to subsection 3.2.1.7, is analyzed. In this article [12], one considers as indicator of the type of kinetics the dimensionless ratio

$$X = \frac{t_h}{\tau_b^{st}}. \tag{3.43}$$

t_h is the conceptual time it would take for a newly created free end to diffuse through the fluid over a distance corresponding to the mean distance between free ends $h = (\frac{L_0}{2\phi})^{1/3}$ (assuming it does not react), and $\tau_b^{st} = \frac{1}{2\omega Q_s^{eq} L_0}$ is the life time of the average chain (in the short time analysis sense where all transitions are considered).

The definition of X can be reformulated using the kinetic constants. We show here that our new kinetic constant k_f defined by equation (3.33) is identical to Q_{rec} of Ref. [12], the recombination rate of two overlapping chain ends of size b. From the definition of k_f, and assuming $\kappa(\omega) \longrightarrow 1$, one has for the recombination rate constant k_r^{st} :

$$k_r^{st} = 4k_f 4\pi \int_0^{R_c} dr r^2 g_{ee}(r) \equiv 4k_f b^3, \tag{3.44}$$

Where b is the chain end size according to the notation of O'Shaughnessy and Yu [12]. According to scission-recombination equilibrium, one has

$$Q_{rec} * b^3 \rho_{ends}^2 = \rho_{ends}/\tau_b, \tag{3.45}$$

where $\rho_{ends} = \frac{1}{h^3}$ is the density of ends. The right hand side represents the breakup rate. As $\rho_{ends} = \frac{2\phi}{L_0}$, $\tau_b = \frac{1}{k_s L_0}$, equations (3.45) can be rewritten as:

$$\frac{1}{2} Q_{rec} * b^3 \left(\frac{2\phi}{L_0}\right)^2 = \frac{1}{2}\left(\frac{2\phi}{L_0}\right)(k_s L_0) = \phi k_s^{st}. \tag{3.46}$$

Notice that in the last equality, we assumed $\kappa(\omega) \longrightarrow 1$ $(k_s \simeq k_s^{st})$. According to equation (3.19),

$$k_s^{st}\phi = \frac{1}{2}\left(\frac{\phi}{L_0}\right)^2 k_r^{st} \tag{3.47}$$

This results in (see (3.44) and (3.46)):

$$Q_{rec} = k_f. \tag{3.48}$$

Further, the authors of [12] introduced a time t^* which corresponds to the average time needed for two chain ends newly created by a scission to recombine with one another. The explicit expression of t^* is related to our kinetic constant k_r^{st}. In fact, we define x_{t^*} the diffusion distance corresponding to t^* (Rouse regime) as

$$x_{t^*}^2 = At^{*1/2}. \tag{3.49}$$

It is equivalent to

$$x_{t^*} = A^{1/2} t^{*1/4}. \tag{3.50}$$

As we have [12]

$$\frac{t^* Q_{rec} b^3}{x_{t*}^3} \approx 1, \tag{3.51}$$

i.e. the total recombination probability at time t^* after a scission is equal to 1. We obtain ((3.50)+(3.51) and (3.44)+(3.48))

$$t^* = \left(\frac{A^{3/2}}{Q_{rec} b^3}\right)^4 = \left(\frac{4A^{3/2}}{k_r}\right)^4, \tag{3.52}$$

On the other hand, we have $h^2 = A t_h^{1/2}$ (Rouse regime), and $h = \left(\frac{L_0}{2\phi}\right)^{1/3}$ giving

$$t_h = \left(\frac{L_0^{1/3}}{(2\phi)^{1/3} A^{1/2}}\right)^4. \tag{3.53}$$

The ratio of t_h to t^* gives

$$\frac{t_h}{t^*} = \left(\frac{L_0^{1/3} k_r}{2^{7/3} \phi^{1/3} A^2}\right)^4 = \left(\frac{L_0^{7/3} k_s}{(2\phi)^{4/3} A^2}\right)^4 \equiv X^4. \tag{3.54}$$

As $k_s^{st} = \frac{1}{\tau_b^{st} L_0}$, equation (3.54) confirms

$$X = \frac{L_0^{4/3}}{(2\phi)^{4/3} A^2} L_0 k_s = t_h L_0 k_s = \frac{t_h}{\tau_b^{st}} \tag{3.55}$$

O'Shaughnessy and Yu [12] defined situations where $X \gg 1$ to obey diffusion controlled kinetics (self-recombination dominate). The opposite cases $X \ll 1$ correspond to mean field kinetics where a chain end recombines with a arbitrary uncorrelated free end. Using our result for the constant A ($A \approx 1$) [18], we have $t_h \approx 1080$ and 4018 for $W = 10$ and 12 respectively, while $\tau_b^{st} = 82\omega^{-1}$ and $170\omega^{-1}$ respectively, this gives values of X for our different state points (listed in Table 3.4). Despite that values of X are larger or around unity, the dynamics of our micellar system at equilibrium may follow MF kinetics predictions for the relaxation of dynamical quantities, provided the rate constants are interpreted as the effective ones (obtained e.g. by a cumulative hazard analysis). This turns out to be equivalent to a renormalization of the rates to eliminate the effects of the unavoidable self-recombinations.

3.2.2 Analysis of the Monomer Diffusion

The mean square displacements (MSD) of the segments of the polymers, as a function of time, is an interesting probe of the polymer dynamics. For a system of unentangled monodisperse dead polymers of size L, the MSD usually follows a Rouse-type behavior for short times (scaling as $t^{0.6}$ or $t^{0.5}$) followed by an Einstein diffusion behavior for long times. The crossover time is on the order of the single chain Rouse relaxation time $\tau_R = \tau_0 L^2$. For "living" polymer system, as the monomers belong to a polydisperse set of chains which continuously break and recombine, the behavior of the MSD is expected to be rather complex. Thus, in this subsection we will focus on the analysis of the coupling between the Rouse relaxation and the effect of scission-recombination mechanism.

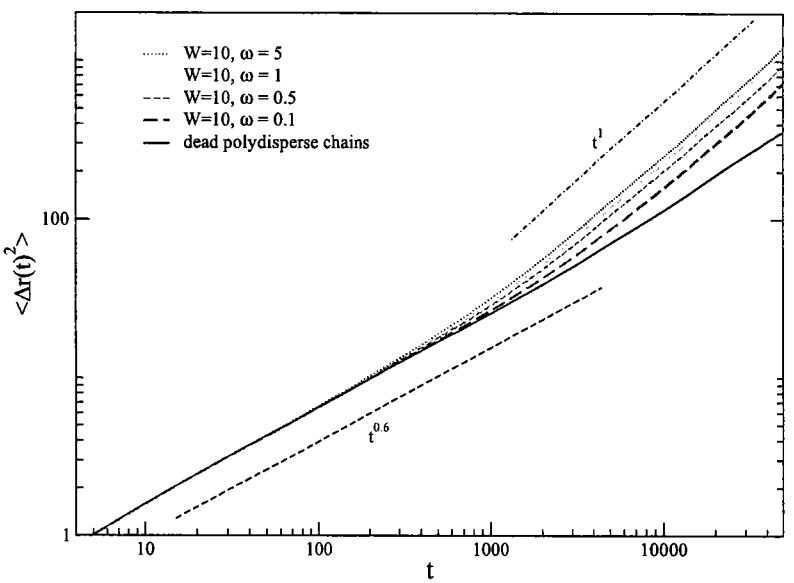

Figure 3.16: Mean square displacements of monomers (semi-dilute case (W=10)). The continuous curve has been obtained for the relevant polydisperse sample but with ω set to zero, averaging over many independent initial configurations. It is a reference from which the other curves depart at decreasing times when increasing values of ω are considered. The cases $\omega = 0.1$ (thick dashed lines), $\omega = 0.5$ (thin dashed lines), $\omega = 1.0$ (dot-dashed lines) and $\omega = 5.0$ (dotted lines) are shown together with two indicative power laws which suggest the evolution of the subdiffusive scaling regime to the normal diffusion limit.

The mean squared displacement (MSD) of all monomers as a function of time is

shown in Figure 3.16 for all ω's in one of the semi-dilute cases (W=10). As shown in figure 3.16, up to a time of 100, the MSD is ω independent and presents a Rouse-like behavior with a time dependence $t^{0.6}$. In the reference case where ω was set to zero (we simulate a polydisperse sample of dead polymers), this power law behavior persists at least up to the time 5000, a time corresponding to the Rouse time of a chain of length 54. When scissions and recombinations are allowed, the MSD deviates from the master curve (of dead polymers) to adopt progressively a MSD linear in time. This takes place sooner and sooner for increasing values of ω. At long times ($t > 2000$), the MSD has evolved towards usual Einstein diffusion with a diffusion coefficient increasing with k_s.

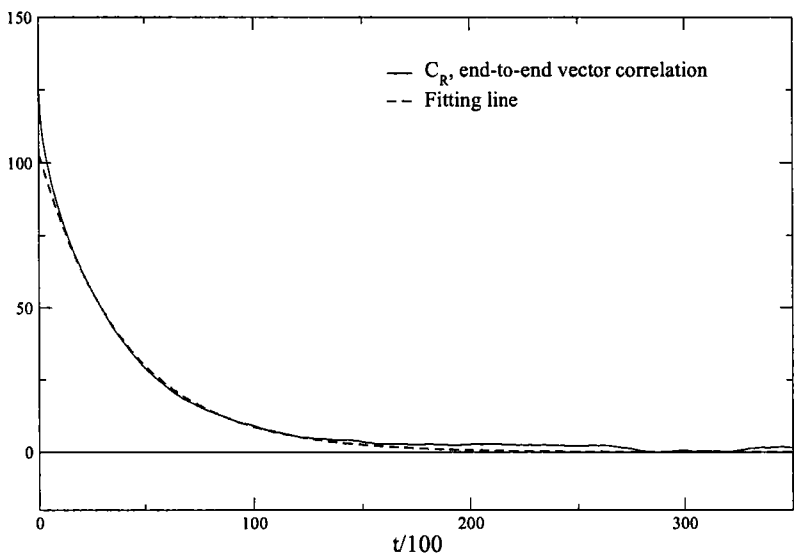

Figure 3.17: The end-to-end vector relaxation function obtained by a Brownian dynamics run on a monodisperse sample of 20 dead polymers of length $L = 50$. The Rouse relaxation time $\tau_R = 4.24\ 10^3$ is given by the fit. Results for $t > 300$ are very noisy and should be zero.

To discuss the monomer mean squared displacement, it is also important to have an estimate of the longest internal relaxation (Rouse) time of the chains. Performing a separate Brownian dynamics run on a monodisperse sample of 20 "dead" polymers of length L=50 (corresponding roughly to the mean polymer length of our living polymer sample) at the same semi-dilute state point ($T = 1$, $\phi = 0.15$, $W = 10$), as shown in figure 3.17, we get from the long-time exponential behavior of the end-to-end vector

relaxation function a value of $\tau_R = 4.24\ 10^3$ [48]. For our very flexible polymers, the scaling of the Rouse time with L in the semi-dilute conditions should be

$$\tau_R(L) = \tau_0 L^2, \tag{3.56}$$

where τ_0 is a constant depending on the solvent conditions and the persistence length [48]. On the basis of our estimated value of τ_{50}, we get $\tau_0 \approx 1.70$.

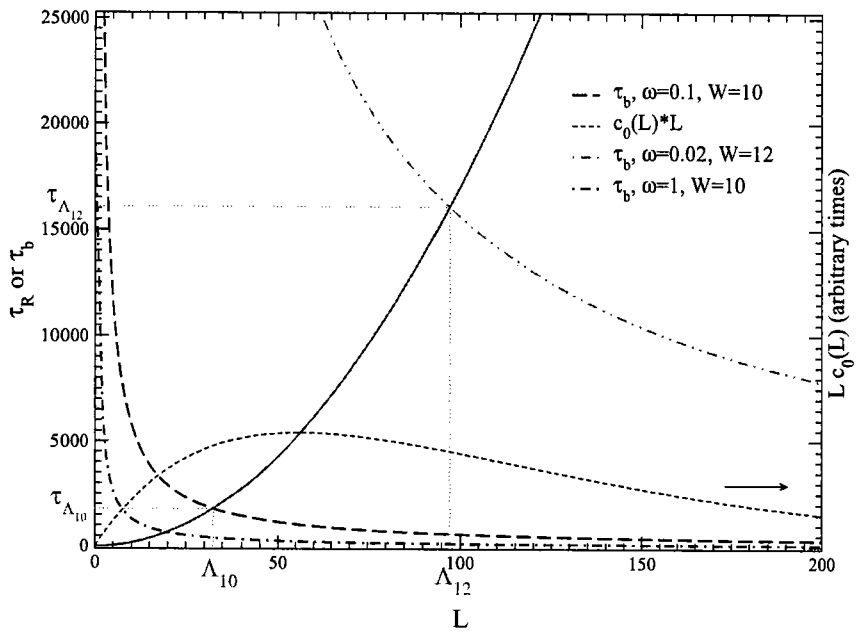

Figure 3.18: Characteristic times as a function of polymer size. The Rouse relaxation time $\tau_R = 1.70 * L^2$, shown as continuous curve, must be compared to the life time of a polymer of size L, given by $\tau_b = (k_s L)^{-1}$. Three frequencies are illustrated, namely $\omega = 1.0$, $W = 10$ (dot-dashed line), $\omega = 0.1$, $W = 10$ (dashed line) and $\omega = 0.02$, $W = 12$ (double dot dashed line) using effective k_s values. The largest values of length Λ for the two state points studied are indicated by the *dot lines* namely Λ_{10} and Λ_{12} respectively. The relaxation times corresponding to the two Λ values are also indicated. We show on the same graph the distribution of monomers (thin dashed curve) as a function of the size of the polymer to which they belong to for the case $W = 10$ (see text).

For living polymers, the degree to which the relaxation of chains is affected by the scission and recombination kinetics depends on their relative time scales. The time scale for the scission/recombination process has been estimated so far in terms of the

Table 3.5: Table of Λ, τ_Λ, τ^* and the diffusion coefficient D for the cases of $W = 10$ and $W = 12$.

W	ω	k_s	Λ	τ_Λ	τ^*	D	L_0
10	0.1	$1.72\ 10^{-5}$	32.43	1788	4401	2.4210^{-3}	56.2(6)
10	0.5	$5.51\ 10^{-5}$	22.02	824	2283	3.1410^{-3}	56.2(1)
10	1	$7.63\ 10^{-5}$	19.75	663	1465	3.7410^{-3}	56.2(2)
10	5	$1.26\ 10^{-4}$	16.72	475	1199	4.0510^{-3}	56.6(6)
12	0.02	$6.39\ 10^{-7}$	97.28	16087	42076	7.0110^{-4}	151(4)
12	0.1	$2.57\ 10^{-6}$	61.17	6361	14616	1.1310^{-3}	150.7(5)
12	1	$9.54\ 10^{-6}$	39.50	2653	6427	1.6310^{-3}	150.4(6)

average survival time $\frac{1}{k_s L_0}$ for the chain of average size, a quantity which was found to vary from $\approx$ 100 up to $\approx$ 10000 in the investigated ω range (see table 3.3). In the present context, we consider the explicit L dependent survival time $\propto \frac{1}{k_s L}$, at a given ω value, and figure 3.18 shows the resulting functions for two such frequencies. In figure 3.18 the distribution of monomers as a function of the size of the chain to which they belong to is also given.

On the basis of the above considerations, it is useful to recall the definition (see Chapter 1) of the particular chain length Λ for which the Rouse time is equal to the survival time [36, 14] ,

$$\tau_\Lambda = \tau_0 \Lambda^2 = \frac{1}{k_s \Lambda}, \tag{3.57}$$

giving

$$\Lambda = (\tau_0 k_s)^{-1/3} \tag{3.58}$$

and

$$\tau_\Lambda = \tau_0^{1/3} k_s^{-2/3} \tag{3.59}$$

where $\tau_0 = 1.70$.

Using our previous estimations of k_s (Table 3.3), Λ and τ_Λ are calculated and listed in Table 3.5. Chains longer than Λ have their internal dynamics strongly altered by the kinetics, while chains shorter than Λ should have an internal dynamics little affected with respect to dead polymers of the same size. As figure 3.18 illustrates, when the scission attempt frequency increases, the fraction of monomers which belong to chains whose dynamics is little affected by scissions decreases. The inequality $\Lambda < L_0$ verified

in our simulations implies that the chain dynamics is strongly affected by the scission-recombination mechanism. This inequality and equation (3.58) also imply

$$k_s \geq \left(\tau_0 L_0^3\right)^{-1} \tag{3.60}$$

The implications of the scission-recombination mechanism on the mean squared displacement of monomers is analyzed as follows. As we see in figure 3.18, monomers belong dominantly to chains of length $L > \Lambda$ so that, in the absence of scissions, the monomer diffusion within a chain of size L would become Einstein-type after a time $\approx \tau_R(L) = \tau_0 L^2$ needed for all the slowest intramolecular modes to have relaxed to zero. The effect of scissions will restrict the lifetime of a chain fragment of length L' to $\tau_b(L') = 1/(k_s L')$ and thus restrict similarly the life time of any Rouse mode implying a number L' of monomers to $\tau_b(L')$. This means that within a chain of size $L > \Lambda$, the Rouse modes associated with chain fragments of length L' in the range of $\Lambda < L' < L$ will relax artificially fast, on a time scale $\tau_b(L')$ which is even shorter than τ_Λ. On the other hand, the Rouse modes associated with chain fragments of length L' shorter than Λ will relax as in similar fragments of dead polymers. Consequently, at long times, the monomer mean squared displacement will thus become Einstein-type after a time of order of τ_Λ.

The crossover time between Rouse-type and Einstein-type is verified. In figure 3.19, we show the mean squared displacement of monomer for $\omega = 0.1, 0.5, 1, 5$ for the case $W = 10$ and $\omega = 0.02, 0.1, 1$ for the case $W = 12$. We plot the asymptotes of the short time ($t^{0.6}$) and long time (t^1). Their intercept defines the crossover time τ^*. Numerical values of τ^* for the different ω and W are listed in Table 3.5.

Figure 3.20 shows τ^* vs k_s on a log-log scale. A two parameters fit gives $\ln \tau^* = 1.06 - 0.67 \ln k_s$. This shows $\tau^* \propto k_s^{-2/3}$, i.e. the k_s dependence of τ^* is identical to that of τ_Λ. Using equation (3.59) and the value of the prefactor, we obtain $\tau^* \approx 2.4\tau_\Lambda$, as indicated by Table 3.5 as well. This confirms that τ_Λ is indeed the relaxation time regarding the dynamics of the living polymer chains.

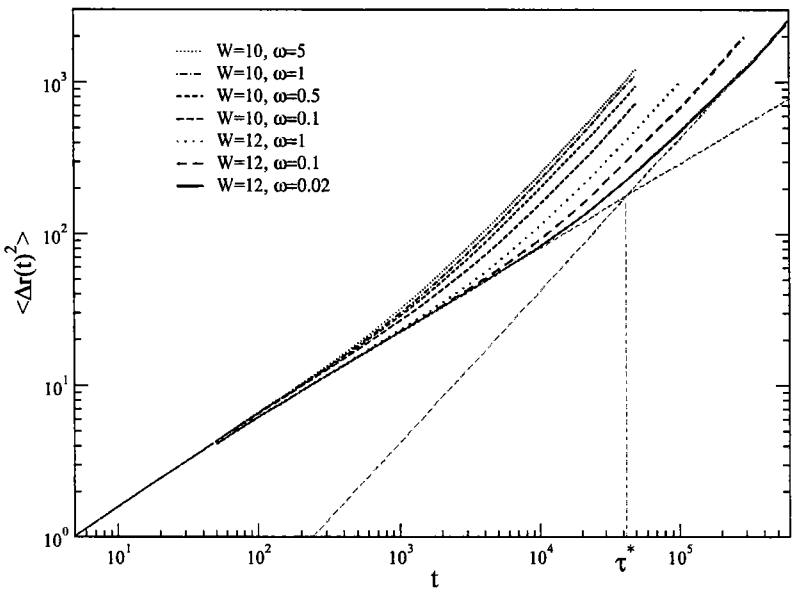

Figure 3.19: Mean squared displacements of monomers for $\omega = 0.1, 0.5, 1$ and 5 for the case $W = 10$ and for $\omega = 0.02, 0.1$ and 1 for the case $W = 12$. For $\omega = 0.02$ the short time ($t^{0.6}$) and long time (t^1) asymptotes are drawn. Their intercept defines the crossover time t^*.

3.2.2.1 Self-diffusion coefficient D of the monomers versus the scission rate constant k_s

The mean square displacement in the long time limit gives the self-diffusion coefficient of a monomer. The diffusion coefficient D can be obtained by using the relation:

$$D = \lim_{t\to\infty} \frac{1}{6t} \left\langle |\overline{r}(t) - \overline{r}(0)|^2 \right\rangle \tag{3.61}$$

The value of D for the studied cases are listed in Table 3.5. We can plot D as a function of k_s. As shown in figure 3.21 the diffusion coefficient D is observed to scale like $k_s^{1/3}$ in the explored ω range. The result is in good agreement with the 1/3 power law behavior observed by Milchev with the lattice bond fluctuation model (BFM) [14]. The 1/3 power law scaling can be explained by assuming that clusters of Λ monomers are responsible for the long time behavior of living polymers, giving

$$D \propto \frac{R_g^2(\Lambda)}{\tau_{Rouse}(\Lambda)} \propto \frac{\Lambda}{\Lambda^2} \propto \Lambda^{-1} \propto k_s^{1/3}. \tag{3.62}$$

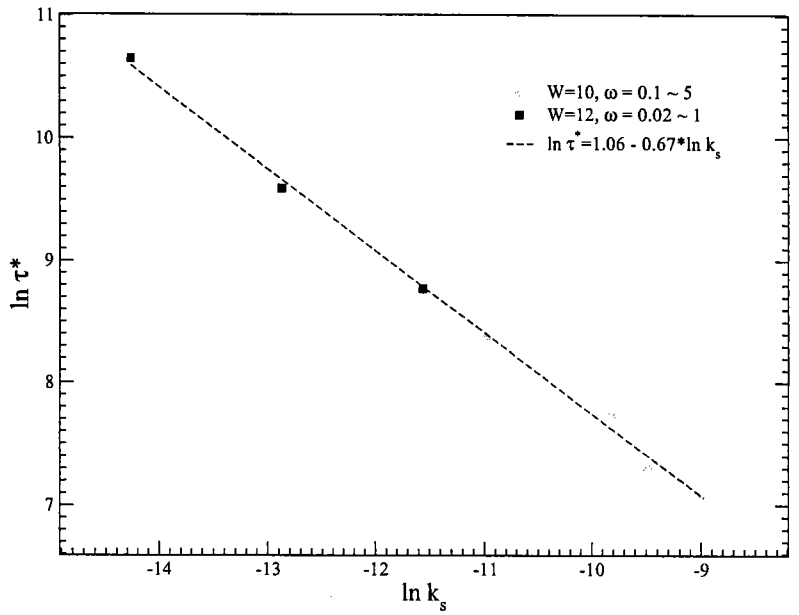

Figure 3.20: τ^* is plotted versus k_s on a log-log scale. The *dashed line* with slope $(-2/3)$ corresponds to a power law $\tau^* \propto k_s^{-2/3}$

This result shows again the relevance of the characteristic length Λ in describing the dynamics of the living polymers.

3.2.3 Zero-shear stress time autocorrelation functions

The stress relaxation function is an important macroscopic relaxation function for micellar system. Our dynamically unentangled system must indeed be the object of a coupling between the stress relaxation and the scission-recombination process if the corresponding times scales distributions of both processes overlap.

According to the theoretical description presented in chapter I, the stress relaxation function is

$$G(t) = \sum_{p=1}^{\infty} W_p G_p'(t) \tag{3.63}$$

where the weight function W_p can be obtained from the distribution of chain lengths $c_0(L)$, and where

$$G_p'(t) = G_0 \frac{1}{p} \sum_{q=1}^{p} \exp\left(-\frac{t}{\tau_\Lambda}\left[\frac{p}{q_\Lambda} + 2\left(\frac{q\Lambda}{p}\right)^2\right]\right) \tag{3.64}$$

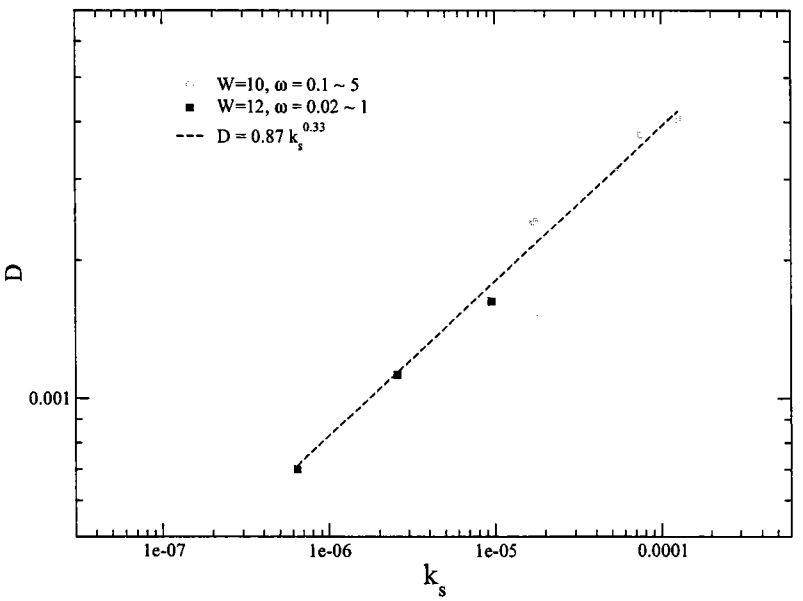

Figure 3.21: Monomeric Einstein diffusion coefficient as a function of k_s for the two semi-dilute cases ($W = 10$ and $W = 12$). The value of D is obtained from the long time behavior of the monomeric mean square displacement shown in figure 3.19. The *dashed line* represents a $k_s^{1/3}$ power law.

is the relaxation function for chains of length p. It is an equation with only three parameters, namely G_0, k_s, and τ_0 or equivalently G_0, Λ, and τ_0. Actually, in the case where $L_0 > \Lambda$, the long time ($t \gg \tau_\Lambda$) asymptotic expression of the stress relaxation function becomes independent of the chain length distribution and one gets [36]

$$\lim_{t \gg \tau_\Lambda} G(t) = A\sqrt{\frac{\tau_0}{t}} \exp(-t/\tau_{relax}), \tag{3.65}$$

where the relaxation time $\tau_{relax} = (2^{2/3}/3)\tau_\Lambda$ and where $A = G_0\sqrt{\pi/3}$

We have performed at equilibrium, a series of long runs, with three of our ω values, namely $\omega = 0.1, 1$, and 5, to compute the stress-stress time correlation function. Within the linear response theory, this stress-stress time correlation function is related to the stress relaxation function in case of weak external perturbation. From our LD trajectories, we estimated the zero shear stress relaxation modulus $G(t)$ via the equilibrium stress tensor time correlation function [8]

$$G(t) = \frac{V}{k_B T} \langle \sigma_{xy}(t)\sigma_{xy}(0) \rangle \tag{3.66}$$

As it has often been experienced in the past, these functions are extremely noisy and require very long runs to get a signal out of the noise. We therefore applied an aliasing procedure with time window equal to 400. Given the noise in our data, we simply checked the plausibility of expression (1.64) by estimating it with the known values of τ_0 and Λ mentioned in Section 3.2.2. Adjusting G_0 as the single free parameter to match simultaneously the three curves corresponding to ω=0.1, 1, and 5, we get $G_0 \approx 0.22$. The resulting curves shown in figure 3.22 indicate a reasonable agreement with simulation data for $t > \tau_{relax}$, confirming that our equilibrium polymer system behaves in a way consistent with the hypotheses of Faivre and Gardissat, on the basis of the effective rate constants determined separately.

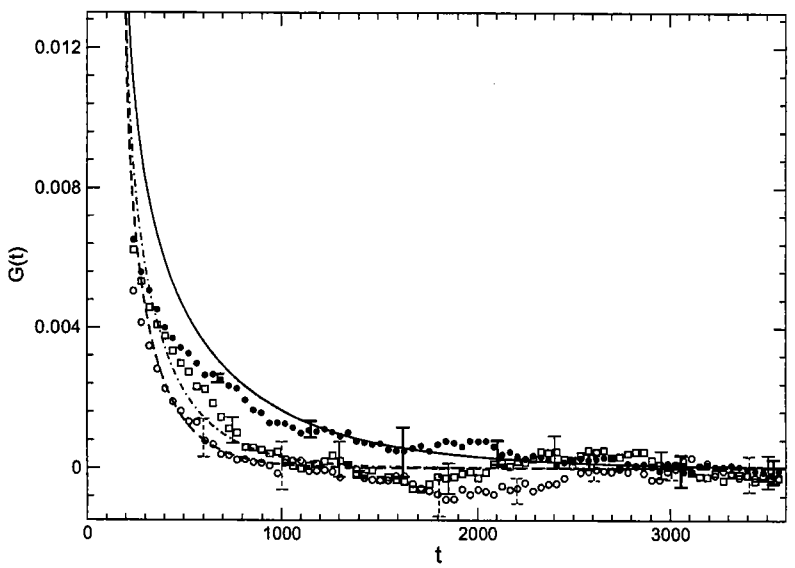

Figure 3.22: Simulation results of the zero shear stress relaxation modulus $G(t)$ for $\omega = 0.1$ (dots), $\omega = 1$ (squares), and $\omega = 5$ (circles). The lines represent the theoretical curves based on equation (3.63), after fitting the amplitude G_0 (see text).

3.2.4 Macroscopic relaxation behavior

In order to make another check of the macroscopic relevance of the effective kinetic constants determined at temperature T=1.0 for various attempt frequencies ω, we performed a T-jump experiment [27, 46] in a particular case. First, the system is equilibrated at a temperature T_0 with average length $L_0(T_0)$. At some arbitrary time,

chosen as time origin, we switch the temperature to $T < T_0$ in the LD simulations and we follow the transient evolution of the averaged chain length from $L_0(T_0)$ to $L_0(T)$. The theoretical expression for the macroscopic relaxation behavior of a T-jump has been given in chapter I. In equations (1.46) and (1.47), τ can be related to the average chain length life time τ_b [Equation (1.36)] through

$$\tau = \frac{1}{2k_s(T)L_0(T)} = \frac{1}{2}\tau_b(T). \tag{3.67}$$

Notice that $\tau_b(T)$ (or $k_s(T)$) are already known by equilibrium simulations

In figure 3.23, we display our results of the transient mean chain length $< L(t) >$ versus t for ω=1 based on an average of 50 independent LD trajectories, starting with equilibrium at T_0=1.2 [at which $L_0(T_0) = 26$] and setting T=1 [having $L_0(T) = 56.5$] abruptly. The data correspond to state point 2. The simulation results are fitted with the theoretical curve [Equation (1.45)], using a single free parameter τ, giving an estimate of the kinetic constant $k_s = 8.02 \times 10^{-5}$, using equation (3.67), in good agreement with our previous estimates based on microscopic kinetics, 7.63 10^{-5} (Table 3.3).

3.3 General comments

In this chapter, we have exploited our mesoscopic model of cylindrical micelles to study the structure and the dynamics of these complex systems at dilute and at semi-dilute equilibrium state points. The results of static properties, found to be governed by the monomer density and the end cap energy, are consistent with the theory and previous simulation works. The dynamics and kinetics at the semi-dilute state points has been more specifically investigated. Our study is focused on the evolution of various dynamical properties when, for the two state points corresponding to semidilute situations, the barrier height of the scission/recombination process is varied over a large range. This range is however, restricted in this study to the most interesting situation where a significant coupling exists between the intramolecular relaxation of the "temporary" chains and the scission/recombination mechanism.

The simple mean-field kinetic model of Cates [9, 27] is found to be valid for times of the order and beyond the mean lifetime of a chain of average size provided that the "short time" kinetic constants computed directly from the number of Monte Carlo

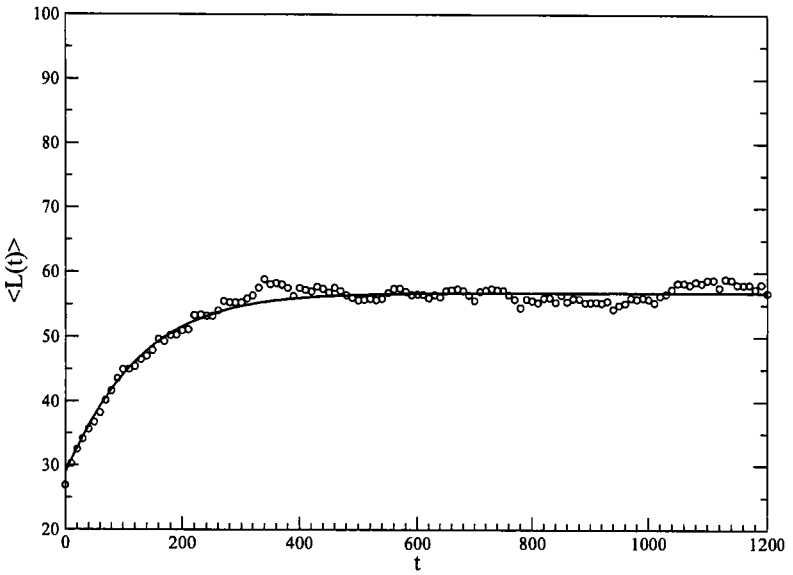

Figure 3.23: Time evolution of $\langle L(t) \rangle$ for the T-jump experiments, with w=1, starting at equilibrium at temperature T_0=1.2 and setting at t=0 the temperature to T=1. Simulation results are shown as circles and the theoretical curve according to equation (1.45) by the continuous line.

accepted binding/unbinding changes are rescaled by a transmission coefficient κ. The quantity $(1-\kappa)$ can be interpreted as a measure of the fraction of unsuccessful scissions which are almost immediately followed by a recombination of the two ends just created. Dynamic properties sensitive to the "intermediate" and "long" time effects of the scission/recombination kinetics, such as the average chain length time dependence in a T-jump experiment, the monomer diffusion and the stress relaxation, were all found to be related to the effective rate constants, according to mean-field-like theories. These effective constants need to be distinguished from their short time values and we note that the correcting transmission coefficient was found to vary from 0.93 down to 0.12 when going from the lower to the hightest ω values chosen.

We observed that, as it could be expected, the transmission coefficient estimated on the basis of a time scale separation turns out to be close to the fraction of recombinations involving the reunion of a chain end with a new partner with respect to the partner it originally detached from. The effective rate constants have been estimated by different techniques. The cumulative hazard technique introduced by Helfand to com-

pute isomerization rates in chain molecules has been found to be particularly efficient as it avoids the need of binning recombination time data or the explicit computation of time correlation functions. The distribution of first recombination times $\psi(t)$ remains, however, a central function. At short times, it is dominated by its self-recombination contribution which follows the $t^{-5/4}$ power law decay predicted by O'Shaughnessy and Yu [12]. At long times, it becomes exponential with a time decay characterized by the average chain length lifetime $\frac{1}{(k_s L_0)}$ providing an estimate of the effective rate constants.

To sum up, we find that in cylindrical micellar solutions the distinction between mean-field and diffusion controlled kinetics can be entirely related to the value of the transmission coefficient κ. When this value is close to unity, the kinetics is purely mean field and no recombination with the original partner is observed within the process of relative separation of the newly created chain ends by diffusion. When κ is much smaller than unity, the diffusion controlled kinetics model applies but simply means that only a fraction $(1-\kappa)$ of scissions survive on the long time scale which can still be described by the mean-field kinetics model of Cates, provided that rescaled kinetics constants are used. The kinetic constants can be related to the structural functions, i.e. the distribution of bonding lengths $P(r)$ and the chain ends pair correlation function $g_{ee}(r)$. This analysis allows us to verify the micro-reversibility of the system and to estimate the macroscopic energy of scission E and the barrier energy of recombination B. The latter analysis shows that the pair potential bonding energy parameter W of our model plays a role equivalent to E, i.e. $L_0 \propto \exp\left(\frac{\beta W}{2}\right)$. The barrier B increases when ω decreases, and as expected, it follows $\omega\kappa(\omega) \propto \exp(-\beta B)$. By the studies of the monomer diffusion and zero-shear stress functions, we also find that the main relaxation time in the system is indeed τ_Λ, the life time of the dynamical units of chain size Λ for which the life time of chain $\frac{1}{(k_s \Lambda)}$ is equal to it's Rouse relaxation time $\tau_0 \Lambda^2$, which is found to play an essential role in the linear viscoelasticity.

Chapter 4

Non-equilibrium properties

In this chapter we are interested in the rheology and the kinetics of scission-recombination of giant cylindrical micelles in a dynamically unentangled semi-dilute solution. The main goal of our study is to investigate the viscous and structural responses to the imposition of an homogeneous shear flow in this particular self-assembling system when the micelle scission-recombination kinetics and the shear flow influence are strongly coupled.

Based on the analysis of monomer diffusion at equilibrium addressed in section 3.2.2, we can expect a coupling between the shear flow ordering effects and the scission-recombination relaxation mechanism when the life time of the equilibrium average size chain is smaller than its Rouse relaxation time,

$$\tau_b(L_0) < \tau_R(L_0) = \tau_0 L_0^2. \tag{4.1}$$

The ω values for the equilibrium state were precisely chosen to satisfy this inequality, and thus, we have kept the same four values $\omega = 0.1$, 0.5, 1 and 5 for the non-equilibrium state. We are led to define a central parameter which is the reduced shear rate

$$\beta_\Lambda = \dot{\gamma}\tau_\Lambda \tag{4.2}$$

and we show in this chapter that most physical properties of our system are universal functions of this reduced rate.

Shear flow was maintained by setting up Lees Edwards boundary conditions [49, 51] together with imposing a solvent velocity field $\bar{u}(y) = \dot{\gamma} y \bar{1}_x$. After eliminating the transient period needed to reach stationary conditions at the imposed temperature, all

simulation runs were followed for a total time of $T_{max} = 2.5\ 10^5$ corresponding to $5\ 10^7$ time steps. Values of shear rates were selected in the range $5.6\ 10^{-5} \leq \dot{\gamma} \leq 0.21$ to adjust specific reduced shear rates $\beta_\Lambda = 0.1, 0.25, 0.5, 1, 5, 10, 50$ and 100 for the four ω values studied at equilibrium (see table 4.1).

4.1 Collective rheological behavior

The present section deals with the collective rheological behavior of giant cylindrical micelles in semi-dilute solution, the main point under investigation being the influence of the scission-recombination kinetics upon the viscous and structural responses to shear for this type of complex fluids, which, otherwise, shares many analogies with polymer solutions [54, 53].

4.1.1 Orientation of the chains

To investigate the orientational properties of the cylindrical micelles system subjected to a simple shear flow, we have adapted the methodology used to standard polymer solution. When polymer solutions are subjected to shear flow, the chains in the solution are oriented (on average) and deformed by the flow. Birefringence and neutron or light scattering experiments [59] reveal that individual polymers increasingly deform and orient along the flow direction as the shear rate increases. Those phenomena can be quantitatively probed through the anisotropy arising in any relevant tensorial quantity, such as the bond order parameter tensor $\bar{\bar{O}}$, the polymer bond stress tensor $\bar{\bar{\sigma}}$, and the radius of gyration tensor $\bar{\bar{G}}$ defined respectively as

$$\bar{\bar{O}} = \frac{1}{\sum_\alpha \{N(\alpha) - 1\}} \sum_\alpha \sum_{i=1}^{N(\alpha)-1} \left\langle \frac{\bar{u}_{i\alpha}\bar{u}_{i\alpha}}{u_{i\alpha}^2} - \frac{\bar{\bar{1}}}{3} \right\rangle \tag{4.3}$$

$$\bar{\bar{\sigma}} = -\frac{1}{V} \left\langle \sum_{i=1}^{N} m_i \bar{v}_i \bar{v}_i + \sum_{i=1}^{N-1} \sum_{j=i+1}^{N} (\bar{R}_i - \bar{R}_j)\bar{F}_{ij} \right\rangle \tag{4.4}$$

$$\bar{\bar{G}}(L) = \frac{1}{2L^2} \sum_{n=1}^{L} \sum_{m=1}^{L} \left\langle (\bar{R}_n - \bar{R}_m)\,(\bar{R}_n - \bar{R}_m) \right\rangle \tag{4.5}$$

where $N = \sum_\alpha N(\alpha)$ is the total number of polymeric monomers, α an index over all polymers in the system and $N(\alpha)$ the number of monomers of polymer α. Where

$\bar{u}_i = \bar{R}_{i+1} - \bar{R}_i$, $\bar{\bar{1}}$ is the unit tensor, and $\bar{F}_{ij}$ is the force exerted by particle j on particle i. At equilibrium the system is isotropic and the tensorial quantity, say $\bar{\bar{A}}$ reduces to a scalar. In the presence of a shear flow $\bar{u}_s(\bar{r}) = \dot{\gamma} y \bar{l}_x$, any tensoral quantity takes the structure

$$\bar{\bar{A}} = \begin{pmatrix} A_{xx} & A_{xy} & 0 \\ A_{yx} & A_{yy} & 0 \\ 0 & 0 & A_{zz} \end{pmatrix} \tag{4.6}$$

as a result of the symmetry.

The extinction angle χ_O, defined through the relation

$$\cot(2\chi_O) = \frac{O_{xx} - O_{yy}}{2O_{xy}}, \tag{4.7}$$

measures the rotation around z-axis of the principal axes (I, II, III) of the tensor $\bar{\bar{O}}$ with respect to the flow axes (x, y, z). In shear flow, O_{xy} starts linearly with $\dot{\gamma}$ while the first contribution to $O_{xx} - O_{yy}$ is of order $\dot{\gamma}^2$. Therefore the linear (Newtonian) regime is characterized by $\chi_O = \pi/4$. Outside the linear regime, χ_O decrease to zero for increasing shear rate.

Single polymer theories[8] have shown that, for a polymer solution with chains of size L, the birefringence angle χ_O decreases with shear rate according to

$$\cot(2\chi_O^L) = \frac{\beta_L}{m_O}, \tag{4.8}$$

where m_O, know as the flow resistance, is a constant which depends upon the solvent quality and the importance of hydrodynamic interactions. At larger shear rates, equation 4.8 is still used as a definition of the effective flow resistance $m_O(\beta_L)$, a quantity which has been measured by simulation of polymers in shear flow, as shown in Ref [53]. It is found that m_O follows an effective power law $m_O = c\beta_L^{0.6}$. This leads to

$$\cot(2\chi_O^L) = c^{-1}\beta_L^{\alpha}, \tag{4.9}$$

where $\alpha = 0.4$ for the extinction angle. The crossover from the linear regime taking place around $\beta_L \approx 2$

Similarly to the birefringence angle χ_O, the anisotropy can also be probed through the stress tensor $\bar{\bar{\sigma}}$ or the average single chain gyration tensor $\bar{\bar{G}}$, defining χ_σ and χ_G using equation 4.8. For χ_G, we note that equation (4.9) applies also to χ_G with $\alpha = 0.46$ [53].

Applying the expressions (4.9) to individual chains within a polydisperse sample, longer chains will be oriented closer to the flow direction than shorter ones. If χ_O^L (or χ_σ^L) the conceptual orientation angle specific to the subset of chains of size L within the sample subject to shearing flow, one should have

$$\cot\left(2\chi_O^L\right) = c^{-1}\dot{\gamma}^\alpha \tau_0^\alpha L^{\mu\alpha}, \tag{4.10}$$

where we have assumed that $\tau_L = \tau_0 L^\mu$ in terms of the monomer local time scale τ_0 and the effective exponent $\mu = 2\nu + \nu'$ depending upon the exponents related to the chain size $R \propto L^\nu$ and the chain hydrodynamic radius $R_H \propto L^{\nu'}$.

4.1.1.1 Orientation order parameter and extinction angle

The bond orientation and the degree orientation has been computed in terms of the orientation order parameter. The principal axis system I, II, III is such that axis I corresponds to the orientation of the eigenvector with the largest eigenvalue S_I and its orientation with respect to the flow direction x corresponds to the extinction angle χ_O if the intrinsic birefringence dominates. The values of $\chi_O(\omega, \dot{\gamma})$ and $S_I(\omega, \dot{\gamma})$ are listed in Table 4.1. As shown in figure 4.1 (S_I) and figure 4.2 (χ_O), the data were plotted as a function of reduced shear rate β_Λ and as a function of absolute shear rate $\dot{\gamma}$ respectively. A clear trend to universality is observed for data plotted against β_Λ. As the shear rate increases, χ_O decreases from its 45 degrees value for ($\dot{\gamma} \to 0$) down to 0 degrees, while the scalar order parameter S_I increases from 0 to 1 asymptotically.

4.1.1.2 Average bond length versus β_Λ

The bond length elongation due to shear flow has also been investigated. The average bond length over all bonds $\langle l \rangle$ are listed in Table 4.1. Figure 4.3 shows the average bond length increase due to shear flow as a function of the absolute shear rate for each ω value. For the sake of comparison, we also show the bond elongation obtained in a test experiment where, starting from configurations generated at equilibrium from a normal run at finite scission rate, we follow at finite shear rate the Langevin Dynamics at $\omega = 0$ (i.e., interrupting completely the kinetic process) the establishment of the stationnary state for a similar "dead polymer" polydisperse system under shear. As expected, the bonds of the temporary chains do not reach the "dead" polymer average value, because the bond extension which is governed by the relaxation time of the polymer it belongs

Table 4.1: Average bond length β_Λ, average extinction angle χ_O, reduced viscosity η/η_0, and average orientation order parameter S_I for each set of $(\omega, \dot{\gamma})$ (see text)

ω	$\dot{\gamma}$	β_Λ	$\langle l \rangle$	χ_O	$\frac{\eta}{\eta_0}$	S_I
0.1	0	0	0.970732(3)	-	-	-
0.1	0.000056	0.1	0.970732(8)	42(4)	1.0(2)	0.001
0.1	0.00014	0.25	0.970734(5)	39(2)	1.05(9)	0.003
0.1	0.00028	0.5	0.970735(7)	37.339(8)	0.97(8)	0.007
0.1	0.00056	1.0	0.970752(3)	32.20(4)	0.97(5)	0.016
0.1	0.0028	5.0	0.97092(2)	16.6676(3)	0.62(3)	0.075
0.1	0.0056	10	0.97121(3)	12.915(7)	0.49(3)	0.126
0.1	0.028	50	0.97289(2)	8.762(5)	0.221(3)	0.275
0.1	0.056	100	0.97403(3)	8.422(1)	0.151(6)	0.332
0.5	0	0	0.970732(3)	-	-	-
0.5	0.00012	0.1	0.970737(7)	42(7)	0.9(2)	0.002
0.5	0.0003	0.25	0.970742(4)	41.9(2)	1.04(5)	0.006
0.5	0.0006	0.5	0.970751(5)	36.961(1)	0.95(2)	0.011
0.5	0.0012	1.0	0.970752(8)	31.08(8)	0.89(2)	0.023
0.5	0.006	5.0	0.970991(8)	17.156(6)	0.565(6)	0.094
0.5	0.012	10	0.97135(1)	13.709(5)	0.431(6)	0.150
0.5	0.06	50	0.97332(2)	9.777(2)	0.195(4)	0.305
0.5	0.12	100	0.97460(2)	9.1765(8)	0.133(2)	0.366
1	0	0	0.970730(3)	-	-	-
1	0.00015	0.1	0.970733(7)	42(2)	1.0(1)	0.002
1	0.00038	0.25	0.970729(9)	40(2)	1.00(5)	0.006
1	0.00075	0.5	0.970736(6)	36.751(1)	0.883(8)	0.012
1	0.0015	1.0	0.970753(5)	31.67(9)	0.88(1)	0.025
1	0.0075	5.0	0.971016(6)	17.718(6)	0.547(9)	0.099
1	0.015	10	0.97136(1)	14.3344(4)	0.407(5)	0.153
1	0.075	50	0.97330(1)	10.221(1)	0.185(1)	0.309
1	0.15	100	0.97459(1)	9.668(1)	0.127(2)	0.370
5	0	0	0.970724(7)	-	-	-
5	0.00021	0.1	0.970733(5)	40.7(6)	0.95(5)	0.003
5	0.00053	0.25	0.970742(4)	41.09(2)	0.96(4)	0.007
5	0.00105	0.5	0.970743(3)	35.8(3)	0.92(1)	0.014
5	0.0021	1.0	0.970762(3)	30.92(2)	0.867(8)	0.029
5	0.0105	5.0	0.971056(5)	18.263(3)	0.532(4)	0.105
5	0.021	10	0.971376(4)	15.214(4)	0.395(5)	0.158
5	0.105	50	0.97313(1)	11.346(1)	0.176(2)	0.305
5	0.21	100	0.97439(1)	10.673(1)	0.122(1)	0.368

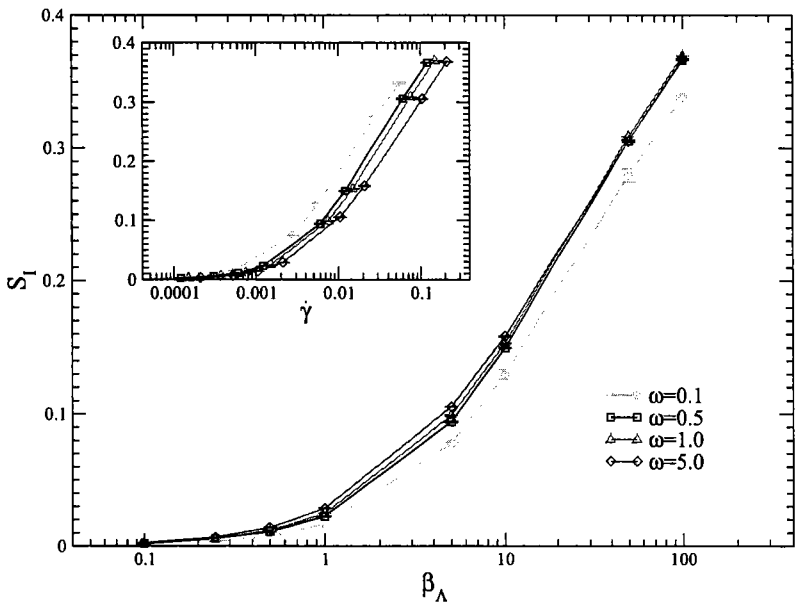

Figure 4.1: Orientation order parameter S_I as a function of the reduced shear rate β_Λ and, in inset, as a function of the bare shear rate $\dot{\gamma}$. Data corresponds to $\omega = 0.1$(circle), $\omega = 0.5$(square), $\omega = 1$(triangle) and $\omega = 5$(diamond). Notice that the results for $\omega = 0.1$ is a little off, because of its $\Lambda = 32$, quite close to $L_0 = 56$.

to, cannot achieve its dead polymer long time limit as a result of continuous scissions and recombinations. For a given shear rate $\dot{\gamma}$, the less elongated bonds are those where the ω rate is highest and this suggests plotting again the same results as a function of the shear rate reduced by the inverse of the characteristic time of the dynamical units β_Λ. The inset of Figure 4.3 shows indeed a universal behavior of the effective elongation respect to equilibrium case in terms of this reduced shear rate.

4.1.2 Viscosity

In connection with rheological experiments, we observe a strongly non-Newtonian character for the viscosity η expressed as a function of $(\omega, \dot{\gamma})$. In our non-equilibrium stationary simulations, the rheology can be determined by measuring the average of the instantaneous stress tensor. Under a shear flow in the x direction, $\eta(\omega, \dot{\gamma})$ is obtained by dividing the xy component of the stress tensor by the absolute shear rate $\dot{\gamma}$:

$$\eta(\omega, \dot{\gamma}) = \frac{\langle \sigma_{xy}(\omega, \dot{\gamma}) \rangle}{\dot{\gamma}} \tag{4.11}$$

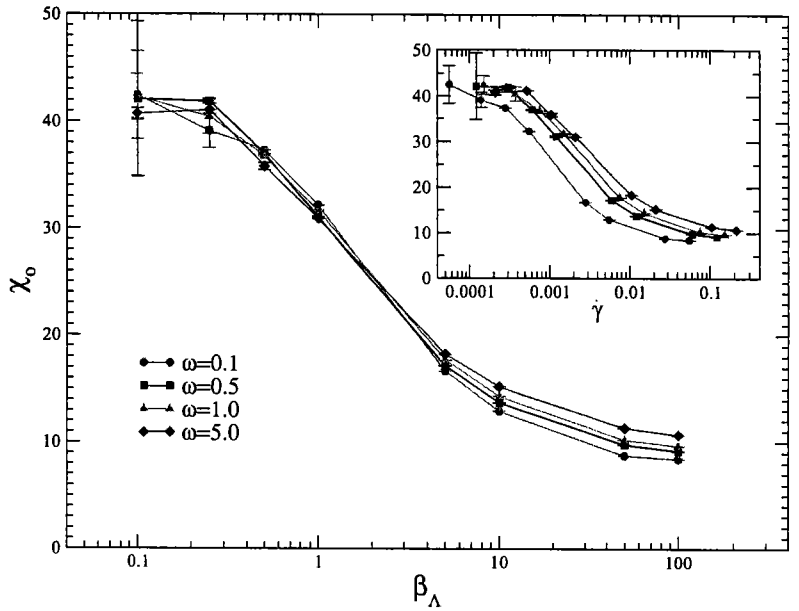

Figure 4.2: Extinction angle χ_O as a function of the reduced shear rate β_Λ and, in inset, as a function of the bare shear rate. Data correspond to $\omega = 0.1$ (circles), $\omega = 0.5$ (squares), $\omega = 1$ (triangles) and $\omega = 5$ (diamonds).

A recent experimental observation on entangled micelles showing shear thinning behavior has expressed that the effective viscosity of micelles under flow is decreasing exponentially with a local orientational order parameter [55]. By analogy we plot the shear viscosity for each $(\omega, \dot{\gamma})$ as a function of the corresponding order parameter. We observe in figure 4.4 an exponential behavior $\eta = \eta_0 \exp(-a_1 S_I)$ for each set of points relative to a particular ω value. Therefore, the Newtonian viscosity at zero shear rate, η_0, has been estimated by the extrapolation using a simple exponential fitting for the non-Newtonian viscosity. The η_0 values obtained are 8.3(6), 5.6(2), 5.1(1), and 4.33(7) for $\omega = 0.1$, $\omega = 0.5$, $\omega = 1$, and $\omega = 5$ respectively. Figure 4.5 shows that the ratio η/η_0 is a universal exponential function of S_I, which is obtained by a single free parameter fitting giving $a_1 = 5.68$.

We previously estimated η_0 for different choices of k_s (and hence of τ_Λ) by the integration of stress-stress correlation function in our earlier BD simulation work [18]. Due to the large noise on the simulation data, the Faivre-Gardissat $G(t)$ expression [36] at equilibrium could only be verified qualitatively. Here, by extrapolation of the effec-

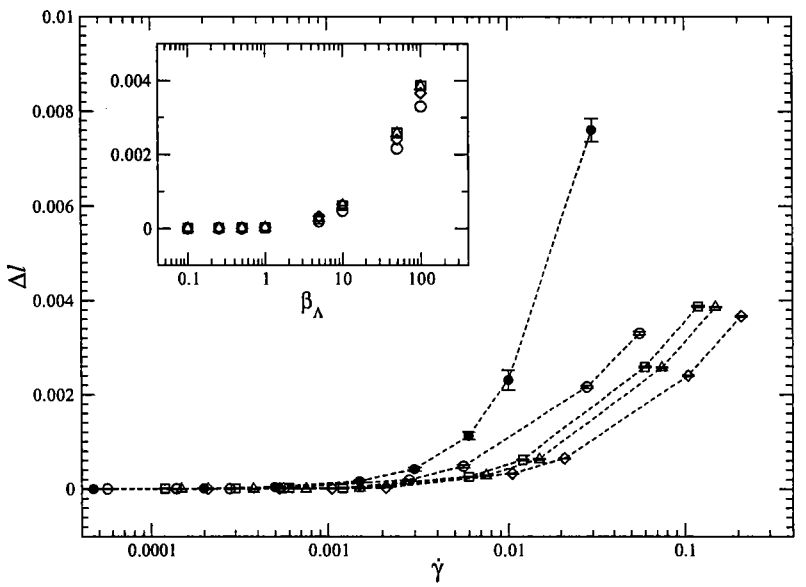

Figure 4.3: Average bond length extension Δl with respect to equilibrium, as a function of the bare shear rate and, in inset, as a function of the reduced shear rate β_Λ. Data corresponds to $\omega = 0.1$ (circle), $\omega = 0.5$ (square), $\omega = 1$ (triangle) and $\omega = 5$ (diamond). The remaining data (filled circles) correspond to a polydisperse "dead" polymer sample structurally similar to the micellar solution

tive viscosity obtained in non-equilibrium Langevin Dynamics simulation at high shear rates, we get a more precise estimate of η_0. The zero shear viscosity expressed in terms of τ_Λ can be tested by the expression of Faivre-Gardissat [36]. Using a single parameter G_0 in the integrated form of equation (1.70) of chapter I, the functional form with free parameter G_0, in figure 4.6, with $G_0 = 0.26(1)$, represents quite well the increase of the zero shear rate viscosity as the scission rate decreases. In figure 4.7, we show that $\eta_0 \propto \tau_\Lambda^{1/2}$, as predicted by [36].

As shown in figure 4.1, S_I itself is a function of β_Λ. Therefore the ratio of viscosities η/η_0 must also be a function of that reduced shear rate, which is indeed shown in figure 4.8. In the regime $0 \leq \beta_\Lambda \leq 100$, the shear thinning behavior of the viscosity (reduced by the corresponding Newtonian value), appears to be a universal function represented by the ad hoc function

$$\frac{\eta}{\eta_0} \equiv f(x) = \exp\left[-a(\ln(1+x))^b\right] \tag{4.12}$$

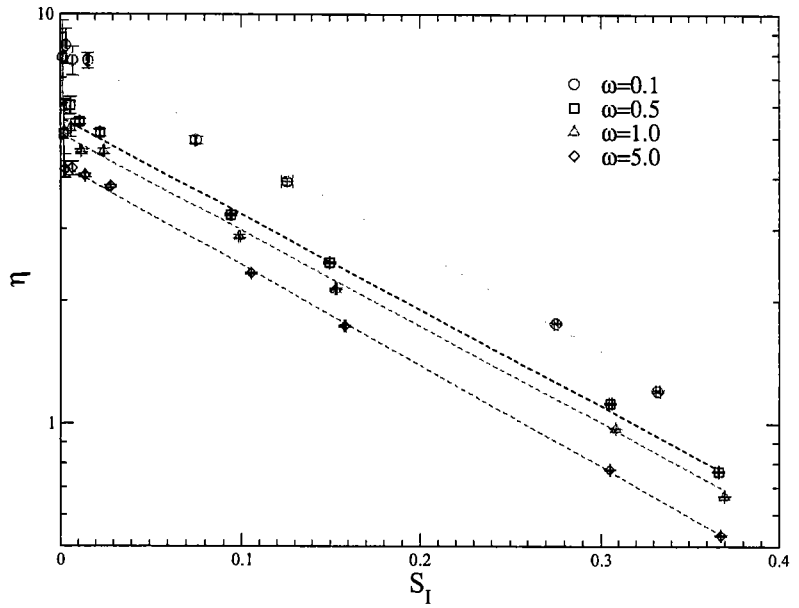

Figure 4.4: Shear viscosity as a function of the order parameter S_I. Data correspond to $\omega = 0.1$ (circle), $\omega = 0.5$ (square), $\omega = 1$ (triangle), $\omega = 5$ (diamond) and dashed lines are two parameters exponential fits (see text).

where $x = \beta_\Lambda$ for $a = 0.2838, b = 1.3045$.

With the analysis of the collective properties, one notes that for shearing rates in the non-linear response regime, the extinction angle χ_O for the system, the collective order parameter S_I, the average bond length between successive monomers, and the effective viscosity reduction $\frac{\eta}{\eta_0}$ appear to be universal properties of a unique parameter β_Λ which combines the shear rate and the scission rate constant, i.e. $\beta_\Lambda = \dot{\gamma}\tau_\Lambda$. This could be expected as the main relaxation time in the system is indeed the life time of the dynamical units of size Λ which was found to play an essential role in the linear viscoelasticity and in the relaxation dynamics at equilibrium.

4.2 Chain length distribution and chain size dependent properties

4.2.1 Effect of shear flow on distribution of chain lengths

We first remind here that the distribution $c_0(L/L_0)$ of lengths of the micelle at equilibrium for a semi-dilute solution presents a simple exponential form, i.e. $c_0(L) \propto$

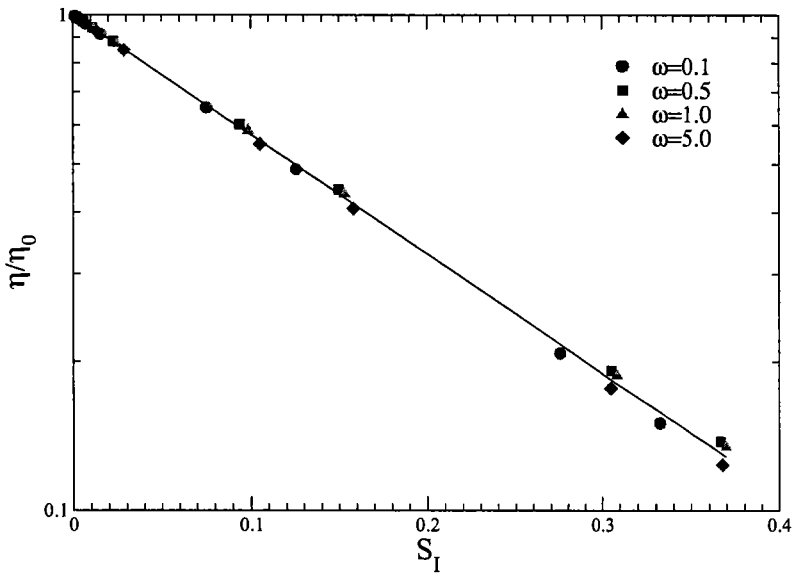

Figure 4.5: The shear thinning factor $\frac{\eta}{\eta_0}$ as a function of the order parameter S_I for all pairs of $\dot{\gamma}$ and ω demonstrates the universality of the relationship and its exponential decay character. The zero shear rate viscosity $\eta_0(\omega)$ has been obtained by linear fitting of $\ln(\eta)$ against S_I for a series of points corresponding to various shear rate.

$\exp(-L/L_0)$ (see section 3.1). When a stationary planar Couette flow is switched on, the distribution of chain lengths is qualitatively modified, as figure 4.9 illustrates. For comparison, the equilibrium case with $\omega = 0.5$ is given and we observe that it is indeed very close to an exponential. In presence of shear flow, the distribution of chain lengths is $\sim \exp(-\gamma L/\langle L \rangle)$ when $\langle L \rangle$ is the non-equilibrium stationary chain length average and γ a prefactor larger than 1. Increasing of shear rate leads to an increase of γ. This observation is in agreement with recent Monte Carlo [26] and Molecular Dynamics simulation [17, 44] works. The change in the distribution of lengths in shear flow is interpreted as the result of the breaking of long chains to reduce the tension remaining in the bonds after the alignment of a chain.

The values of $\langle L \rangle$ for each ω and each $\dot{\gamma}$ are listed in Table (4.2). Essentially, $\langle L \rangle$ decreases with increasing shear rate in agreement with previous studies [17, 26, 44]. Figure 4.10 shows that the average micelle length $\langle L \rangle$ as a function of the absolute shear rate $\dot{\gamma}$, for the various ω's (notice that L_0 is the equilibrium mean length). All results lie on a unique master curve which decreases with increasing shear rate. The

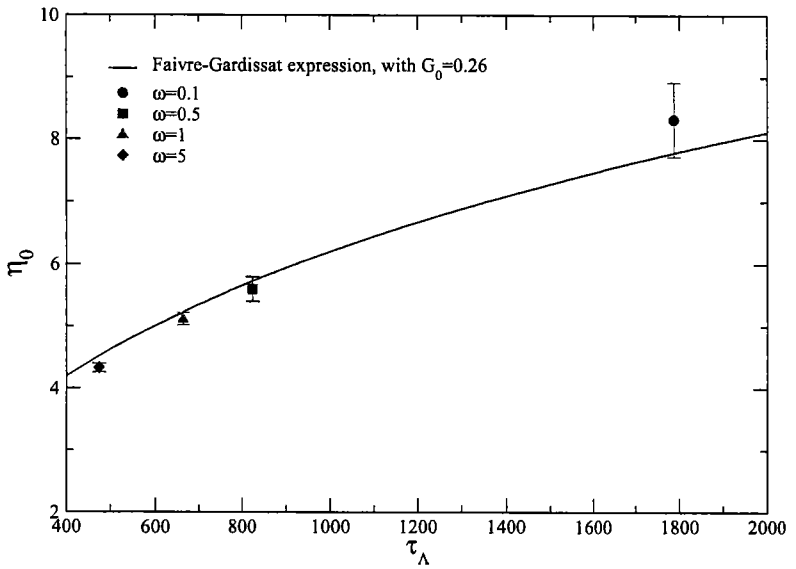

Figure 4.6: The Newtonian shear viscosity is plotted against the corresponding τ_Λ value. Data are fitted by the single parameter G_0 with the Faivre-Gardissat expression, equations ((1.68)+(1.69)+(1.70)).

inset illustrates that the average micelle length is not an universal function of the reduced shear rate β_Λ. We will come back to this curve later when we analyze kinetic rates in shear flow.

4.2.2 Saturation effect on orientational properties

Our micelles system is polydisperse with chain length of life time $\frac{1}{k_s L}$ depending upon their size. To investigate the effect of scission-recombination mechanism on the orientation angle as function of chain size, it is useful to perform two additional experiments with "dead" chain:

1. A monodisperse system. The parameter set up at $L \equiv N = 57$, $k_BT = 1$, $\phi = 0.15$, reduced shear rate $\beta_N = \dot{\gamma}\tau_L$ equal to 0.26, 0.89, 1.12, 0.89, 1.68, 2.79, 8.83, 16.76, 33.53, 55.89, 167.67, and 279.45.

2. A polydisperse system made of a series of configurations with the equilibrium chain length distribution of our micellar system with average chain length $\simeq 56$, $k_BT = 1$, $\phi = 0.15$, that we study under shear at absolute shear rate $\dot{\gamma} = 0.01$ and 0.03.

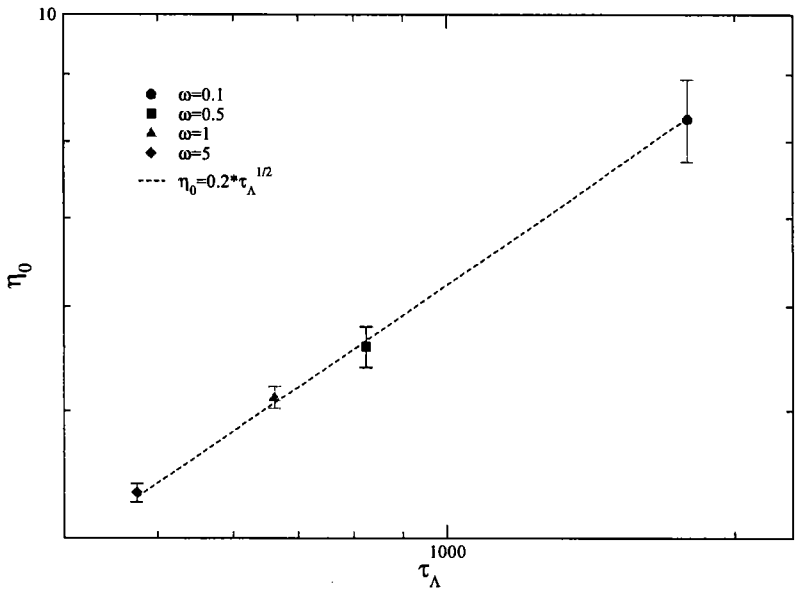

Figure 4.7: The Newtonian shear viscosity is plotted against the corresponding τ_Λ value. Data are fitted with the integral form of the long time ($t \gg \tau_\Lambda$) asymptotic expression of the stress relaxation function of Faivre-Gardissat, equations (3.65). With the exponent fixed at 1/2, the fit gives a prefactor $A \simeq 0.2$. This fit confirms the expected relation $\eta_0 \propto \tau_\Lambda^{1/2}$.

For the monodisperse case, the extinction angle χ_O, and the orientation angle χ_G for each value of β_N have been computed based on equations 4.3 and 4.7. In figure 4.11 we plot $\cot(2\chi_O)$ and $\cot(2\chi_G)$ as a function of β_N. We find that $\cot(2\chi_O) \propto \beta_N$ for the small shear rate region ($\beta_N < 3$) and $\cot(2\chi_O) \propto \beta_N^{0.4}$ for $\beta_N > 3$ for both χ_O and χ_G. This confirms the results of Ref [53].

The work is then focused on the comparison between our micellar system and the "dead" polydisperse system. Figure 4.12 shows the extinction angle χ_O^L as a function of the chain size L for the two systems. Two different shear rates are considered and for each of them we compare the case of "dead" polydisperse polymers (Langevin Dynamics with the scission-recombination mechanism being switched off) to "living" polymers characterized by a particular attempt frequency rate ω. As expected, for the polydisperse "dead" polymers, χ_O^L decreases monotonously with increasing L. We have observed in figure 4.11 that the large reduced shear rate behavior predicted by equation (4.9) is valid for rates above $\beta_L \approx 2 - 3$. It implies that the large reduced

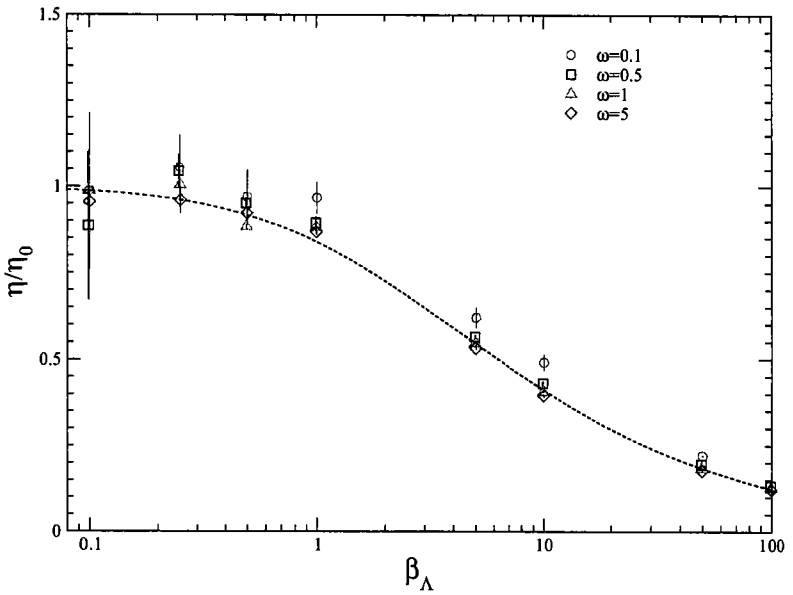

Figure 4.8: Shear viscosity reduced by its Newtonian limit, as a function of the reduced shear rate β_Λ. Data corresponds to ω=0.1 (circle), ω=0.5 (square), ω=1 (triangle) and ω=5 (diamond). The dotted line is an ad hoc function (see text).

shear rate behavior should be observed for $L > L_c$ where $L_c \approx 1.2\dot{\gamma}^{-1/2}$. The value of L_c is then 12 and 7 for the chosen shear rates $\dot{\gamma} = 0.01$ and $\dot{\gamma} = 0.03$ respectively. As shown in the figure 4.12, for the chains $L > L_c$ we observe a behavior roughly consistent with $\cot(2\chi_O) \propto L^{\mu\alpha}$ with $\mu\alpha = 0.8$, supposing here unentangled chains with $\mu = 2(\nu = 0.5, \nu' = 1)$, which is the situation rather closely satisfied in our simulation performed in the semi-dilute regime [19, 18] and in which hydrodynamic interactions are not taken into account. For "living" polymers, the results correspond to the case $\omega = 0.1$ $\dot{\gamma} = 0.03$ and $\omega = 0.5$ $\dot{\gamma} = 0.01$, giving equilibrium rates $k_s = 5.4 * 10^{-5}$ for $\omega = 0.5$ and $k_s = 1.7 * 10^{-5}$ for $\omega = 0.1$. For the average size chain at equilibrium, it corresponds to life times T=328, and T=1043 respectively, to be compared to the much longer Browian relaxation time of a "dead" polymer of similar size τ_{L_0}=5523. For "living" polymers, we thus expect a strong coupling between the flow and the internal kinetics. In figure 4.12, the evolution of the extinction angle towards a plateau value as L increase is the very new observation. This saturation effect at large polymer size must be related to the too short time, giving their finite life time, for these long polymers to reach the stationnary state observed for "dead" polymers of similar size under the

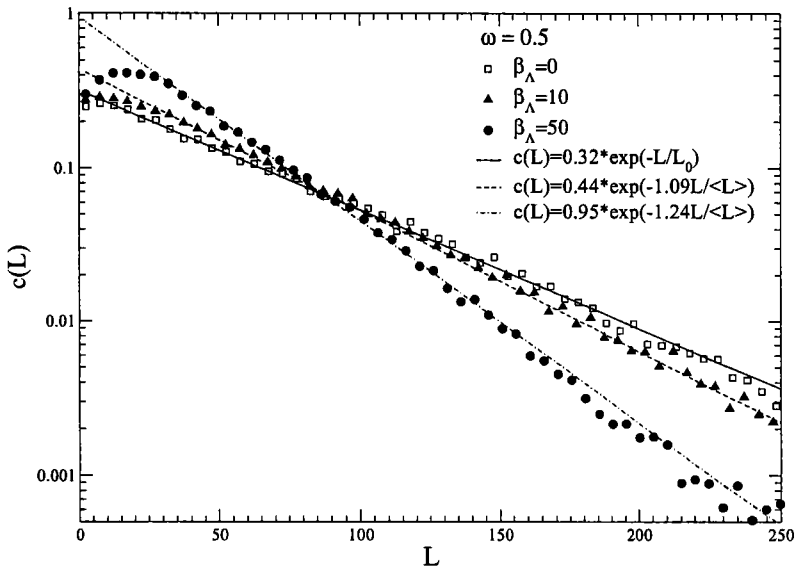

Figure 4.9: Distribution of chain lengths at equilibrium and under shear flow. For the attempt frequency $\omega = 0.5$, we compare the equilibrium case (squares) with two different shear rates $\beta_\Lambda = 10$ (triangles) and $\beta_\Lambda = 50$ (dots) (see text).

same shear flow.

On the contrary, short chains with $L < \Lambda$ (where Λ, obtained by using equation 1.66, is the particular crossover chain size for which the life time and the Brownian relaxation time are equal, namely τ_Λ) orient similarly to dead polymers of similar size. The values of Λ (computed with equation (1.66)) are $\Lambda = 22$ and $\Lambda = 32$ for $\omega = 0.5$ and $\omega = 0.1$ respectively.

By a closer look in the region where $L < \Lambda$, we observe that the chains of this region are slightly more oriented than the corresponding "dead" polymers. The reason of this slight opposite effect is that a fraction of the chains where $L < \Lambda$ are the scission fragments of the originally longer chains which were somewhat more oriented and more elongated.

The saturation effect observed on χ_O^L is also seen on the order parameter S_I. In figure 4.13 we compare the order parameter versus chain length L for the "dead" polymers and the "living" polymers characterized by the same attempt frequency ω and $\dot{\gamma}$ as those for the extinction angle. For the two "dead" polymers, the order parameter increase monotonously with L. For "living" polymers, the order parameter

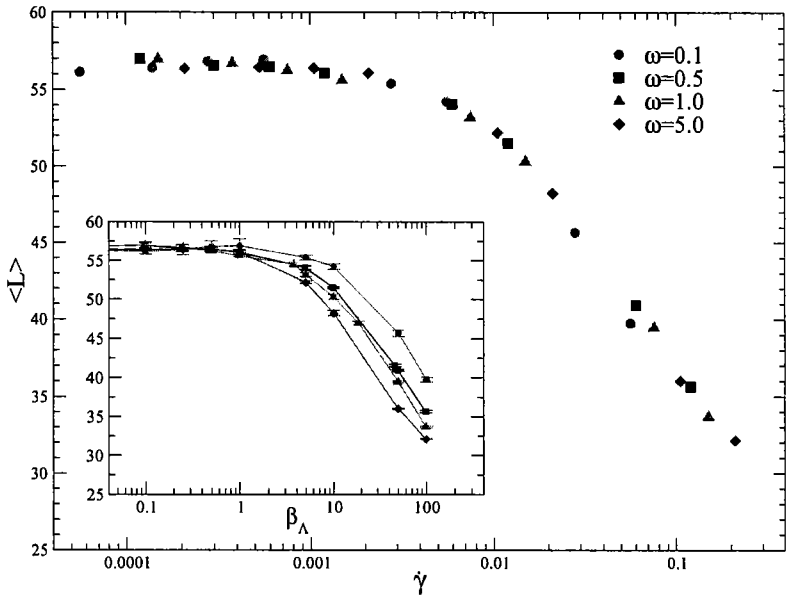

Figure 4.10: Average micelle length as a function of shear rate for various ω. Data correspond to $\omega = 0.1$ (circles), $\omega = 0.5$ (squares), $\omega = 1$ (triangles), and $\omega = 5$ (diamonds). We observe that the average micelle length is independent of ω. Inset illustrates that the average micelle length is not an universal function of the reduced shear rate.

increases with L for $\Lambda < L$ and then levels off again.

The chain length Λ is thus a crossover critical length. For chains $L < \Lambda$, "living" polymers orient and order as "dead" polymer, while for chains length $L > \Lambda$, the systematic orientation and ordering trend is interrupted by the scission-recombination mechanism. This point is also confirmed by the plot of the orientation angle χ_G versus the chain length. For "living" polymer, a universal behavior and a saturation effect are expected at the chain length Λ for different attempt frequency ω. In figure 4.14 we plot $\cot(2\chi_G)/\beta_\Lambda^\alpha$ ($\alpha = 0.46$, see Ref.[53]) versus the reduced chain length L/Λ for the four ω with different $\dot{\gamma}$: $\omega = 0.1(\dot{\gamma} = 0.03)$, $\omega = 0.5(\dot{\gamma} = 0.01)$, $\omega = 1(\dot{\gamma} = 0.015)$, $\omega = 5(\dot{\gamma} = 0.021)$. The four curves show a universal behavior. The increase of the orientation angle appears for chain lengths $L/\Lambda < 1$ and saturates at $L/\Lambda = 1$ with $\cot(2\chi_G)/\beta_\Lambda^{0.46} = c^{-1}$ ($c \simeq 1$) for all the four cases.

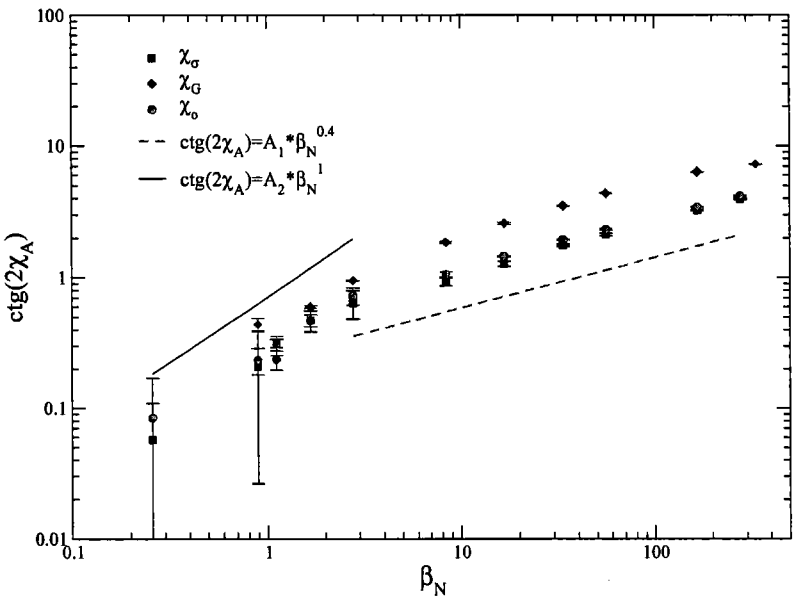

Figure 4.11: Extinction angle χ_O, stress orientation angle χ_σ and gyration tensor orientation angle χ_G for monodisperse chains. For $\beta_N < 3$, the three angles follow $ctg(2\chi_A) \propto \beta_N$ and for $\beta_N > 3$, $ctg(2\chi_A) \propto \beta_N^{0.4}$. For all value of β_N investigated $\chi_O \sim \chi_\sigma$.

4.3 Scission-recombination kinetics under flow

The previous sections have shown that under shear flow, the single chain orientational properties and the rheological properties appear to be universal properties of β_Λ which depends on both the values of attempt frequency ω and the shear rate $\dot{\gamma}$. On the contrary the average micelle length $\langle L \rangle$ was found to decrease with increasing shear rate, independently from the scission rate constant value, just as it was the case for the equilibrium situation [19, 18].

To understand the origin of the independence of the micelle length from the kinetic parameter ω, we will compare the non-equilibrium situation to what happens at equilibrium. When a planar Couette flow is introduced, the system becomes anisotropic so that all rates obtained from the actual number of transitions or from the cumulative hazard analysis of free ends life times, represent an orientational average over nonequivalent directions. We thus interpret the $\dot{\gamma}$ dependence of the average micelle length $\langle L \rangle$ as the result of the cancellation of ω dependent terms in the effective scission

Table 4.2: Average chain length $\langle L \rangle$, and the short time scission and recombination probabilities Q_s and Q_r for each set of $(\omega, \dot{\gamma})$ (see text).

ω	$\dot{\gamma}$	β_Λ	$\langle L \rangle$	$Q_s * 10^4$	Q_r
0.1	0	0	56.2(6)	1.077	4.535
0.1	0.000056	0.1	56.1(3)	1.101	4.628
0.1	0.00014	0.25	56.4(7)	1.159	4.917
0.1	0.00028	0.5	56.8(7)	1.067	4.595
0.1	0.00056	1.0	56.9(8)	1.115	4.820
0.1	0.0028	5.0	55.4(3)	1.111	4.547
0.1	0.0056	10	54.2(3)	1.083	4.244
0.1	0.01	17.9	52.2(4)	1.186	-
0.1	0.02	35.8	48.7(5)	1.389	-
0.1	0.028	50	45.7(4)	1.528	4.249
0.1	0.056	100	39.7(3)	2.060	4.340
0.5	0	0	56.6(1)	1.102	4.705
0.5	0.00012	0.1	57.0(4)	1.105	4.784
0.5	0.0003	0.25	56.6(4)	1.097	4.680
0.5	0.0006	0.5	56.5(3)	1.085	4.616
0.5	0.0012	1.0	56.1(3)	1.137	4.767
0.5	0.006	5.0	54.1(3)	1.156	4.504
0.5	0.012	10	51.5(1)	1.159	4.100
0.5	0.06	50	40.9(1)	1.637	3.657
0.5	0.12	100	35.6(2)	2.222	3.763
1	0	0	56.2(2)	1.077	4.534
1	0.00015	0.1	57.0(3)	1.091	4.721
1	0.00038	0.25	56.7(3)	1.089	4.672
1	0.00075	0.5	56.2(2)	1.094	4.615
1	0.0015	1.0	55.6(1)	1.090	4.496
1	0.0075	5.0	53.2(2)	1.143	4.311
1	0.01	6.6	52.5(3)	1.177	-
1	0.015	10	50.3(3)	1.173	3.957
1	0.02	13.3	48.6(4)	1.257	-
1	0.075	50	39.5(1)	1.624	3.372
1	0.15	100	33.7(1)	2.185	3.305
5	0	0	56.6(2)	1.092	4.666
5	0.00021	0.1	56.4(1)	1.097	4.649
5	0.00053	0.25	56.5(2)	1.099	4.670
5	0.00105	0.5	56.4(3)	1.097	4.655
5	0.0021	1.0	56.1(2)	1.105	4.634
5	0.0105	5.0	52.2(2)	1.135	4.123
5	0.021	10	48.3(3)	1.191	3.698
5	0.105	50	36.0(1)	1.560	2.699
5	0.21	100	32.13(3)	2.006	2.761

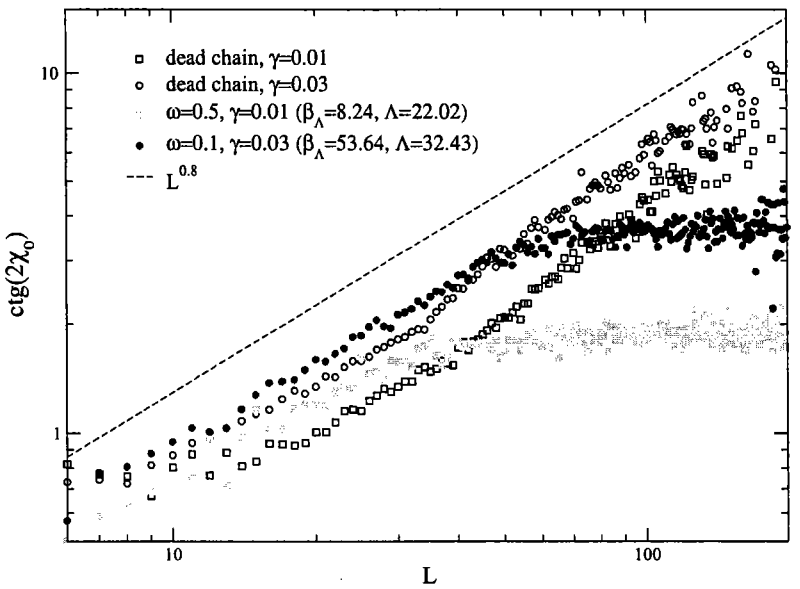

Figure 4.12: Extinction angle $\left(\cot(2\chi_O^L)\right)$ as a function of the micelle length. Shown is the single molecule deformation and alignment within a polydisperse system subject to a stationary shear flow. For a given shear rate, we compare a polydisperse dead polymer solution and a solution of living polymers characterized by a particular attempt frequency rate ω. Open circle and open square refer to a polydisperse system of dead polymers subjected to a shear flow with $\dot{\gamma} = 0.03$ and 0.01 respectively. Filled circles and filled squares refer to living polymer with attempt frequencies $\omega = 0.1$ and $\omega = 0.5$ respectively.

and recombination rates according to a balance between scissions and recombinations in a non-equilibrium situation. Exploiting all dependencies in ω and $\dot{\gamma}$, the number of scissions or recombinations (per unit time and unit volume) are expressed as

$$\begin{aligned} n_s^{eff}(\omega,\dot{\gamma}) &= \kappa(\omega,\dot{\gamma})n_s^{st} = \kappa(\omega,\dot{\gamma})n_r^{st} \\ &= k_s(\omega,\dot{\gamma})\phi = \frac{1}{2}\left(\frac{\phi}{\langle L(\dot{\gamma})\rangle}\right)^2 k_r(\omega,\dot{\gamma}) \end{aligned} \tag{4.13}$$

where, based on our results, one supposes that the micelle average length is independent of ω and where the effective rate constants can be expressed in terms of the non-equilibrium quantities

$$k_s(\omega,\dot{\gamma}) = 2\omega\kappa(\omega,\dot{\gamma})Q_s(\omega,\dot{\gamma}) \tag{4.14}$$

$$k_r(\omega,\dot{\gamma}) = 2\omega\kappa(\omega,\dot{\gamma})Q_r(\omega,\dot{\gamma}), \tag{4.15}$$

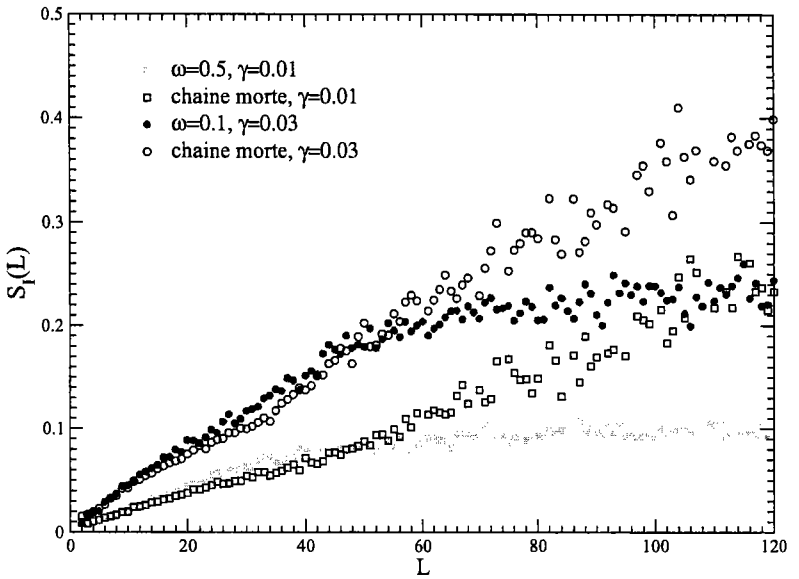

Figure 4.13: Order parameter S_I as a function of chain size L. Open circles and open squares refer to a polydisperse system of dead polymers subjected to a shear flow with $\dot{\gamma} = 0.03$ and 0.01 respectively. Filled circles and filled squares refer to living polymers with attempt frequencies $\omega = 0.1$ ($\dot{\gamma} = 0.03$) and $\omega = 0.5$ ($\dot{\gamma} = 0.01$) respectively.

where Q_s is now the probability in an anisotropic Coutte flow that a selected bond, its replacement by two free ends is accepted by our algorithm. And the recombination term Q_r is the average probability for two randomly selected chain ends to form a new bond (the ends belonging to the same chain being excluded). The values of Q_s, Q_r and $\kappa(\omega, \dot{\gamma})$ for each $(\omega, \dot{\gamma})$ were computed on the basis of the value of k_s and k_r obtained by cumulative hazard function computed under shear and listed in Table (4.2). The way to interpret the dependency of the average micelle length on the shear rate can be based on equation (4.13). At a fixed ω value, the rate constants both increase with $\dot{\gamma}$ but much more strongly in the case of k_s than in the case of k_r. Therefore, the micelles must be shorter to increase the chain end density so that equation (4.13) remains satisfied. At a given shear rate, the effective scission/recombination rate constants both increase with ω in a way which turns out to be identical to the way it depends of ω in the equilibrium situation. This is illustrated in figure 4.15. Based on our results, for the scission case, one finds that the effective rate constants at finite $\dot{\gamma}$ are equal to

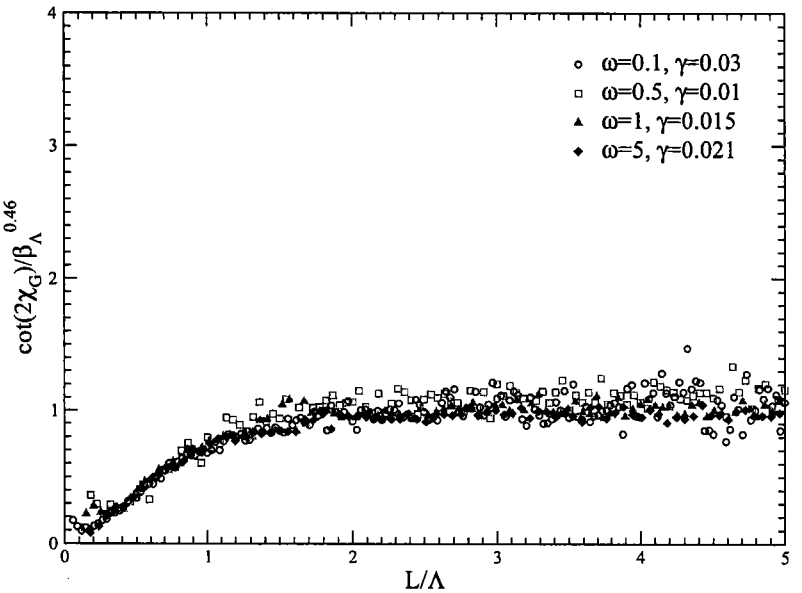

Figure 4.14: $\left(\frac{cot(2\chi_G)}{\beta_\Lambda^{0.46}}\right)$ versus reduced chain length L/Λ for various sets $\omega = 0.1$ ($\dot{\gamma} = 0.03$), $\omega = 0.5$ ($\dot{\gamma} = 0.01$), $\omega = 1$ ($\dot{\gamma} = 0.015$), and $\omega = 5$($\dot{\gamma} = 0.021$). A universal behavior is observed.

$$k_s(\omega, \dot{\gamma}) = \omega\kappa(\omega)(1 + 18.5|\dot{\gamma}|)Q_s^{eq} \tag{4.16}$$

and for the recombination case,

$$k_r(\omega, \dot{\gamma}) = \omega\kappa(\omega)(1 + 2.5|\dot{\gamma}|)Q_r^{eq} \tag{4.17}$$

where the equilibrium transmission coefficient $\kappa(\omega)$ is involved and where Q_s^{eq} and Q_r^{eq} are the factor introduced in equations (3.17) and (3.18) of chapter III.

Substituting equation (4.16) and (4.17) into (4.13) leads to

$$\frac{L_0^2}{\langle L \rangle^2} = \frac{1 + 18.5|\dot{\gamma}|}{1 + 2.5|\dot{\gamma}|}. \tag{4.18}$$

The above relation is verified and shown in figure 4.16.

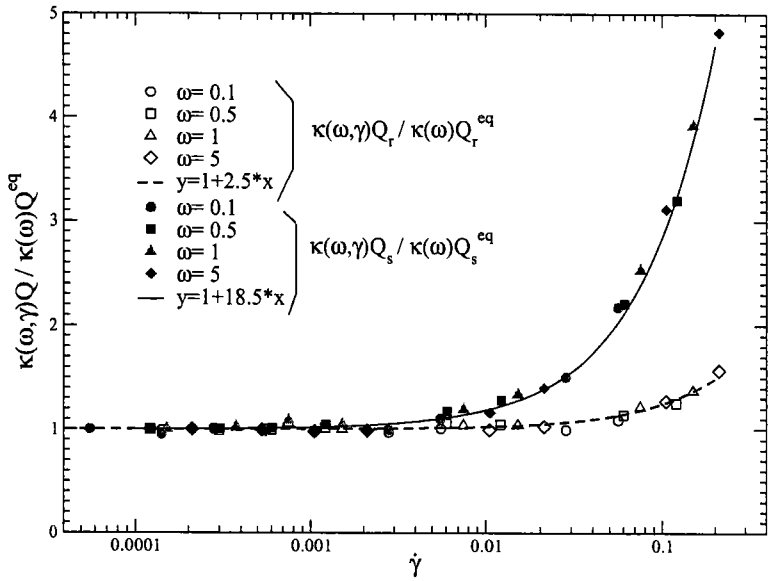

Figure 4.15: The ratio $\frac{k_s(\omega,\dot{\gamma})}{k_s^{eq}(\omega)} \approx 1 + 18.5|\dot{\gamma}|$ (filled symbols) and the ratio $\frac{k_r(\omega,\dot{\gamma})}{k_r^{eq}(\omega)} \approx 1 + 2.5|\dot{\gamma}|$ (open symbols) turn out to be functions of shear rate only. The increase of the effective scission rate k_s with shear rate is faster than that of effective recombination rate k_r.

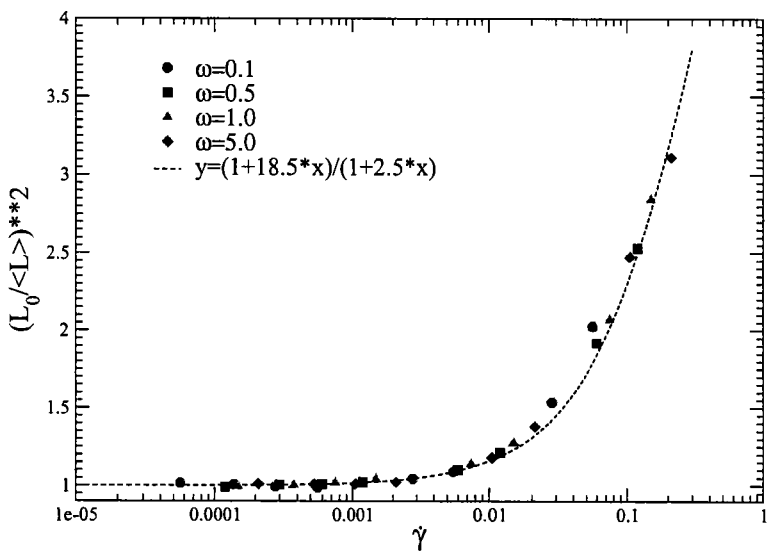

Figure 4.16: The agreement between $\frac{L_0^2}{\langle L \rangle^2}$ and $\frac{1+18.5|\dot{\gamma}|}{1+2.5|\dot{\gamma}|}$.

Chapter 5

Conclusions

Cylindrical micelles are self-assembled curvilinear unidimensional supramolecular "polymers" consisting of amphiphilic molecules.

In the first chapter, we have reviewed the statistical theory of these systems which, at equilibrium, minimize their free energy by producing a phase of cylindrical micelles having a broad specific distribution of lengths. Crucial parameters determining the static properties are the "monomer" density, the reduced energy βE required to split a micelle into two parts (and thus creating two new end-caps) and the solvent quality. The static properties of these particular complex fluids systems are now well understood theoretically [9, 2] thanks also to intensive simulation studies [22, 13, 44].

The dynamical properties of micelles are also interesting because very little is known at the individual micelles level in this potentially very rich domain. Quite generally, one expects a coupling between the flexible micelle dynamical relaxation and their scission-recombination kinetics but the manifestations of this coupling could show up in diverse ways, depending on the monomer density, the solvent quality, and more importantly the reactive time scale of the kinetics with respect to other relaxation processes. The key parameter determining the scission-recombination kinetics is the reduced barrier energy βB in the free energy profile along a reaction coordinate path which describes the progressive fusion of two micelle chain ends, starting from free ends.

In this thesis, we have studied by a Langevin Dynamics simulation technique the static and dynamic properties of a new variant of a mesoscopic model of cylindrical micelles. We have decided to restrict ourselves to the dilute and semi-dilute regimes, where calculations are somewhat more practical than for entangled systems which could

be studied using the same model. A large part of our work is devoted to the rheological properties of our model system for the same solutions.

In chapter II, we have introduced a micelle model as a temporary linear assembly of Brownian particles. Two pair potentials are defined in the model, the precise form being unessential: sufficient to mention that the bonded form allows to form the linear assemblies while the unbounded form, which is a short distance purely repulsive potential, applies between all non connected pairs. At this stage, this model is a popular and standard polymer model. By allowing in addition interchanges of these two potentials (potential swaps) for a pair of monomers in an appropriate relative distance window, we introduce the micelle kinetics model in terms of three "operational" key parameters:

1. βW is the fixed reduced energy by which the bonded potential minimum is shifted with respect to the unbound pair energy level at large distance. It indirectly fixes the reduced energy βE which governs the average size of the model micelles.

2. 2ω is the frequency at which bonded pairs and unbounded pairs are sampled to try, on the basis of a Metropolis Monte-Carlo like algorithm (satisfying detailed balance at equilibrium), a potential swap. Pair potential interchanges are further only attempted if the relative distance between monomers lies within a restricted window ($0.96 < \frac{r}{\sigma} < 1.2$) which is a fraction of the total range allowed for bounded pairs (strictly confined in the window Γ defined by $0 < \frac{r}{\sigma} < \frac{R_c}{\sigma} = 1.5$ where R_c is the distance at which the bounded potential diverges as the bond length increases (σ is the LJ hard core diameter of the monomers). The combined choice of ω and Γ indirectly fixes the reduced barrier energy βB which governs the scission and recombination rates.

The explicit link between the key operational variables (W and ω) and the theoretically relevant physical variables E and B is explicitly discussed in chapter III (see section 3.2.1.7). The quantity βE is defined as the natural logarithm of the ratio of the total number of bonded pairs over the total number of free ends pairs at close distance, close distance being defined as the range $0 < r < R_c$. Similarly B is defined in terms of the rate at which pairs of free ends at close distance are closing up.

Our model has the great advantage over closely related models like the FENE-C model that the structural and dynamical effects can be separately analyzed without mutual interferences. The structural properties at equilibrium are strictly independent

of the attempted rate ω, which allows us to perform global averages over our equilibrium static results for a set of experiments performed at the same state point (βW,$\phi\sigma^3$), but different attempt frequencies ω. Moreover, we can single out how kinetics effects affect the dynamics at a unique (structural and thermodynamical) state point, varying the rates over a large spectrum.

The results of our work are gathered into two main chapters. Chapter III reports all results at equilibrium, for both static and fluctuation dynamics properties while Chapter IV reports the rheological results at a single state point ($\beta W = 10$, $\phi\sigma^3 = 0.15$). The main results are the following:

At equilibrium, four state points have been investigated by LD with a total of M=1000 monomers, mainly

The states ($\beta W = 8$, $\phi\sigma^3 = 0.05$) and ($\beta W = 10$, $\phi\sigma^3 = 0.15$) while a few experiments have also been conducted for the cases ($\beta W = 11$, $\phi\sigma^3 = 0.15$) ($\beta W = 12$, $\phi\sigma^3 = 0.15$). For the two first cases, the average micelle length turns out to be $L_0 = 11.48(1)$ ($\beta W = 8$, $\phi\sigma^3 = 0.05$) and $L_0 = 56.4(4)$ for the case ($\beta W = 10$, $\phi\sigma^3 = 0.15$). The distribution of lengths is found to be characteristic of good solvent conditions in the first case, which is fully coherent with dilute solution conditions as the monomer density predicts a semi-dilute blob size of $L^* = 50$. In the second case, an exponential chain length distribution indicating ideal chain statistics is found. This suggests a large screening of excluded volume interactions for this semi-dilute case where the average chain length turns out to be five times larger than the blob size $L^* = 12$. The latter system and the two other experiments at the same monomer density but different values of W remain in the semi-dilute regime (giving $L_0 = 91.2$ and $L_0 = 151.4$) and are found to be consistent with the ideal chain prediction $L_0 = C^{1/2}(\phi\sigma^3)^{1/2}\exp(\beta\frac{E}{2})$ where $C \simeq 11.5$ and $E \simeq W+2.5$. We thus empirically observe a constant (possibly slightly ϕ and T dependent) shift between the operational variable βW and the relevant quantity βE defined as stated earlier.

The dynamical properties at equilibrium are very sensitive to the specific choice of our attempted frequency ω parameter, the Γ range where potential swaps are possible being supposed to be fixed once for all. It must be noticed that each ω value leads, for a given state point, to a specific scission (k_s) and recombination (k_r) rate constant which are quantities defined as effective overall constants, supposed to be valid for all bonds or for any free end pair. On the basis of a very detailed analysis, we found that

these rates can be expressed as the product of a kinetic factor and a static factor. For the bond scission rate, we get $ks = 2\omega\kappa(\omega)Q_s(\phi, W)$ where 2ω is the rate at which a given bond is selected and Q_s the probability the opening is accepted, that is the outcome of the Monte-Carlo procedure where the acceptance probability involves first the need to be in the Γ range and in addition, the difference between both potentials for the particular r value. The extra factor $\kappa(\omega)$ is the probability that a given bond opening resulting from a successful Monte-Carlo potential swap is a "real" one and not a "inefficient" one. We indeed found that quite generally, our algorithm produces at short times some correlated events where typically a bond scission is immediately followed by a bond recombination between the same partners. The fraction $(1 - \kappa)$ of such correlated transitions increases as ω increases: we show in our thesis that this fraction can be properly estimated by a data analysis, known as the cumulative hazard analysis [30], in which a subset of non-Poisson distributed random events at short times is extracted from the analysis to compute the effective "long time" kinetic rates.

We mainly studied the kinetics at the state point ($\beta W = 10, \phi\sigma^3 = 0.15$), which is also the state point for which rheological studies were performed (see chapter IV). In addition, we studied kinetic aspects in various LD simulations at equilibrium performed at the same monomer density but for increasing W energy, in order to deal with longer chains at the same monomer density. The choice of ω was always guided by the request that the average chain life time, given by $1/(k_s L_0)$, was shorter than the Rouse relaxation time of the same average chain. Indeed, this condition appears to be crucial to get a coupling between relaxation dynamics (dominated by polymer relaxation) and the kinetic processes. The same condition can be expressed as $\Lambda < L_0$ where Λ is the particular micelle size (denominated as dynamical unit in the following) for which the chain relaxation time and its life time are equal. This condition implies a minimum value for ω and thus forced us, given the L_0 values mentioned earlier, to adopt relatively high values for ω for which the κ factor was found to range between 0.93 and 0.11. In chapter III, we discuss the single monomer diffusion, the stress tensor time auto-correlation function and a so called T-jump experiment in which a sudden temperature change drives the system towards a new chain length distribution, appropriate to the new state point. All these studies underline the relevance of the Cates kinetic model in which the effective rates k_s and k_r were first introduced, and confirm our prediction that relevant rate constants involve only the effective transitions.

The rheology of micelles was studied by Langevin Dynamics in shear flow (with Lees-Edwards boundary conditions) on the basis of our model at the well investigated semi-dilute state point ($\beta W = 10$, $\phi\sigma^3 = 0.15$), varying both the shear rate $\dot{\gamma}$ and the operational kinetic parameter ω. In shear flow, it is well known that the relevant physical parameter is the reduced shear rate $\beta_L = \dot{\gamma}\tau_{relax}$ where τ_{relax} is the equilibrium internal relaxation time of the solute. Polymers of size L are strongly deformed and oriented by the shear flow when the reduced shear rate $\beta_L = \tau_0 L^2\dot{\gamma} > 1$. When we analyze the orientation and the deformation of our micelles in a given shear flow $\dot{\gamma}$, we observed the following situation: for small size chains with $L < \Lambda$, there is a systematic increase of the deformation and ordering as the size increases, as predicted by the increasing reduced shear rate β_L while for chains longer than Λ, one gets a saturation effect in the ordering because, it is the reduced shear rate β_Λ which is pertinent for all longer chains as the life time of the dynamical unit becomes the relevant time scale of the relaxation and thus governs the importance of the shearing effects. This is confirmed by our results on the global properties of our sheared micelles system: the bond length increase, the birefringence extinction angle, the alignment order parameter S_I (largest eigenvalue of the overall bond order tensor) and more importantly the ratio η/η_0 of the effective viscosity over its zero shear rate value, are found to approach universal functions when these properties are plotted as a function of the reduced shear rate β_Λ. Regarding more precisely the effective viscosity, we found a simple exponential dependence with respect to the order parameter S_I, as it had been empirically observed experimentally in more concentrated micellar systems [55]. We exploited this exponential behavior to fit a series of viscosity data at fixed ω, but at different shear rates. In this way, we have been able to get rather precise estimates of $\eta_0(\omega)$ and hence the dependency of the zero shear rate viscosity upon the time τ_Λ associated with the relaxation of the dynamical units. Our results confirm the validity of the Faivre-Gardissat theory motivated by the rheology of liquid selenium where single atoms are supposed to bind covalently in non-permanent linear assemblies to form unentangled temporary chain networks. The measured rheological properties of liquid selenium were interpreted in terms of a variant of the Rouse theory where, in addition to polydispersity, the scission/recombination kinetics is included in the theory in an ad hoc way by introducing an extra relaxation mechanism affecting the amplitudes of the contributions of the particular Rouse modes. One of the major results of our thesis

is indeed that our model micellar system leads to a viscosity which decreases as the kinetics gets faster, i.e., as the size of the dynamical units getting smaller.

Finally, our model also predicts that the average micelle size decreases as the shear rate increases. In our case, we found that this decrease is only a function of the bare shear rate and is apparently independent of the kinetics, tuned with the ω parameter. We found that actually the shear rate produces effective scission and recombination rates in which the ω dependence remains the one observed at equilibrium, while the acceptance probability gets larger as the shear rate increases. As the rate relative to the scission process is more strongly increased by the shear rate than the rate controlling the recombination process, the chains need to decrease in size in order to increase the chain end population and satisfy in this way the stationary condition under shear which require an identical number of events of each type.

Many future perspectives are opened by our work:

The study of dense (possibly entangled) micellar systems is a topic of primary interest. Efforts are made presently by different groups. On the basis of a micelle model very similar to ours in which the pair potentials and the Γ range are chosen differently (but this should not affect the general physical context), work is in progress in Strasbourg in J. Wittmer group to study 3D and 2D model fluids at high monomer density.

The study of our model in presence of a planar wall is also an interesting topic as the anisotropy in the diffusion may induce specific inhomogeneity features and lead to unexpected features.

Bibliography

[1] P. van der Schoot, *in "Supramolecular polymers" Ed. A. Ciferri*, 77 (N.Y. 2005)

[2] M.E. Cates and S.J. Candau, *J. Phys: Cond. Matt.* **2**, 6869(1990)

[3] S. Lerouge, J.P. Decruppe and C. Humbert *Phys. Rev. Lett.* **81**, 5457(1998)

[4] H. Hoffmann, S. Hoffmann, A. Rauscher and J. Kalus, *Prog. Colloid Polym. Sci.* **84**, 24(1991)

[5] A. Ott, J.P. Bouchaud, D. Langevin, W. Urbach, Phys. Rev. Lett., **65**, 2201 (1990).

[6] P.G. de Gennes, *Scaling concepts in polymer physics* Cornell University Press, Ithaca(1979)

[7] A.Y. Grosberg and A.R. Khokhlov, *Statistical Physics of Macromolecules* AIP Press, New-York(1994)

[8] M. Doi and S.F. Edwards, *The theory of polymer dynamics* Clarendon, Oxford(1986)

[9] M.E. Cates, *Macromolecules* **20**, 2289(1987)

[10] N.A. Spenley, M.E. Cates and T.C.B. MacLeish *Phys. Rev. Lett.* **71**, 939(1993)

[11] S.M. Fielding and P.D. Olmsted *Phys. Rev. Lett.* **90**, 224501(2003)

[12] B. O'Shaughnessy and J. Yu, *Phys. Rev. Lett.* **74**, 4329(1995)

[13] J.P. Wittmer, A. Milchev and M.E. Cates, *J. Chem. Phys.* **109**, 834(1998)

[14] A. Milchev, *in "Computational methods in colloid and interface science" Ed. M. Borowko and M. Dekker*, 510(N.Y. 2000)

[15] Y. Rouault *J. Chem. Phys.* **111**, 9859(1999)

[16] J.T. Padding and E.S. Boek, *Europhys. Lett.* **66**, 756(2004)

[17] M. Kroger and R. Makhloufi, *Phys. Rev. E* **53**, 2531(1996)

[18] C.-C. Huang, H. Xu, and J.P. Ryckaert, *J. Chem. Phys.* **125**, 094901(2006)

[19] C.-C. Huang, H. Xu, J.-P. Wittmer, F. Crevel, and J.-P. Ryckaert, *"Lecture notes in Physics"* **704** Springer-Verlag, Berlin 379 (2006)

[20] P.van der Schoot, M.A.J. Michels, L. Brunsveld, R. Sijbesma, and Ramzi, *Langmuir* **16** 10076(2000)

[21] A.V. Tobolsky and G.D.T. Owen, *J. Polym. Sci.* **59** 780(1962)

[22] J.P. Wittmer, A. Milchev and M.E. Cates *Europhys. Lett.* **41**, 291(1998)

[23] D. Chandler, *Introduction to Modern Statistical Mechanics* , Oxford University Press (1987)

[24] K. Kremer and G.S. Grest, *J. Chem. Phys.* **92**, 5057(1990)

[25] D.L. Ermak and J.A. McCammon, *J. Chem. Phys.* **63**, 1352(1978)

[26] A. Milchev, J.P. Wittmer, and D.P. Landau Eur. Phys. J. B, 12, 2, pp. 241-251 (1999); cond-mat/9905336.

[27] C.M. Marques, and M.E Cates, *J Phys. II*, **1**, 489(1991)

[28] A. Milchev, J.P. Wittmer, P. van der Schoot, D. Landau Europhysics Letters, 54 58-64 (2001); conf-mat/0008276.

[29] J.P. Wittmer, M. Milchev, P. van der Schoot, J.-L. Barrat J. Chem. Phys., 113 (2000) 6992-7005; cond-mat/0006465.

[30] E. Helfand, *J. Chem. Phys.* **69**, 1010(1978)

[31] D. Brown and J.H.R. Clarke, *J. Chem. Phys.*, 4117(1990)

[32] Y. Rouault and A. Milchev, *Eur. Phys. Lett.* **33**, 341(1996)

[33] R. L. Scott, *J. Phys. Chem.***69**, 261(1965)

[34] J. C. Wheeler, S. J. Kennedy, and P. Pfeuty, *Phys. Rev. Lett.* **45**, 1748(1980)

[35] S. J. Kennedy, J. C. Wheeler, *J. Phys. Chem.***78**, 953(1984)

[36] G. Faivre and J.L. Gardissat, *Macromolecules***19**, 1988(1986)

[37] F. Oozawa and S. Asakura, *Thermodynamics in the Polymerization of Proteins* Academic, New York, 1995

[38] A. Milchev, *Polymer* **34**, 362(1993)

[39] A. Milchev and D.P. Landau, *Phys. Rev. E* **52**, 6431(1995)

[40] A. Milchev and D.P. Landau, *J. Chem. Phys.* **104**, 9161(1996)

[41] Y. Rouault and A. Milchev, *Phys. Rev. E* **51**, 5905(1995)

[42] I. Carmesin and K. Kremer, *Macromolecules* **21**, 2819(1988)

[43] J. Wittmer, W. Paul, and K. Binder, *Macromolecules* **25**, 7211(1992)

[44] J. T. Padding and E. S. Boek, *Phys. Rev. E* **70**, 031502(2004)

[45] C.-C. Huang, H. Xu, and J.-P. Ryckaert, *Submitted* (2007)

[46] A Milchev, and Y, Rouault, *J. Phys. II Frnace* 5, 343(1995)

[47] J.P. Hansen and I.R. McDonald, *Theory of simple liquids* Acad. Pr., (1986)

[48] M. Doi, *Introduction to polymer physics* Clarendon Oxford, (1996)

[49] M. P. Allen and D. J. Tildesley, *Computer Simulation of Liquids* Clarendon Press, Oxford, (1987)

[50] M. G. Paterlini, D. M. Ferguson, *Chem. Phys.* 236, 243(1998)

[51] A. W. Lees and S. F. Edwards, *J. Phys.* C5, 1921(1972)

[52] M.Milchev, J.P. Wittmer, and D.P. Landau, *Phys. Rev. E* 61, 2959(2000)

[53] C. Aust, M. Kröger, and S. Hess, *Macromolecules* 32, 5560(1999)

[54] C. Pierleoni, and J.P. Ryckaert, *Macromolecules* 28, 5097(1995)

[55] S. Förster, M. Konrad and P. Lindner, *Phys. Rev. Lett.* 94, 017803(2005)

[56] M.E. Cates and S.M. Fielding *Advances in Physics* **55**, 7992006

[57] J.T. Padding, E.S. Boek, and W.J. Briels *J. of Phys. Cond. Mat.* **17**, S3347 2005

[58] M. Kroger, *Physics Reports* **390**, 453(2004)

[59] P.J. Flory, *Statistical Mechanics of Chain Molecules* Interscience Publisher, John Wiley & Sons (New York, 1969)

Université Paul Verlaine - Metz

Année 2006-2007

Propriétés statiques, dynamiques et rhéologiques de solutions micellaires par simulation

Thèse en cotutelle avec l'Université libre de Bruxelles

par

Chien-Cheng HUANG

Directeurs : Hong XU et Jean-Paul RYCKAERT

Les propriétés statiques, dynamiques, rhéologiques et la cinétique de scissions et recombinaisons de micelles linéaires auto-assemblées sont étudiées à l'équilibre et sous-écoulement par simulations sur ordinateur, en utilisant un modèle mésoscopique nouveau. Nous représentons les micelles comme des séquences linéaires de billes browniennes dont l'évolution spatio-temporelle est gouvernée par la dynamique de Langevin. Un algorithme de Monte-Carlo contrôle l'ouverture des liens ou la fusion de deux chaînes par les bouts. Un paramètre cinétique ω, qui modélise l'effet une barrière le long d'un chemin de réaction, est introduit dans notre model.

A l'équilibre, nous nous concentrons sur les mécanismes de scission/recombinaison au temps court et au temps long. Nos résultats montrent que pour les temps plus grands que le temps de vie d'une chaîne moyenne, la cinétique est en accord avec le modèle champ-moyen de Cates. L'étude de phénomènes de relaxation macroscopique tels que l'évolution de la longueur moyenne après un T-jump (saut en température) et la fonction de relaxation de contrainte à cisaillement nul confirme que nos constantes cinétiques effectives obtenues aux temps longs sont en effet les paramètres pertinents quand ces relaxations macroscopiques sont couplés à la cinétique scission/recombinaison des micelles.

Pour la situation hors équilibre, nous étudions les effets du couplage entre un écoulement de cisaillement et la cinétique de scission et recombinaison, sur les propriétés structurales et rhéologiques du système micellaire. Nous nous plaçons dans un régime semi-dilué et dynamiquement 'unentangled'. Le paramètre ω est choisi de façon à ce que la durée de vie d'une chaîne moyenne soit plus courte que son temps de relaxation de Rouse le plus long. Nos analyses font apparaître une longueur dynamique Λ, le fragment de chaîne dont la durée de vie τ_Λ est égale à son temps de Rouse. Nous trouvons que les propriétés telles que le rhéo-fluidification, l'anisotropie du tenseur de giration, l'orientation des chaînes et l'étirement des liens sont des fonctions du taux de cisaillement réduit $\beta_\Lambda = \dot{\gamma}\tau_\Lambda$ (où $\dot{\gamma}$ est le tau de cisaillement, alors que la longueur moyenne des micelles est une fonction décroissante du taux de cisaillement, Indépendamment de la barrière du processus scission/recombinaison.

0.0 Introduction

Les solutions de micelles linéaires font partie de systèmes macromoléculaires auto-assemblés qui ont attiré beaucoup d'attention ces dernières années[1, 2]. Ces derniers, comprenant également, entre autres, l'empilement de disques auto-assemblés ou chaînes de molécules bi-fonctionnelles, possède une caractéristique commune, càd qu'ils peuvent être vus comme des systèmes polydisperses de polymères flexibles. Ils ont néanmoins une spécificité : ces 'polymères' sont sans cesse soumis à des processus de scission (d'une chaîne en deux) ou de recombinaison (de deux chaînes en une) par les bouts. C'est pourquoi on les appelle le 'polymères vivants' (en anglais 'equilibrium polymers'). Cette spécificité leur confère des propriétés rhéologiques tout à fait particulières. Sur le plan expérimental, les solutions micellaires ont fait objet d'investigations depuis une dizaine d'années. Le caractère Maxwellien de ces solutions a été constaté[3]. D'autres phénomènes, tels que les bandes de cisaillement[4] et la transition de rhéo-épaississement[5] ont été observés. Etant donné la complexité de ces systèmes, il n'est pas aisé d'interpréter les résultats en repérant les facteurs dominants. Une des complexités est que c'est un système à échelles multiples. Dans une solution micellaire, différentes échelles spatiales et temporelles sont présentes. Il y a par exemple l'échelle moléculaire du surfactant, ou l'échelle de la dynamique de la micelle qui est compliquée par le fait qu'elle est 'vivante' (par scission/recombinaison). Alors que la théorie des polymères est bien établie depuis 50 ans[6, 7, 8], l'étude de polymères vivants est relativement récente[1, 2]. Etant donné qu'il est impraticable de construire une approche théorique à l'échelle moléculaire, des approches basées sur l'approximation 'champ moyen' ou équations phénoménologiques non-locales ont été proposées avec certain succès[9, 10, 11], au prix d'approximations raisonnables mais souvent drastiques, dont certaines ont été questionnées depuis. Par exemple, concernant la cinétique scission/recombinaison des micelles, une étude théorique par O'Shaughnessy et Yu[12] propose qu'à part le modèle 'champ moyen', la cinétique peut aussi se passer selon un mécanisme contrôlé par la diffusion (diffusion controlled). D'autres parts, les études théoriques ont pour la plupart étudié les régimes semi-dilués et concentrés, là où les phénomènes de rhéologie non-linéaire sont les plus spectaculaires et là où le champ moyen est plus applicable. Il y a donc un 'espace' à explorer concernant des régimes à la limite entre dilué et semi-dilué, où la théorie de Rouse classique doît être élargie[8]. Citons, sur ce sujet, les travaux de Faivre et Gardissat[13], qui traite la viscoélascité linéaires de polymères vivants en régime 'unentangled', qui permit d'interpréter la rhéologie du sélénium liquide (possédant un réseau de liens transitoires).

Parallèlement, les simulations par ordinateur peuvent éclairer beaucoup d'aspects de ces systèmes, grâce aux techniques empruntées de la simulation des polymères. Par une modélisation mésoscopique, les micelles linéaires sont représentées par des chaînes de polymères vivants capables de scission et de recombinaison. L'avantage des simulations numériques est leurs possibilités d'être comparées soit aux expériences soit à la théorie, étant donné que ces systèmes sont difficiles à caractériser expérimentalement et que les résultats ne sont pas simples à interpréter. Le modèle sur réseau 'bond fluctuation model' (BFM) a été utilisé pour étudié les propriétés statiques et dynamiques des polymères vivants à l'équilibre[14, 15]. Concernant les approches dans l'espace continu, on peut citer [16, 17, 18, 19], pour des propriétés d'équilibre ou sous cisaillement, avec néanmoins des modèles de micelles qui ne semblaient pas satisfaire la

micro-réversibilité.

Nous adoptons donc une approche dans l'espace continu, en proposant un nouveau modèle de micelle respectant la microréversibilité. L'évolution spatio-temporelle des monomères est régie par la dynamique de Langevin, et les transitions scission/recombinaisons sont contrôlées par un algorithme Mont Carlo. Nous introduisons dans notre modèle un paramètre de fréquence de transition ω qui permet de modifier la cinétique des micelles sans changer les propriétés statiques, telles que la distribution de longueurs, ou la longueur moyenne. Ce paramètre nous permet de révéler des aspects fondamentaux de la dynamique des micelles.

La thèse est organisée comme suit : Ch1 est consacré à une révision théorique, Ch2 présente le modèle mésoscopique des micelles ainsi que l'algorithme numérique utilisée. Dans Ch3 nous présentons nos résultats du système à l'équilibre, notamment concernant la cinétique et les propriétés dynamiques, tandis que Ch4 traite la situation du système sous cisaillement, avec l'accent mis sur le couplage entre la cinétique et le champ d'écoulement. Dans Ch5 nous donnons les conclusions.

0.1 Cadre théorique

Dans ce chapitre, nous présentons le cadre théorique de physique statistique qui étudie un système de polymères vivants à l'équilibre. Ce problème a vu un progrès considérable depuis les travaux de Cates et d'autres auteurs[2]. Nous avons également revu certaines notions fondamentales dans un article récents[20]. Dans les sections suivantes nous allons présenter : 1) La distribution des chaînes à l'équilibre; 2) Le modèle de cinétique de Cates et 3) La relaxation macroscopique et 4) La viscoélasticité des polymères vivants.

0.1.1 La fonction de distribution des chaînes à l'équilibre

Considérons un système de chaînes de polymères vivant, défini par M monomères dans un volume V, la densité des monomères est $\phi = M/V$, l'energie de scission est E et la température du solvant est T. Comme nous avons montré dans [20], la mécanique statistique d'équilibre permet de calculer la distribution des longueurs $c_0(L)$ et la longueur moyenne L_0. Nous avons, notamment, pour les chaînes idéales :

$$c_0(L) = \frac{\phi}{L_0^2} \exp\left(-\frac{L}{L_0}\right) \tag{1}$$

et

$$L_0 = B^{1/2}\phi^{\frac{1}{2}} \exp\left(\frac{\beta E}{2}\right). \tag{2}$$

où $B = eb^3/C_1$ est une constante dépendant notamment de la taille des monomères b.

Pour une solution diluée, nous avons Une distribution de Schulz-Zimm :

$$c_0(L) = \frac{\exp(-\beta E)}{B} L^{(\gamma-1)} \exp\left(-\gamma\frac{L}{L_0}\right) \tag{3}$$

et

$$L_0 = \left(\frac{\gamma^\gamma}{\Gamma(\gamma)}\right)^{\frac{1}{1+\gamma}} B^{\frac{1}{1+\gamma}} \phi^{\frac{1}{1+\gamma}} \exp\left(\frac{\beta E}{(1+\gamma)}\right). \tag{4}$$

où $\gamma = 1.167$ est une constante universalle des marches au hasard auto-évidente.

Pour une solution semi-diluée, la distribution est donnée par :

$$c_0(L) = \frac{\phi}{L_0^2} \exp\left(-\frac{L}{L_0}\right) \tag{5}$$

et la longueur moyenne par :

$$L_0 \propto \phi^\alpha \exp\left(\frac{\beta E}{2}\right) \tag{6}$$

où $\alpha = \frac{1}{2}(1 + \frac{\gamma-1}{3\nu-1})$ est environ 0.6 ($\nu = 0.588$ est la constante de Flory).

0.1.2 Modèle cinétique de Cates pour la scission et la recombinaison

Soit $c(t, L)$ la distribution des chaînes au temps t, Cates[9] a proposé l'équation cinétique suivante :

$$\frac{dc(t,L)}{dt} = -k_s L c(t,L) + 2k_s \int_L^\infty c(t,L')dL' \tag{7}$$

$$+ \frac{k_r}{2}\int_0^L c(t,L')c(t,L-L')dL' - k_r c(t,L)\int_0^\infty c(t,L')dL' \tag{8}$$

où k_s et k_r sont des constantes cinétique de scission (recombinaison). Naturellement la distribution d'équilibre $c_0(L)$ est la solution stationnaire, et k_s et k_r sont reliés par :

$$\phi \frac{k_r}{2k_s} = L_0^2 \tag{9}$$

La théorie champ moyen suppose qu'un polymère de longueur L_0 a une durée de vie $\tau_b = 1/(k_s L_0)$. Le processus de scission et de recombinaison suit une loi de Poisson. Ce qui implique que la distribution des temps de premières scissions est de la forme :

$$\Psi(t) = \exp\left(-\frac{t}{\tau_b}\right) \tag{10}$$

pour une chaîne de taille moyenne. Pour le bilan détaillé, $\Psi(t)$ est aussi la distribution des premières recombinaisons.

0.1.3 Relaxation macroscopique

La relaxation que nous présentons ici correspond à une expérience T-jump (saut de température). Un calcul théorique en champ moyen permet d'exprimer l'évolution de la longueur moyenne des chaines vers l'équilibre, après un saut brutal de température[21]. Si le système est équilibré à T_0 et qu'il est brutalement amené à la température $T < T_0$ (T-jump), la longueur moyenne évolue de $L_0(T_0)$ vers $L_0(T)$ selon :

$$< L(t) >= L_0(T) / \coth\left(\frac{t + t_0}{2\tau}\right) \tag{11}$$

où

$$t_0 = 2\tau \coth^{-1}\left[L_0(T)/L_0(T_0)\right] \tag{12}$$

avec τ relié au temps de vie moyen $\tau_b(T)$ par :

$$\tau = \frac{1}{2k_s(T)L_0(T)} = \frac{1}{2}\tau_b(T) \tag{13}$$

Donc, cette relaxation de longueur moyenne est intimement reliée à la constante cinétique $k_s(T)$.

0.1.4 La viscoélasticité des polymères vivants

La viscoélasticité des polymères vivants est fortement influencée par la cinétique scission/recombinaison. Pour les systèmes semi-dilués et concentrés, Cates et al.[2] ont prédit une relaxation à un temps, du type Maxwell, avec $\tau_{relax} = \sqrt{\tau_b \tau_{rep}}$ où τ_{rep} est un temps de reptation d'une chaîne. Pour nous systèmes qui sont semi-dilués mais proches du régime dilué, les chaînes sont 'unentangled' sur le plan dynamique. Nous devons donc appliquer la théorie de Faivre de Gardissat[13] qui généralise le modèle de Rouse[8]. Il est prédit, notamment, que la relaxation du module de cisaillement s'exprime :

$$\lim_{t>>\tau_\Lambda} G(t) = G_0 \sqrt{\frac{\pi}{3}} \sqrt{\frac{\tau_0}{t}} \exp\left(-t/\tau_{relax}\right) \tag{14}$$

où le temps de relaxation $\tau_{relax} = (2^{2/3}/3)\tau_1$, où $\tau_1 = \tau_b^{2/3}(L_0)\tau_{Rouse}^{1/3}(L_0)$. Ce temps τ_1 n'est rien d'autre que le temps caractéristique τ_Λ, qui correspond à une longueur de chaîne Λ telle que son

temps de Rouse est égal à son temps de vie (cf[15]) : $\tau_{Rouse}(\Lambda) \equiv \tau_0 \Lambda^2 = \tau_b(\Lambda) \equiv 1/(k_s \Lambda)$. Donc Λ est τ_Λ dépendent de k_s :

$$\tau_\Lambda = \tau_0^{1/3} k_s^{-2/3}; \quad \Lambda = (\tau_0 k_s)^{-1/3} \tag{15}$$

Nous allons montrer l'importance de τ_Λ aux Ch3 et Ch4.

0.2 Un modèle mésoscopique de polymères vivants

Dans ce chapitre, nous présentons un nouveau modèle de polymère vivant qui sert de modèle de base pour nous études numériques des Ch.3 et Ch.4. Nous présentons aussi les algorithmes numériques qui gouvernent l'évolution spatio-temporelle des monomères et celle du réseau de liens entre monomères. Notre modèle est inspiré de celui des polymères FENE[22], tout en tenant compte de l'aspect scission/recombinaison des chaînes, caractéristiques des polymères vivants. Par rapport aux modèles existants, il préserve la micro-réversibilité par construction et il permet la variation de la barrière de recombinaison, conduisant à des études intéressantes sur la cinétique scission/recombinaison. Nous présenterons d'abord le potentiel de pair liées et non-liées, ensuite nous expliciterons la technique de la Dynamique de Langevin, ensuite nous présenterons la méthode Monte Carlo utilisé pour faire évoluer le réseau de liaisons.

0.2.1 Le potentiel de paire

Dans notre modèle, les monomères s'intéragissent via un potentiel de paire, dont la forme diffère selon qu'ils sont liés ou non-liés. En effet, les monomères non-liés s'intéragissent avec U_2 qui est un potentiel de Lennard-Jones répulsif, et les paires liées sont sous U_1 qui consiste en un potentiel FENE additionné de U_2. La figure1donne un schéma des potentiels U_1 et U_2.

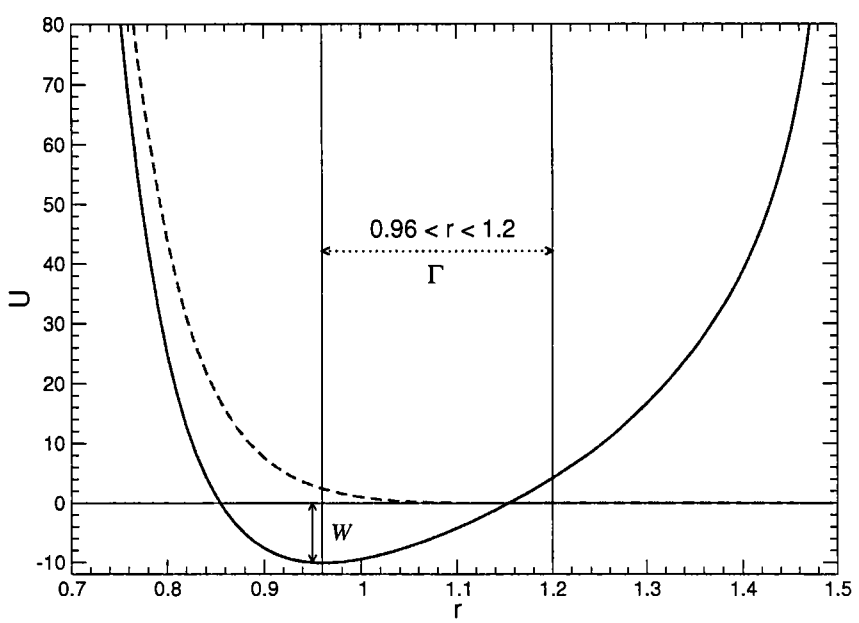

FIG. 1 – Le potentiel d'une paire liée $U_1(r)$ (courbe continue) et non-liée $U_2(r)$ (courbe en pointillés). W représente l'énergie nécessaire pour ouvrir un lien. La région Γ où les potentiels s'échangent pendant la simulation en dynamique de Langevin est aussi indiquée.

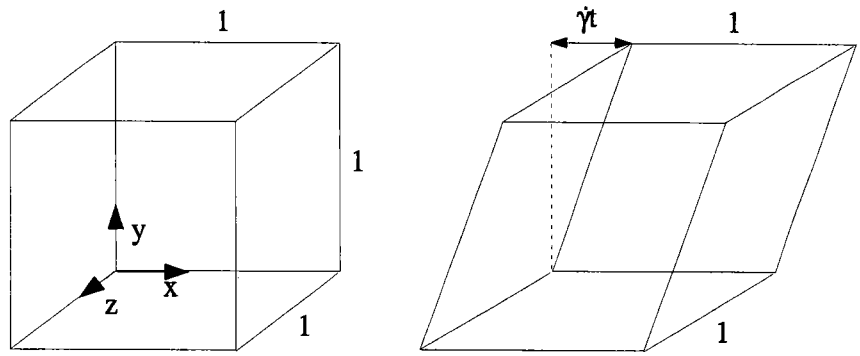

FIG. 2 – Représentation schématique d'un écoulement de Couette plan.

0.2.2 La dynamique de Langevin

Durant nos simulations, l'évolution spatio-temporelle des monomères est régie par la dynamique de Langevin, qui représente les mouvements de particules browniennes dans un solvant. En absence d'écoulement macroscopique du solvant, l'équation de Langevin s'écrit :

$$m_i\dot{\vec{v}}_i(t) = -m\xi\vec{v}_i(t)_i + \vec{F}_i(t) + \vec{R}_i(t) \tag{16}$$

Avec, pour les forces aléatoire $\vec{R}_i$, les propriétés suivantes (théorème de fluctuation-dissipation) :

$$< R_{i\alpha}(t)R_{j\beta}(t') >= 2m_i\xi_i k_B T\delta_{ij}\delta_{\alpha\beta}\delta(t-t') \tag{17}$$

où $\alpha(\beta)$ sont les composants x,y ou z. Une résolution numérique (par pas de temps fini) a été proposée par[23] qui est basée sur l'algorithme Velocity-Verlet.

En présence du cisaillement, nous avons un champ de vitesse $\vec{u}$ with $u_x = \dot{\gamma}y$ (voir fig2). L'équation de Langevin devient : Pour assurer le cisaillement à travers les frontières de la boîte de simulation, nous adoptons les conditions aux limites de Lees-Edwards[24] (voir fig3).

0.2.3 Algorithme Monte Carlo

Comme indiqué précédemment, les polymères vivants subissent des scissions et des recombinaisons à cause des fluctuations thermodynamique (et aussi sous l'effet du cisaillement quand celui-ci est présent). Nous considérons donc qu'à chaque instant le système est représenté par $2M$ liens, donc certains sont des vrais liens, d'autres des 'bras pendants' (chaque monomère a deux bras, peuvent donc avoir 0, 1 ou 2 liens). Nous proposons d'utiliser un algorithme Monte Carlo pour controler la transition entre un état m et un état n du réseau de liens. Cet algorithme est expliqué en détail dans[20]. Notons que cette probabilté de transition est proportionnelle à ω, la fréquence d'essai par bras. Et les transitions se passent quand deux monomères se trouvent dans la zone de distance Γ (voir fig1). Le paramètre ω est introduit afin de modéliser une barrière de recombinaison selon $\omega \propto \exp(-B)$. Dans nos simulations, ω est la fréquence d'essai pour l'exchange U_1 à U_2 ou l'inverse, par bras de monomère (chacun ayant 2 bras).

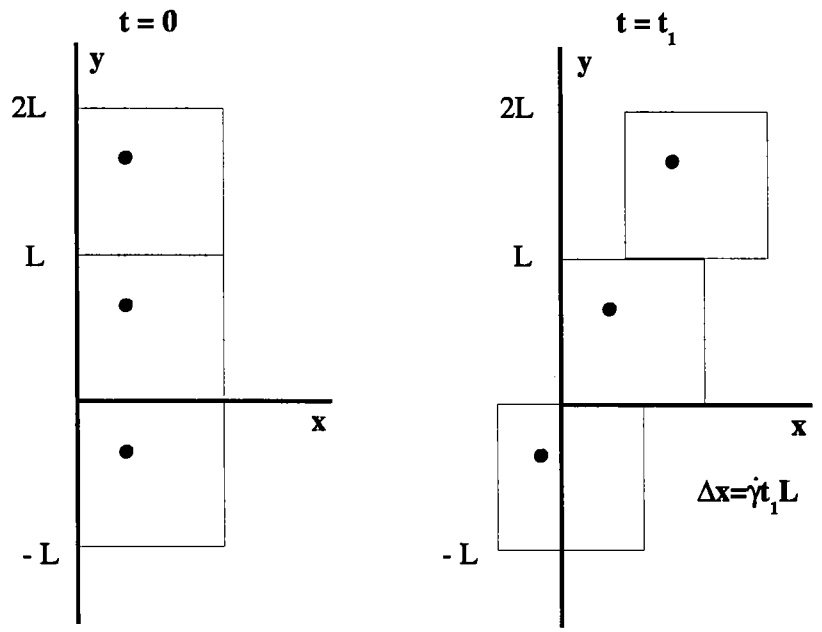

FIG. 3 – Représentation schématique de conditions périodiques en cas d'écoulement de Couette plan.

0.3 Propriétés à l'équilibre

Ce chapitre est consacré aux propriétés à l'équilibre de nos solutions micellaires, selon le modèle mésoscopique du Ch2. Nos systèmes sont composés de M monomères, dans un volume V, dans un solvant à température T. Nous fixons la température, ainsi que la viscosité du solvant. Trois états thermodynamiques ont été explorés. Ces états sont déterminés par les paramètres W (énergie de liaison entre monomères) et $\phi = M/V$ la densité des monomères. En adoptant les unités de Lennard-Jones, nous avons, pour les trois états, les couples (W, ϕ) suivants : 1.(8,0.05) ; 2.(10,0.15) et 3.(12,0.15), la température $T = 1/k_B$ et la viscosité $\eta = 1$. Le nombre de monomères dans la boîte de simulation a été fixé à $M = 1000$. Nous avons pris pour chaque état plusieurs valeurs de fréquences ω. Les résultats de ce chapitre ont fait l'objet de deux publications[20, 25].

0.3.1 Propriétés statiques

Les premières proriétés statiques sont la distribution de longueur de chaîne $c_0(L)$ et la longueur moyenne L_0. Comme attendu, ces résultats sont indépendants de ω. Nous obtenons $L_0 = 11.5$, 56 et 151 pour les trois états respectivement. Il s'ensuit que l'état 1 est dilué et les 2 autres semi-dilué. Nous avons vérifié l'accord avec les prédictions théoriques de Ch1, avec E identifiable à W, à une constante additive près. Les résultats de conformation des chaînes confirment les lois d'échelle bien connues, selon le régime de concentration.

0.3.2 Propriétés dynamiques

Cette partie constitue une contribution originale que notre modèle permet de faire, grâce à sa capacité à varier ω, pour le même état thermodynamique. En effet, les propriétés dynamiques, aussi bien la cinétique de scission/recombinaison que la diffusion des monomères, dépendent fortement de ω.

L'un des 1ers calculs que nous avons fait concerne l'estimation de constantes cinétiques de scission et de recombinaison k_s et k_r apparaîssant dans la théorie champ moyen de Cates[9]. Nous avons montré qu'il est très important de séparer les échelles de temps dans tout processus dynamique. En effet, au temps court, les transitions de scission ou recombinaison sont souvent tout de suite suivies par une transition dans le sens inverse. Ces événement corrélés ne contribuent pas à la transition 'vraie', au sens champ moyen, qui implique, par exemple, une recombinaison de 'i' avec 'k' après s'être séparé de 'j' et avoir diffusé. Une façon d'estimer les constantes cinétiques effectives est de calculer la fonction de distribution des temps de premières recombinaison après une cassure de lien, qui donne le temps de vie τ_b et permet de calculer k_s et k_r à travers les relations du Ch1. Sur la fig4, nous montrons cette distribution $\Psi(t)$ en fonction du temps pour un cas semi-dilué et à $\omega = 0.5$. Nous séparons les recombinaisons 'self' (avec son ancien partenaire suivant une séparation) et les recombinaisons 'cross' (avec un autre partenaire que celui duquel le monomère est séparé). Nos courbes montrent clairement qu'au temps court, les recombinaisons 'self' dominent, et qu'au temps long, la tendance est inversée. Le comportement au temps long correspond à un processus de Poisson et permet d'estimer τ_b.

Sur la fig5, nous présentons $\Psi(t)$ pour plusieurs valeurs de ω. Nous montrons ainsi que plus ω est petit, plus vite la limite 'champ moyen' est atteinte. Ce qui s'explique par une plus grande possibilité pour les monomères de diffuser avant une nouvelle recombinaison.

Bien que $\Psi(t)$ permette d'estimer les constantes cinétiques, elle présente un inconvénient technique dû au manque de statitiques au temps long. Une autre méthode plus précise due à Helfand[26, 20] a été appliquée à nos systèmes. La fonction $H(t)$ (hasard cumulé) relative aux statistiques de recombinaisons est engendrée durant nos simulations. Au temps long, cette fonction est linéaire dont le pente donne $1/\tau_b$. L'interception de $H(t)$ avec l'axe des ordonnées donne $-\ln\kappa$, où κ est le coefficient de transmission, càd la proportion de transitions qui sont effectives au sens 'champ moyen'. Sur la fig6, nous montrons $H(t)$ pour l'état 3 (semi-dilué), illustrant ainsi les comportement aux temps long et court. Les différentes méthodes d'estimation de k_s et k_r ont été présentées et commentées dans[25].

Une autre propriété dynamique que nous avons étudiée est le déplacement quadratique moyen (DQM) des monomères. Comme ceux-ci appartiennent à des chaînes de longues différentes qui subissent sans cesse des scissions et recombinaisons, l'interprétation du DQM n'est pas aisée. Cependant, suivant l'idée de Milchev[15] invoquée au Ch1, nous pouvons examiner le DQM sous l'angle de τ_Λ. Fig7 montre le DQM des monomères pour les deux états semi-dilué que nous avons étudiés et pour plusieurs valeurs de ω. Nous constatons un changement de comportment (Rouse/Einstein) au temps de croisement τ^* qui dépend de ω. Connaissant le temps τ_Λ par ailleurs (à travers k_s), nous observons que $\tau^* \approx 2.4\tau_\Lambda$ pour tous les cas étudiés, montrant qu'en réalité, c'est τ_Λ qui gouverne ce 'cross-over' du DQM. Pour renforcer cette observation, nous

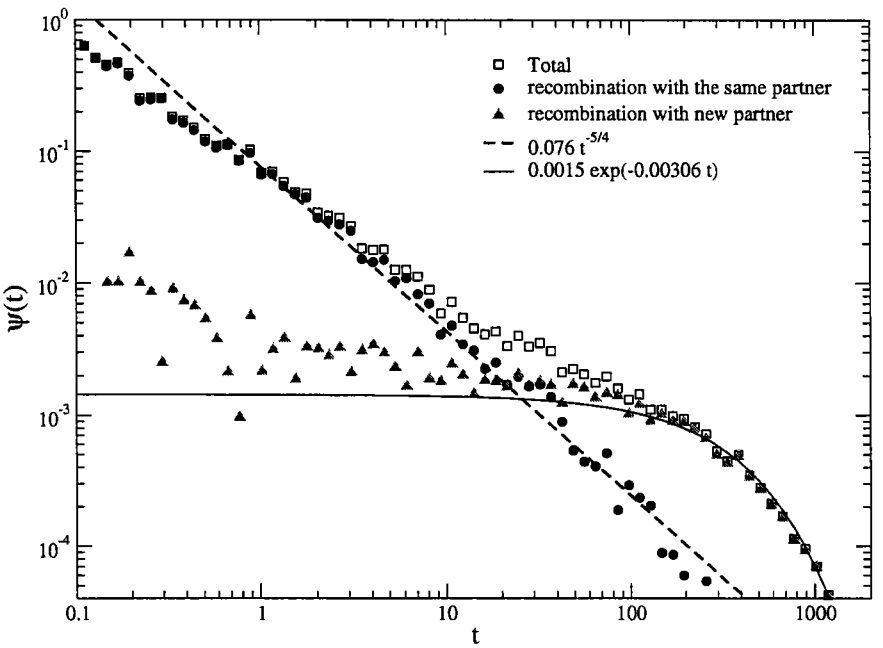

FIG. 4 – Distribution des temps de premières recombinaisons $\Psi(t)$ pour le cas semi-dilué ($W = 10$) avec une fréquence d'essai $\omega = 0.5$. Nous distinguons la recombinaison avec le même partenaire (cercles pleins) ou avec un nouveau partenaire (triangles pleins). La ligne en pointillés (avec une pente $-5/4$ représente une loi de puissance $t^{-5/4}$ attendue au temps courts[18]. La ligne solide indique la prédiction 'champ moyen' au temps long (pour $t > 30$).

portons dans fig8 τ^* vs k_s pour chaque ω, nous observons en effet une loi de puissance $-2/3$, comme pour τ_Λ.

Dans cette partie de thèse, nous avons aussi étudié la fonction d'auto-corrélation des contraintes $G(t)$, ainsi qu'une relaxation macroscopique (T-jump)[25]. Nous avons vérifié que $G(t)$ suit la prédiction de Faivre et Gardissat invoquée au Ch1. Nous avons pu fitter nos résultats avec cette théorie en ayant un seul paramètre libre G_0. Pour la T-jump, notre expérience numérique de la relaxation de la longueur moyenne $< L(t) >$ après un T-jump est tout à fait en accord avec la prédiction théorique[21] basé sur une approche 'champ moyen', pourvu que l'on prenne les constantes cinétiques effectives (estimation au temps long).

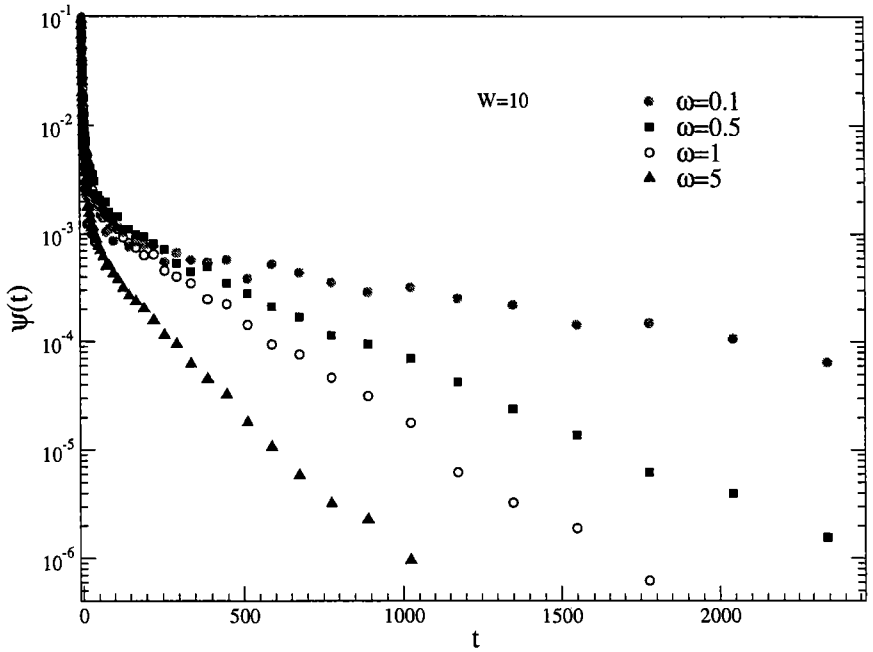

FIG. 5 – Distribution des temps de premières recombinaisons $\Psi(t)$ pour le cas semi-dilué ($W = 10$) pour 4 fréquences d'essai, $\omega = 0.1$ (cercle plein), 0.5 (carré plein), 1 (cercle vide) et 5 (triangle pleins). La longueur moyenne pour cet état est $L_0 = 56.4$ et est indépendant de ω.

0.4 Propriétés sous écoulement

Ce chapitre est consacré à l'étude de nos solutions micellaires sous cisaillement. Le modèle est toujours celui du Ch2. L'état choisi est un état semi-dilué, avec $L_0 = 56$ à l'équilibre. Forts de nos expériences du Ch3, nous avons choisi les valeurs de ω pour qu'il y ait un fort couplage entre la dynamique des chaînes et le processus scission/recombinaison, càd $L_0 > \Lambda$. Le but est d'étudier le couplage entre l'écoulement de cisaillement et cette cinétique de scission/recombinaison. Cette coulage se manifeste à deux niveaux, d'une part sur les propriétés rhéologiques collectives, d'autre part sur les propriétés dépendant de longueur de chaînes.

0.4.1 Comportement rhéologique collectif

Sous l'écoulement, les micelles ont tendance à s'aligner dans la direction de celui-ci. Cette propriété peut être mesurée par l'angle d'extinction χ_O en fonction du taux de cisaillement $\dot{\gamma}$. Cette propriété est tracée en fig9. On constate que comme prévu, χ_O est une fonction monotone décroissante de $\dot{\gamma}$, de 45° pour $\dot{\gamma} \to 0$ à quelques degrés pour les grandes valeurs de $\dot{\gamma}$. Nous remarquons également que cette décroissance est plus lente quand ω diminue, dû à un plus faible k_s. Ce qui est remarquable, c'est quand nous réduisons $\dot{\gamma}$ par le temps caractéristique τ_Λ, en traçant χ_O vs $\beta_\Lambda = \dot{\gamma}\tau_\Lambda$, nous trouvons une courbe universelle (indépendante de ω). Ce résultat montre que l'important pour le système, c'est $\dot{\gamma}/(1/\tau_\Lambda)$, et non pas $\dot{\gamma}$ seul.

Dans fig.10, nous traçons la variation de la longueur de liaison moyenne Δl sous l'effet

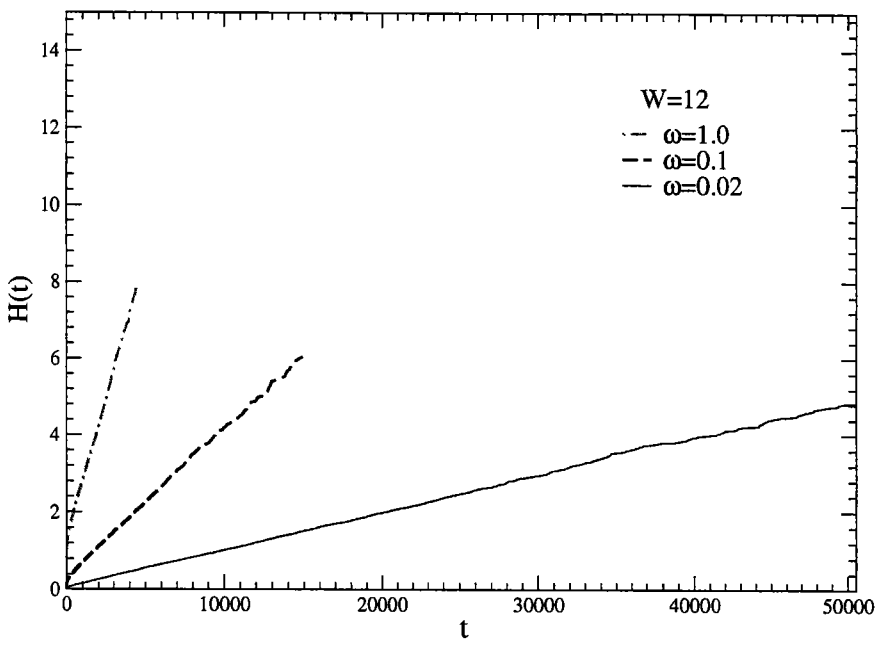

FIG. 6 – La fonction du hasard cumulé $H(t)$ pour le cas $W = 12$. La longueur moyenne est $L_0 = 151.4$. Les courbes correspondent à plusieurs fréquences d'essai ω, qui a pour valeur 0.02 (ligne continue), 0.1(ligne en pointillés) et 1(pointillés et tirets). Remarquons que la cas de$\omega = 0.02$, présentant une interception $H_I \approx 0$ est très proche du cas 'mean field', avec un coefficient de transmission $\kappa = 0.93$.

du cisaillement. C'est une fonction croissante de $\dot{\gamma}$, et cette croissance dépend de ω. Ainsi, ω grand donne une plus faible croissance, due aux scissions/recombinaisons plus nombreuses. En revanche, quand nous traçons Δl vs β_Λ, le même comportement universel est observé.

La viscosité du système se calcule avec la formule $\eta = \sigma_{xy}/\dot{\gamma}$. D'après[27], cette propriété est reliée à la structure du système, notamment le paramètre d'ordre d'orientation S_I, à travers la relation $\eta \propto \exp(-aS_I)$. Nos expériences numériques vérifient en effet cette relation (voir fig11). Une extrapolation permet de trouver avec précision la limite Newtonnienne η_0 pour chaque ω.

Dans fig12, nous traçons η/η_0 en fonction du taux réduit β_Λ. D'abord, nous remarquons que nous avons une courbe maîtresse (indépendante de ω), ensuite, nous constatons que le système est rhéo-fluidifiant, comme attendu.

L'intérêt de connaître avec précsion η_0 pour différente valeurs de ω réside dans le fait qu'il permet de remonter à la théorie de Faivre et Gardissat (viscoélasticité linéaire). Dans Ch1, nous avons donné $G(t)$ qui dépend de deux paramètres libres, τ_Λ et G_0. Or, l'intégrale de $G(t)$ donne η_0. En traçant η_0 en fonction de τ_Λ dans fig13, nous trouvons G_0 par un fit. La valeur trouvée est très proche du fit basé sur un calcul direct de $G(t)$ [25], avec, là-bas beaucoup de bruits numériques.

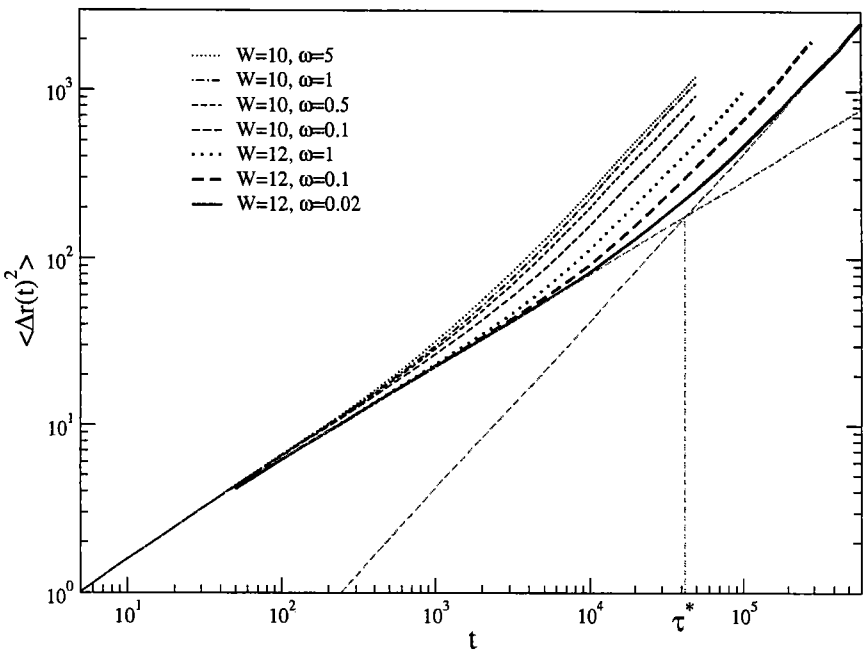

FIG. 7 – Déplacement quadratique moyen des monomères pour $\omega = 0.1, 0.5, 1, 5$ du cas $W = 10$ et $\omega = 0.02, 0.1, 1$ du cas $W = 12$. Pour $\omega = 0.02$, les comportements au temps court ($t^{0.6}$) et au temps long (t^1) sont représentés. Ces asymptotes se croisent au temps τ^*.

0.4.2 Analyse des propriétés dépendant de la longueur des chaînes

Nos études des propriétés dépendant de la longueur ont montré un résultat remarquable : il y a un phénomène de saturation des propriétés matériels, telles que l'angle d'extinction, ou le paramètre d'ordre d'orientation, en fonction de la longueur. Cette situation est mise en évidence quand nous comparons le comportement de nos polymères vivants avec celui de systèmes polydisperses 'morts', qui eux, suivent des lois d'échelles déjà observées par d'autres auteurs[28, 29, 30]. Et cette saturation arrive pour une longueur $L \approx \Lambda$ (voir fig14). Ceci montre que les chaînes plus longues que Λ se 'cassent' avant d'être alignées par l'écoulement, démontrant de nouveau le couplage fort entre la cinétique et l'écoulement.

Une autre propriété structurale que nous avons mesurée est la longueur moyenne des chaînes $< L >$ en fonction du taux de cisaillement (voir fig15). Contrairement aux autres propriétés, celle-ci, une fonction décroissante de $\dot{\gamma}$, est indépendante de ω, comme à l'équilibre. L'explication de ce constat n'est pas encore complète. Il semble que ce soit lié au fait qu'en écoulement stationnaire, $< L >$ doit satisfaire $< L >^2 = \phi k_r/(2k_s)$. Or nous avons constaté que, sous cisaillement, $k_s(\omega, \dot{\gamma}) = \kappa(\omega) Q_s(\dot{\gamma})$ et $k_r(\omega, \dot{\gamma}) = \kappa(\omega) Q_r(\dot{\gamma})$, où $\kappa(\omega)$ est le coefficient de transmission à l'équilibre. Ce qui résulte le comportement de la longueur moyenne en fonction du taux de cisaillement.

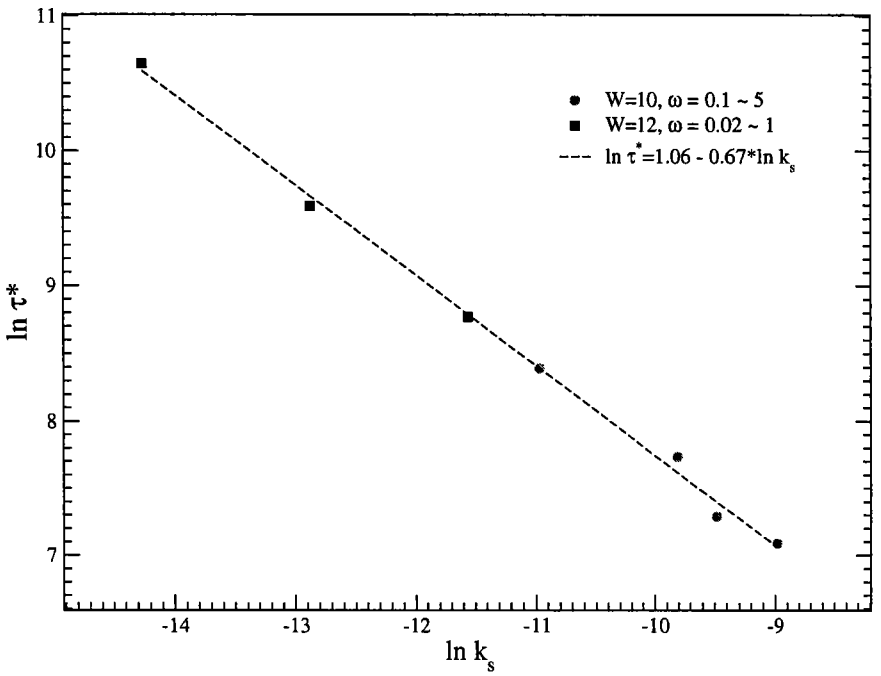

FIG. 8 – τ^* est représenté en fonction de k_s dans une écjelle log-log. La ligne en pointillés avec une pente $-2/3$ correspond à une loi de puissance $\tau^* \propto k_s^{-2/3}$.

0.5 Conclusions

Dans cette thèse, nous avons proposé une nouvelle version de modèle mésoscopique de polymères vivants en solution. Et nous avons exploré ce modèle pour étudier la structure, la dynamique et la rhéologie de ces systèmes complexes à l'aide de simulations numériques et aux points thermodynamiques en régimes dilués et semi-dilué.

La dynamique et la rhéologie d'un état semi-dilué ont été spécifiquement étudiées. Cet état présente une longueur de contour moyenne $L_0 = 57$ monomères. Cette chaîne peut être vue comme une collection de 'blobs' de taille $g \approx 37$. Etant donné le caractère très flexible de nos chaînes et le fait que le système est modérément semi-dilué, nous sommes dans un régime dynamique 'non-entangled'. Par consequent, le temps de relaxation d'une chaîne de longueur L suit une dépendance en L^2. Ainsi, nous avons défini une longueur dynamique Λ telle que son temps de vie est égal à son temps de Rouse. Il n'ensuit que les chaînes plus longues que Λ voient leur dynamqiue fortement influencée par la cinétique scission/recombinaison. Nous avons choisi l'intervalle du paramètre de barrière ω telle que l'on a des systèmes où $L_0 > \Lambda$. Nous avons pu mettre en évidence de façon convaincante l'aspect unversel de Λ et de τ_Λ concernant la dynamique des solutions micellaires. Nos études ont aussi permis d'apporter un éclairecissement sur la distinction entre 'mean field' ou 'diffusion contrôlled' concernant la cinétique des micelles. En fait le passage entre l'un et l'autre se manifeste par un coefficient de transmission $\kappa < 1$ qui mesure la proportion de transitions au sens 'champ moyen'. Nous avons pu à la fois quantifier κ et estimer les constantes cinétiques effectives au sens 'mean field'. Ces derniers prédisent des

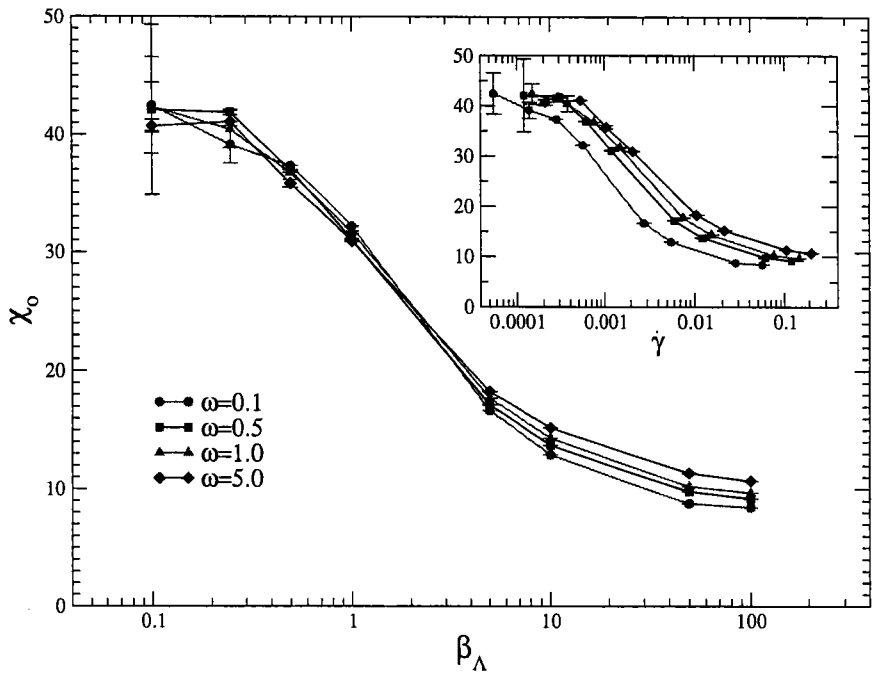

FIG. 9 – L'angle d'extinction χ_O en fonction du taux de cisaillement réduit β_Λ, et, dans l'encart, en fonction du taux de cisaillement $\dot{\gamma}$. Les symboles correspondent à $\omega = 0.1$(cercle), 0.5 (carré), 1 (triangle) et 5 (diamand).

relaxations macroscopiques cohérentes avec les théories existantes. En soumettant le système à un écoulement de cisaillement, nous avons, pour la 1ère fois concernant les systèmes micellaires, obtenu des courbes maîtresse de rhéologie et de structure du système en portant ces propriétés en fonction du taux de cisaillement réduite par un taux dynamique intrinsèque du système $1/\tau_\Lambda$. Ces résultats marquent les 1ers pas d'études de nos systèmes hors équilibre, qui vont être poursuivies avec l'attention sur la cinétique sous cisaillemnt et le lien entre la cinétique et la réponse structurale du système sous cisaillement.

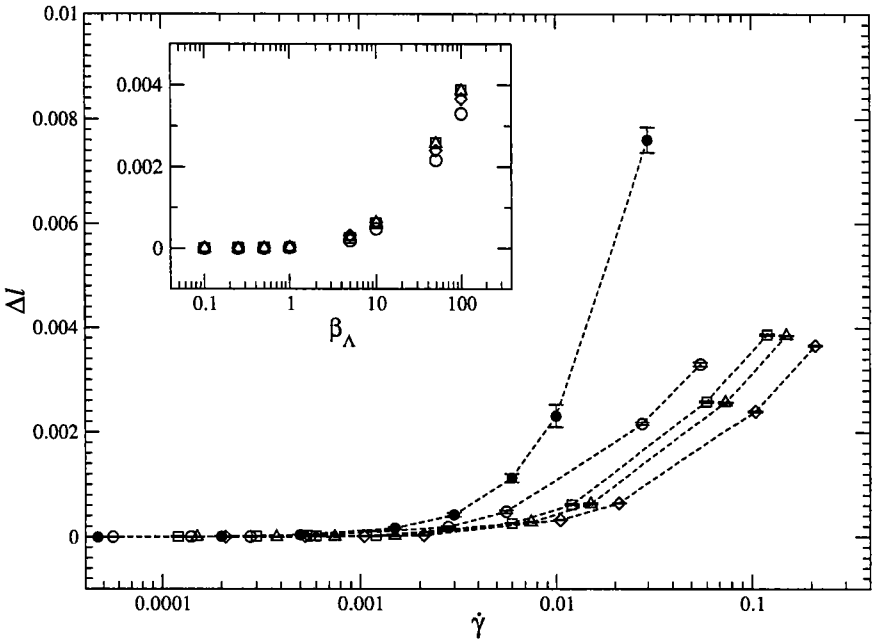

FIG. 10 – L'extension de la longueur moyenne de lien par rapport à l'équilibre, Δl en fonction du taux de cisaillement 'brut' $\dot{\gamma}$, et, dans l'encart, en fonction du taux réduit β_Λ. Les symboles correspondent à $\omega = 0.1$(cercle vide), 0.5 (carré), 1 (triangle) et 5 (diamand). Les cercles pleins sont des résultats d'un système polydisperse de chaînes 'mortes' (sans scission/recombinaison).

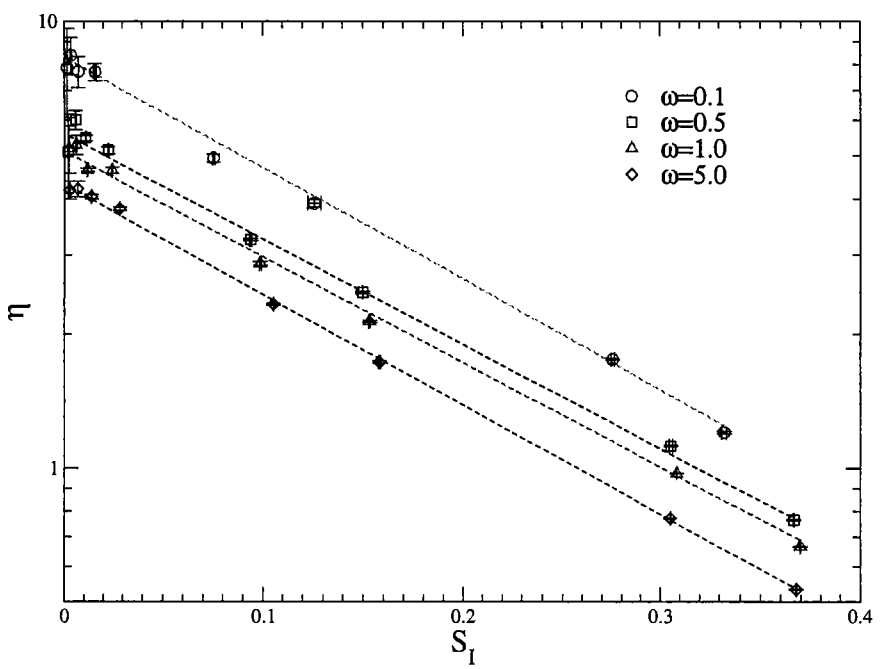

FIG. 11 – La viscosité en fonction du paramètre d'ordre S_I. Les symboles correspondent à $\omega = 0.1$(cercle), 0.5 (carré), 1 (triangle) et 5 (diamand). Les droites en pointillés sont des fits à deux paramètres $\eta = \eta_0 \exp(-aS_I)$.

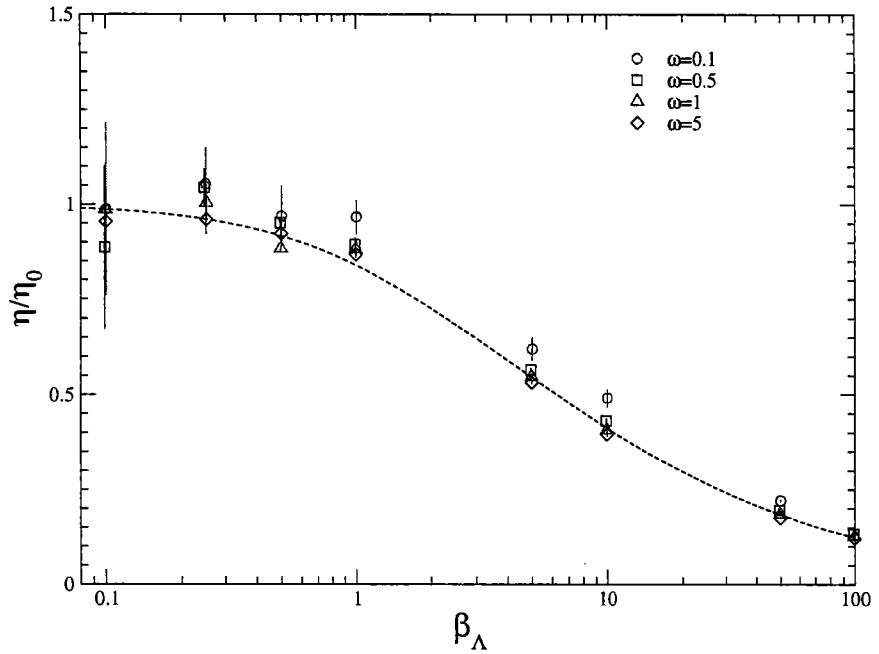

FIG. 12 – La viscosité relative η/η_0 en fonction du taux de cisaillement réduit β_Λ. Les symboles correspondent à $\omega = 0.1$(cercle), 0.5 (carré), 1 (triangle) et 5 (diamand). La courbe en pointillés est une fonction de fit ad hoc $f(\beta_\Lambda) = exp[-a(ln(1+\beta_\Lambda))^b]$ avec $a = 0.2838$ et $b = 1.3045$.

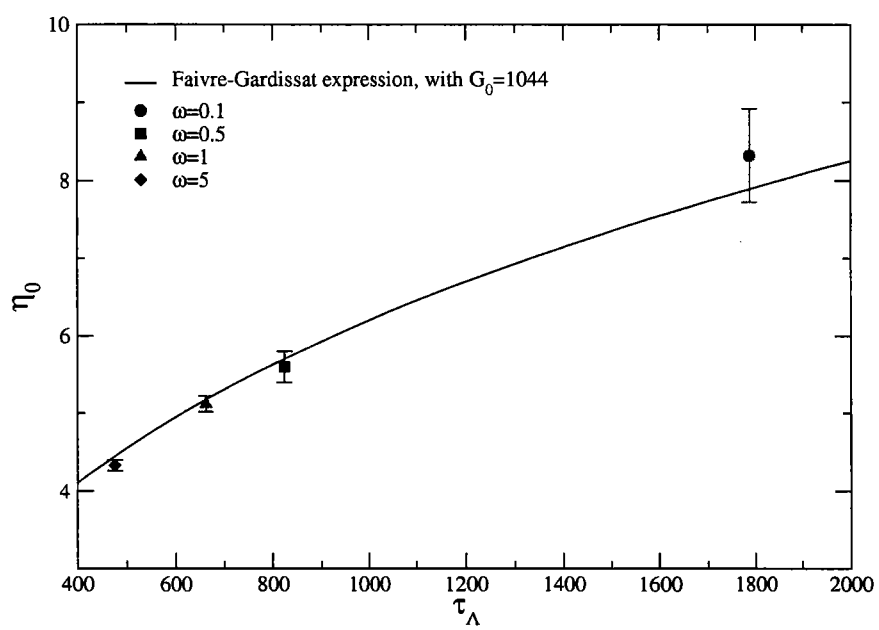

FIG. 13 – La viscosité statique η_0 est tracée en fonction de τ_Λ correspondant, à l'aide d'un fit à un paramètre G_0 et la théorie de Faivre et Gardissat (Ch1).

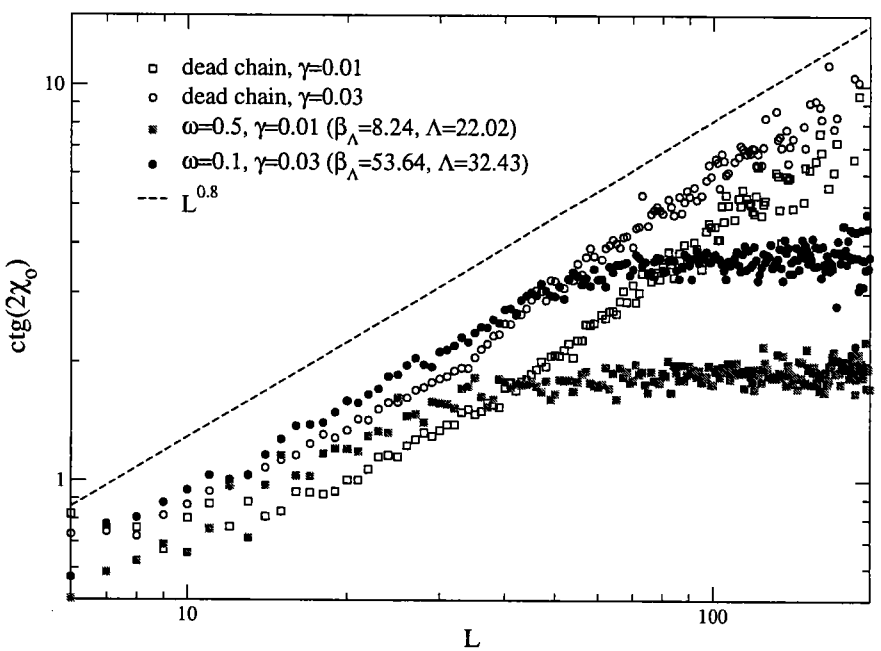

FIG. 14 – L'angle d'extinction $\left(\cot(2\chi_O^L)\right)$ en fonction de la longueur des micelles. Les symboles ouverts correspondent à des systèmes polydisperses de polymères 'morts' tandis que les symboles fermés sont ceux de micelles soumises aux scissions/recombinaisons. Les cercles représentent le cas $\dot{\gamma} = 0.03$ (où $\omega = 0.1$ pour les cercles fermés). Les carrés représentent le cas $\dot{\gamma} = 0.01$ (où $\omega = 0.5$ pour les carrés fermés). La droite en tirets représente la loi pour les chaînes 'mortes' $\left(\cot(2\chi_O^L)\right) \propto L^{0.8}$[30].

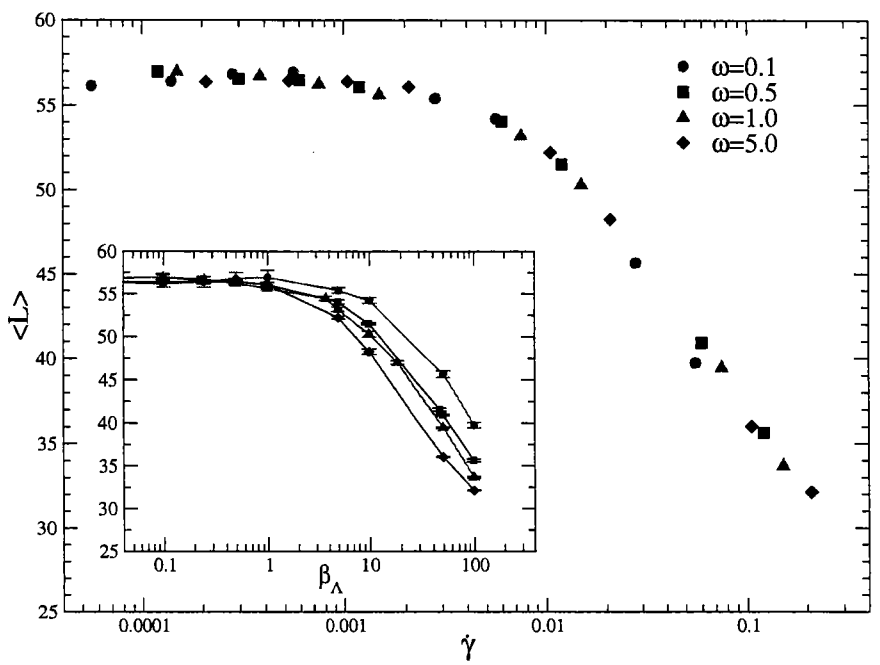

FIG. 15 – La longueur moyenne des micelles $< L >$ en fonction du taux de cisaillement $\dot{\gamma}$. Les symboles correspondent à $\omega = 0.1$(cercle), 0.5 (carré), 1 (triangle) et 5 (diamand). On peut noter que le résultat est indépendant de ω. Dans l'encart $< L >$ est représenté en fonction de β_Λ, où l'on remarque une dispersion des courbes.

Bibliographie

[1] P. van der Schoot, *in "Supramolecular polymers" Ed. A. Ciferri*, 77 (N.Y. 2005)

[2] M.E. Cates and S.J. Candau, *J. Phys : Cond. Matt.* **2**, 6869(1990)

[3] vois par exemple S. Lerouge, *Thèse de Doctorat*, Metz, (2001)

[4] S. Lerouge, J.P. Decruppe and C. Humbert *Phys. Rev. Lett.* **81**, 5457(1998)

[5] H. Hoffmann, S. Hoffmann, A. Rauscher and J. Kalus, *Prog. Colloid Polym. Sci.* **84**, 24(1991)

[6] P.G. de Gennes, *Scaling concepts in polymer physics* Cornell University Press, Ithaca(1979)

[7] A.Y. Grosberg and A.R. Khokhlov, *Statistical Physics of Macromolecules* AIP Press, New-York(1994)

[8] M. Doi and S.F. Edwards, *The theory of polymer dynamics* Clarendon, Oxford(1986)

[9] M.E. Cates, *Macromolecules* **20**, 2289(1987)

[10] N.A. Spenley, M.E. Cates and T.C.B. MacLeish *Phys. Rev. Lett.* **71**, 939(1993)

[11] S.M. Fielding and P.D. Olmsted *Phys. Rev. Lett.* **90**, 224501(2003)

[12] B. O'Shaughnessy and J. Yu, *Phys. Rev. Lett.* **74**, 4329(1995)

[13] G. Faivre and J.L. Gardissat, *Macromolecules* **19**, 1988(1986)

[14] J.P. Wittmer, A. Milchev and M.E. Cates *Europhys. Lett.* **41**, 291(1998) ; *J. Chem. Phys.* **109**, 834(1998)

[15] A. Milchev, *in "Computational methods in colloid and interface science" Ed. M. Borowko and M. Dekker*, 510(N.Y. 2000)

[16] Y. Rouault *J. Chem. Phys.* **111**, 9859(1999)

[17] M. Kroger and R. Makhloufi *Phys. Rev. E* **53**, 2531(1996)

[18] J.T. Padding and E.S. Boek, *Europhys. Lett.* **66**, 756(2004)

[19] Padding J.T.and Boek E.S.,*Phys. Rev. E* **70**, 031502(2004)

[20] C.C. Huang, H. Xu, J.P. Wittmer, F. Crevel and J.P. Ryckaert, *Lecture notes in physics*, **704**, 367-406,Springer (2006)

[21] C.M. Marques and M.E. Cates, *J. Phys. II* **1**, 489(1991)

[22] K. Kremer and G.S. Grest, *J. Chem. Phys.* **92**, 5057(1990)

[23] M.G. Paterlini and D.M. Ferguson, *Chem. Phys.* **236**, 243(1998)

[24] M.P.Allen and D.J. Tildesley, *Computer simulation of liquids*, Clarendon Press, Oxford(1987)

[25] C.C. Huang, H. Xu and J.P. Ryckaert, *J. Chem. Phys.*, **125**, 094901(2006)

[26] E. Helfand, *J. Chem. Phys.* **69**, 1010(1978)

[27] Förster S., M. Konrad M. and Lindner P., *Phys. Rev. Lett.* **94**, 017803(2005)

[28] Bossart J. and Öttinger H-C, *Macromolecules* **28**, 5852(1995)

[29] Pierleoni C. and Ryckaert J.P., *Macromolecules* **28**, 5097(1995)

[30] Aust C., Kröger M.and Hess S., *Macromolecules* **32**,5560(1999)

利用新近提出的中觀模型, 運用計算機模擬, 我們學習了自組線性膠束在平衡狀態以及在剪流下的靜力學, 動力學以及流變學. 本模型將膠束模型化爲由 Langevin 動力學界定時空演變的布朗粒子線性序列. 在本模型中, 蒙特卡羅演算法控制了鍵結斷裂與合併. 同時我們使用一個 ω 變數來模擬重新合併的動力屏障.

在平衡狀態中, 本學習主要專注在剪斷與重新連結的力學在短時間與長時間的行爲. 我們的結果顯示, 在時間尺度大於平均鏈長時間的狀況下, 動能學符合 Cates 所提出的均田動能學理論. 藉由學習宏觀鬆弛現象, 例如平均膠束長度在一個溫度跳躍之後的變化, 單體擴散與零剪切鬆弛函數, 我們驗證了在膠束的動能與宏觀鬆弛耦合時, 有效動能常數是主要的控制變因.

對於非平衡的狀況, 我們研究了剪切流與剪斷和重組動力的耦合效應對於此膠束系統的結構與流變性質的影響. 研究專注在於半稀與非纏繞區域的狀態. 控制變數 ω 選擇在於讓平均鍊子長度的生命時間短於此系統的最長的鬆弛時間 (Rouse relaxation time) 的範圍之內. 本研究的分析中心概念在於系統的動力單位尺寸Λ. 在這個尺寸時, 鍊子的生命時間相等於 Rouse 鬆弛時間. 根據本研究, 剪切變稀效應, 鍊子的旋轉張量各向不同性, 鍊子的朝向, 以及鍵結長度的延展都依據縮簡的剪切速率 $\beta_\Lambda = \gamma\tau_\Lambda$. 我們並發現, 系統的平均鍊長則根據純減切速率的增大而減短, 而此現象獨立於剪斷與合併程序的動力屏障高度.

Statics, Dynamics, and Rheological properties of Micellar solutions by Computer Simulation

Statics, dynamics, rheology and scission-recombination kinetics of self-assembling linear micelles are investigated at equlibrium state and under shear flow by computer simulations using a newly proposed mesoscopic model. We model the micelles as linear sequences of Brownian beads whose space-time evolution is governed by Langevin dynamics. A Monte Carlo algorithm controls the opening of a bond or the chain-end fusion. A kinetic parameter ω, modelling the effect of a potential barrier along a kinetic path, is introduced in our model.

For equilibrium state we focus on the analysis of short and long time behaviors of the scission and recombination mechanisms. Our results show that at time scales larger than the life time of the average chain length, the kinetics is in agreement with the mean-field kinetics model of Cates. By studying macroscopic relaxation phenomena such as the average micelle length evolution after a T-jump, the monomer diffusion, and the zero shear relaxation function, we confirm that the effective kinetic constants found are indeed the relevant parameters when macroscopic relaxation is coupled to the kinetics of micelles.

For the non-equilibrium situation, we study the coupled effects of the shear flow and the scission-recombination kinetics, on the structural and rheological properties of this micellar system. Our study is performed in semi-dilute and dynamically unentangled regime conditions. The explored parameter ω range is chosen in order for the life time of the average size chain to remain shorter than its intrinsic (Rouse) longest relaxation time. Central to our analysis is the concept of dynamical unit of size Λ, the chain fragment for which the life time τ_Λ and the Rouse time are equal. Shear thinning, chain orientation and bond stretching are found to depend upon the reduced shear rate $\beta_\Lambda=\gamma\tau_\Lambda$ while the average micelle size is found to decrease with increasing shear rate, independently of the height of the barrier of the scission-recombination process.

Propriétés statiques, dynamiques et rhéologiques de solutions micellaires par simulation sur ordinateur

Les propriétés statiques, dynamiques, rhéologiques et la cinétique de scissions et recombinaisons de micelles linéaires auto-assemblées sont étudiées à l'équilibre et sous-écoulement par simulations sur ordinateur, en utilisant un modèle mésoscopique nouveau. Nous représentons les micelles comme des séquences linéaires de billes browniennes dont l'évolution spatio-temporelle est gouvernée par la dynamique de Langevin. Un algorithme de Monte-Carlo contrôle l'ouverture des liens ou la fusion de deux chaînes par les bouts. Un paramètre cinétique ω, qui modélise l'effet d'une barrière le long d'un chemin de réaction, est introduit dans notre model.

A l'équilibre, nous nous concentrons sur les mécanismes de scission/recombinaison aux temps long et court. Nos résultats montrent que pour les temps plus grands que le temps de vie d'une chaîne moyenne, la cinétique est en accord avec le modèle champ-moyen de Cates. L'étude de fonctions de relaxation macroscopique confirme que nos constantes cinétiques effectives obtenues aux temps longs sont pertinentes pour ces relaxations.

Pour la situation hors équilibre, nous étudions les effets du couplage entre un écoulement de cisaillement et la cinétique de scission et recombinaison sur les propriétés structurales et rhéologiques du système micellaire. Nous nous plaçons dans un régime semi-dilué et dynamiquement 'unentangled'. Le paramètre ω est choisi de façon à ce que la durée de vie d'une chaîne moyenne soit plus courte que son temps de relaxation de Rouse le plus long. Nos analyses font apparaître une longueur dynamique Λ, le fragment de chaîne dont la durée de vie τ_Λ est égale à son temps de Rouse. Nous trouvons que les propriétés telles que la rhéo-fluidification, l'orientation des chaînes et l'étirement des liens sont des fonctions du taux de cisaillement réduit $\beta_\Lambda= \gamma\tau_\Lambda$, alors que la longueur moyenne des micelles est une fonction décroissante du taux de cisaillement, indépendamment de la barrière du processus scission/recombinaison.

Discipline : Physique
Mots-cles : Modélisation mésoscopique, simulation par ordinateur, systèmes auto-assemblés, solutions micellaires, système sous-cisaillement